MITIGATING THE CHEMICAL DEGRADATION OF MAGNESIA-CHROMITE BRICKS IN CONTACT WITH A PbO BASED SLAG

Lennart SCHEUNIS

Members of the
examination committee

Prof. W. Sansen, chairman
Prof. B. Blanpain, supervisor
Dr. P.T. Jones, supervisor
Dr. A. Malfliet, supervisor
Prof. J. Vleugels
Prof. P. Wollants
Dr. M. Campforts (Umicore)
Prof. W.E. Lee (Imperial College)

Dissertation presented in
partial fulfilment of the
requirements for the
degree of Doctor in
Engineering Science

December 2014

Uitgegeven in eigen beheer, LENNART SCHEUNIS, Beringen

ISBN 978-94-6018-933-3

Legal deposit D/2014/7515/156

Voorwoord

Na 4 jaar zit mijn leven als doctoraatsstudent aan de KU Leuven er bijna op. Voor mij de ideale gelegenheid om even terug te blikken op de laatste jaren en de mensen te bedanken die dit werk mee mogelijk hebben gemaakt. Eerst en vooral wil ik mijn promotoren, Bart, Tom en Annelies, bedanken voor de vrijheid die ze mij hebben gegeven tijdens mijn onderzoek, hun interesse in mijn werk en geduld tijdens het schrijven (en herschrijven) van mijn papers en deze tekst. Mieke, vanuit Umicore heb je er steeds voor gezorgd dat ik de link met de industrie niet uit het oog verloor. Bedankt voor de diepgaande discussies over mijn werk. I would also like to thank the other jury members for their interest in my work and their useful comments on this text. Ik wil ook het IWT en Umicore bedanken om dit werk financieel mogelijk te maken. Binnen Umicore wil ik in het bijzonder Saskia, Mieke, Danny, Jef en Sylvain bedanken voor hun hulp bij het plannen en uitvoeren van mijn experimenten.

At MTM I was fortunate to end up in the basement, sharing an office with Enze, Liang, Bart, Xuan, Jeroen T., Jolien, Recai, Arne, Jeroen H., Thomas and Yuanyuan. Thank you all for making MTM a great place to work! This great atmosphere was also created by the HiTemp members and by the “Alma-gangers”. Bedankt voor het gezever tijdens de middag! Ik wil ook graag mijn studie genoten, Yentl, Niels en Michaël, bedanken voor het aanhoren van mijn frustraties tijdens het schrijven van deze tekst en er steeds weer voor te zorgen dat ik terug gemotiveerd geraakte. Michaël en Niels, ik wens jullie veel succes met het opstarten van Rein4ced.

Eugene, thank you for your interest in my work and the countless hours we spent discussing my results. Ata, I remember the hours and nights we spent in the lab trying to get the setup to work after it, and with it the furnace, failed, yet again. Thank you for never giving up hope that it would eventually work and for showing me around Brisbane and Gold Coast!

Ik wil ook het technisch personeel van MTM bedanken voor hun hulp tijdens het uitvoeren van mijn werk. In het bijzonder Paul, Rudy, Joris, Tom en Pieter. Pieter, je was altijd bereid om mij te helpen als ik (weer eens) een probleem had met de EPMA. Je hulp en inzichten hebben mij zonder enige twijfel dagen, zo niet weken, aan werk uitgespaard. Tenslotte wil ik mijn vrienden, ouders en mijn broer bedanken voor hun onvoorwaardelijke steun tijdens de laatste 4 jaren.

Abstract

Vessel integrity is a vital aspect in the production of metals, determining the efficiency and feasibility of pyrometallurgical production processes. The linings in the reactors are made of refractory bricks, ceramic materials used for their excellent chemical and thermo-mechanical properties at the operational temperature. Nevertheless, failure of the lining occurs over time due to a combination of thermal, mechanical and chemical stresses, requiring a timely and costly replacement of the lining. Reducing the refractory wear would lead to less standstills and thus a more cost efficient production process. The objective of this work is to investigate the in-situ formation of phases by reaction with the slag as a method to limit the chemical refractory degradation caused by PbO-SiO_2 based slags. The chemical degradation of porous magnesia-chromite bricks by PbO-SiO_2 based slags is caused by (1) liquid infiltration into the porous refractory brick and (2) dissolution of MgO from the refractory into this liquid slag. Slag engineering is successfully used to form a protective layer between the liquid and the refractory brick sample, slowing down the dissolution rate as the refractory components have to diffuse through this new layer. For deep infiltration slags, the liquid composition, and thus the chemical corrosion, changes inside the refractory brick and the protective layer no longer forms. The formation of in-situ phases is used to seal off the open pores in the refractory. This has been tested for refractory brick under isothermal conditions and under a temperature gradient. The latter uses a newly designed experimental setup. The ability to seal off the pores before complete infiltration depends on the ratio between the growth rate of the new phases and the infiltration rate of the liquid.

Samenvatting

Integriteit van de reactorwand is een essentieel aspect van metaalproductie, het bepaalt in grote mate de efficiëntie en haalbaarheid van pyrometallurgische productieprocessen. De reactorwanden zijn vervaardigd uit vuurvaste stenen, keramische materialen gebruikt omwille van hun resistentie tegen hoge temperaturen en hun gunstige mechanische eigenschappen bij de werkingstemperatuur van de oven. Niettemin falen deze stenen na verloop van tijd als gevolg van een combinatie van thermische, mechanische en chemische belastingen, waardoor een tijdsintensieve en dure vervanging van de wand moet worden doorgevoerd. Een vermindering van de slijtagesnelheid zou leiden tot minder stilstand en dus een kostenefficiënter productieproces. Het doel van dit werk is om te bepalen of in-situ vorming van fasen gebruikt kan worden om de slijtage van vuurvaste stenen door PbO-SiO_2 gebaseerde slakken te beperken. De twee belangrijkste chemische degradatiemechanismen van poreuze magnesia-chromiet stenen in contact met deze slakken zijn: (1) infiltratie van vloeibaar slak in de poreuze vuurvaste stenen en (2) het oplossen van MgO van de stenen in deze vloeibare slak. Slak engineering wordt succesvol gebruikt om een beschermende laag tussen de vloeibare slak en de vuurvaste stenen te vormen. Hierdoor kunnen de componenten uit de vuurvaste stenen enkel oplossen in het bad als deze door de nieuwe laag diffunderen, hetgeen leidt tot een vertraging van de oplossnelheid. Voor slakken die diep kunnen infiltreren verandert de samenstelling van de vloeibare fase, en dus ook de chemische corrosie, in de steen waardoor de beschermlaag dieper in de steen zich niet langer vormt. De vorming van in-situ fasen wordt gebruikt voor het afdichten van de open poriën van de vuurvaste stenen. Dit werd zowel onder isotherme omstandigheden als onder een temperatuurgradiënt getest. Deze laatste test maakt gebruik van een nieuw ontworpen experimentele opstelling. De mogelijkheid om de poriën af te dichten voor volledige infiltratie is afhankelijk van de verhouding tussen de groei van nieuwe fasen en de infiltratiesnelheid van de vloeistof.

List of minerals and symbols

Minerals

Magnesite	$MgCO_3$
Spinel	$[Mg,Fe,Zn][Al,Cr,Fe]_2O_4$
Forsterite	Mg_2SiO_4
Monticellite	$CaMgSiO_4$
Melilite	$[Ca,Pb]_2[Fe,Mg,Al][Si,Al,Fe]_2O_7$
Wustite	FeO
Chalcopyrite	$CuFeS_2$
Periclase	MgO
Pyrope	$Mg_3Al_2(SiO_4)_3$
Fluorite	CaF_2
Willemite	Zn_2SiO_4
Galena	PbS
Haematite	Fe_2O_3

Symbols

c_p	Heat capacity	$[J.kg^{-1}.K^{-1}]$
k	Heat conductivity	$[W.m^{-1}.K^{-1}]$
l	Infiltration depth	[m]
q_{gen}	Heat generation	$[J.s^{-1}.m^{-3}]$
r	Open pore radius	[m]
t	Reaction time	[s]
T	Temperature	[K]
T_{CF}	Cold face temperature	[K]
T_{HF}	Hot face temperature	[K]
ΔP	Capillary pressure	[Pa]
η	Viscosity	[Pa.s]
θ	Contact angle	[rad]
ρ	Density	$[kg.m^{-3}]$
σ	Surface tension of the liquid	$[N.m^{-1}]$

Table of content

Voorwoord I
Abstract III
Samenvatting V
List of minerals and symbols VII
Table of content IX
Chapter 1 General introduction 1
1.1 Research objectives 3
1.2 Outline of the text 3
Chapter 2 Magnesia-chromite bricks 7
2.1 Production of magnesia-chromite bricks 8
2.2 Behavior in use 13
2.2.1 Thermo-mechanical degradation 13
2.2.2 Chemical degradation 14
2.3 Identification of degradation 16
2.4 Conclusion 17
Chapter 3 Mitigating the chemical wear 23
3.1 Viscosity of the slag 23
3.2 Changing the solubility of refractory components in the slag 23
3.3 Direct-indirect dissolution 26
3.4 Infiltration 28
3.4.1 Fundamentals of infiltration 28
3.4.2 In-situ measurements 29
3.4.3 Changes in slag composition 30
3.4.4 Predicting the slag changes 30
3.4.5 Methods to stop infiltration 34
3.5 Conclusions 37
Chapter 4 Slag engineering for PbO slags 43

4.1 Introduction 43
4.2 Materials and methods 43
4.3 Results 45
4.3.1 Slag S1 47
4.3.2 Slag S2 51
4.4 Discussion 55
4.5 Conclusion 56
Chapter 5 The influence of slag compositional changes on the chemical degradation of magnesia-chromite refractories exposed to PbO-based non-ferrous slag saturated in spinel 57
5.1 Introduction 58
5.2 Experimental procedure 59
5.3 Results 61
5.3.1 Microstructure 61
5.3.2 Composition of the slag inside the sample 69
5.4 Discussion 71
5.5 Effect on the overall degradation of a refractory lining 74
5.6 Conclusions 77
5.7 Acknowledgement 79
Chapter 6 The effect of phase formation during use on the chemical corrosion of magnesia-chromite refractories in contact with a non-ferrous PbO-SiO_2 based slag 85
6.1 Introduction 86
6.2 Experimental procedure 89
6.3 Results and discussion 90
6.3.1 Reacted brick 90
6.3.2 Slag-refractory interaction 98
6.4 Conclusion 108
6.5 Acknowledgement 109

Chapter 7 The effect of a temperature gradient on the phase formation inside a magnesia-chromite refractory brick in contact with a non-ferrous PbO-SiO_2-MgO slag 113
7.1 Introduction 114
7.2 Experimental procedure 116
7.3 Results 119
7.3.1 Temperature measurements 119
7.3.2 Microstructure 121
7.3.3 Slag composition as a function of position 125
7.4 Discussion 129
7.4.1 Local temperature 130
7.4.2 Slag composition 130
7.4.3 Infiltration behavior 131
7.4.4 Effect of external cooling on chemical degradation 134
7.5 Conclusion 136
Chapter 8 Conclusions and future work 141
8.1 Conclusions 141
8.2 Future work 143
List of publications 145
Curriculum Vitae 147

Chapter 1

General introduction

In pyrometallurgy, metal is produced in a high temperature process either directly from ores (called primary production) or by recycling end-of-life products or waste streams (called secondary production). These feeds are melted in a reactor in order to separate them in different phases; typically an alloy, slag and gas phase. The distribution of the components in the feed to the different phases is controlled by the temperature and the applied oxygen partial pressure (pO_2) in the reactor. The latter parameter depends on the ratio between the amount of added oxygen and reducing agent (cokes, natural gas, fuel,…), the amount and the composition of the feed and the interaction between all these phases. The different process materials are contained in a furnace, as schematically shown in Figure 1.1. This furnace consists of a steel shell. Unfortunately, the steel shell cannot withstand the combination of thermal, mechanical and chemical loads when it is in direct contact with the process materials. A lining is therefore placed between the shell and the phases in the process. Two methods are used to protect the steel shell: by using a freeze lining or by using a refractory lining.

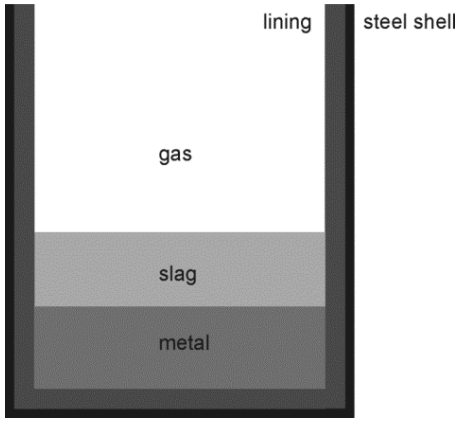

Figure 1.1: Schematic representation of a pyrometallurgical reactor, showing the external steel shell, the lining and phases in the reactor (metal, slag and gas).

By applying external cooling of the shell, a layer of process material (called a freeze lining [1-13]) is deposited on the wall. This freeze lining separates, and thus protects, the furnace wall from the aggressive process materials. The main advantages of the freeze lining approach are its self-healing nature, its compatibility with the process materials and the high thermal resistance of the slag compared to, for example, the alloy. If the layer should fail, for example due to mechanical impact on the lining, a new layer will form by freezing new process materials against the shell. Because the freeze lining is formed by the process materials it is also in chemical equilibrium with the phases present in the reactor, limiting any reaction between the freeze lining and the phases in the reactor. The main downside of a freeze lining approach for vessel integrity is the safety risk when a failure of the lining occurs. When this happens and the process materials come into direct contact with the cooled furnace wall, the latter can fail, resulting in direct contact between the cooling water and the reactor in turn leading to a steam explosion. The layer thickness is controlled by the heat balance over the freeze lining. When the heat input from the bath is larger than the heat removal from the cooling water the freeze lining melts. If the layer thickness becomes too thin, there is a risk of failure. If the heat removal is larger than the supplied heat the freeze lining thickness increases, decreasing the capacity of the reactor. The necessity for a stable layer thickness during the entire lifetime of the furnace is the main limitation to the applicability of freeze linings.

An alternative approach to the application of a freeze lining is the use of a refractory lining [14-18], which is still the most used method. The refractory linings are placed between the steel shell and the process phases. They are ceramic materials with a low thermal conductivity, ensuring that the high temperatures in the reactor can be reached with minimal heat losses while at the same time the steel shell is protected against the high temperature. The second main function of the lining is creating a physical barrier between the steel shell and the process materials. Therefore no reaction between both can occur. However, this means that the refractory lining is in direct contact with the process materials and the refractory materials, therefore, have to be able to withstand the aggressive conditions inside the smelter. With time failure of the refractory still occurs, requiring a costly and time intensive replacement of the lining. The overarching goal in industrial refractory research is to maximize the profit for the smelting process. The strategy to do this differs depending on the area in the reactor. For the area showing the most severe wear the best approach is

usually to determine the conditions that lead to a minimal wear rate and therefore a longer production run. For the less critical areas, cheaper bricks are commonly used. These bricks typically corrode faster, but as long as the wear rate stays below that of the most critical area, it will not affect the overall lifetime of the furnace.

1.1 Research objectives

The main objective of this work is to identify methods to limit the chemical refractory degradation caused by PbO-containing slags. The classic approach to this problem is to develop new refractory bricks with a better chemical resistance. There are, however, limitations to the brick properties that can be achieved. In order to further improve the wear rate this work uses the interaction between the slag and the refractory phases to form protective phases to slow down the chemical degradation.

PbO containing slag systems are known to easily and deeply infiltrate the refractory leading to chemical attack inside the sample as well as on the surface. The research goals are therefore twofold: (1) determine how the slag composition can be modified to limit the dissolution at the surface of the refractory brick and (2) determine how the slag composition can be modified to prevent the infiltration of liquid slag into the open pores of the refractory.

1.2 Outline of the text

Chapters 2 and 3 of the text cover a literature review. In Chapter 2 the production and use of magnesia-chromite bricks are discussed. Based on this the main limitations of the lifetime of the reactors are defined. Chapter 3 focuses on strategies that involve targeted changes in the slag composition as a way to limit the chemical degradation and also discusses the effect of infiltration of the liquid slag into the porous brick on the occurring degradation.

The results covering the research goals are discussed in chapters 4-7. In Chapter 4 the effect of slag engineering on the chemical dissolution at the hot face of a refractory sample is investigated, thereby showing how the MgO dissolution is decreased by the formation of a protective spinel layer. In Chapter 5 it is further clarified how the formation of such a protective layer influences the chemical degradation inside the sample.

In the final two chapters methods are investigated that seal off the porous refractory sample from the liquid PbO slags. The first method consists of the formation of new phases in the pores by the reaction between the infiltrating slag and the refractory phases and is discussed in Chapter 6. Chapter 7, finally, investigates what happens to the slag-refractory interaction when a temperature gradient is applied over the refractory sample as a way to slow down the infiltration rate.

Chapter 8 gives the main conclusions of this work as well as some suggestions for future work.

Chapters 5-7 are based on the author's papers published in or submitted to international peer-reviewed journals. On the first page of each of these chapters a bibliographic reference of the publication is made and the contribution of the author to the work is discussed.

References

1. Campforts, M., Blanpain, B., and Wollants, P., *The importance of slag engineering in freeze-lining applications.* Metallurgical and Materials Transactions B-Process Metallurgy and Materials Processing Science, 2009. **40**(5): p. 643-655.
2. Campforts, M., Jak, E., Blanpain, B., and Wollants, P., *Freeze-lining formation of a synthetic lead slag: Part I. Microstructure formation.* Metallurgical and Materials Transactions B-Process Metallurgy and Materials Processing Science, 2009. **40**(5): p. 619-631.
3. Campforts, M., Jak, E., Blanpain, B., and Wollants, P., *Freeze-lining formation of a synthetic lead slag: Part II. Thermal history.* Metallurgical and Materials Transactions B-Process Metallurgy and Materials Processing Science, 2009. **40**(5): p. 632-642.
4. Campforts, M., Verscheure, K., Boydens, E., Van Rompaey, T., Blanpain, B., and Wollants, P., *On the mass transport and the crystal growth in a freeze lining of an industrial nonferrous slag.* Metallurgical and Materials Transactions B-Process Metallurgy and Materials Processing Science, 2008. **39**(3): p. 408-417.
5. Campforts, M., Verscheure, K., Boydens, E., Van Rompaey, T., Blanpain, B., and Wollants, P., *On the microstructure of a freeze lining of an industrial nonferrous slag.* Metallurgical and Materials Transactions B-Process Metallurgy and Materials Processing Science, 2007. **38**(6): p. 841-851.
6. Fallah-Mehrjardi, A., Hayes, P.C., and Jak, E., *Investigation of freeze lining in copper-containing slag systems: Part III. High-temperature experimental investigation of the effect of bath agitation.* Metallurgical and Materials Transactions B-Process Metallurgy and Materials Processing Science, 2013. **44**(6): p. 1337-1351.
7. Fallah-Mehrjardi, A., Hayes, P.C., and Jak, E., *Investigation of freeze-linings in copper-containing slag systems: Part I. Preliminary experiments.* Metallurgical and Materials Transactions B-Process Metallurgy and Materials Processing Science, 2013. **44**(3): p. 534-548.
8. Fallah-Mehrjardi, A., Hayes, P.C., and Jak, E., *Investigation of freeze linings in copper-containing slag systems: Part II. Mechanism of the deposit stabilization.* Metallurgical and Materials Transactions B-Process Metallurgy and Materials Processing Science, 2013. **44**(3): p. 549-560.

9. Jansson, J., Taskinen, P., and Kaskiala, M., *Freeze-lining formation in continuous converting calcium ferrite slags. I.* Canadian Metallurgical Quarterly, 2013. **53**(1): p. 1-10.
10. Verscheure, K., Campforts, M., Verhaeghe, F., Boydens, E., van Camp, M., Blanpain, B., and Wollants, P., *Water-cooled probe technique for the study of freeze lining formation.* Metallurgical and Materials Transactions B-Process Metallurgy and Materials Processing Science, 2006. **37**(6): p. 929-940.
11. Fallah-Mehrjardi, A., Hayes, P., and Jak, E., *Understanding slag freeze linings.* JOM:The Journal of The Minerals, Metals & Materials Society (TMS), 2014. **66**(9): p. 1654-1663.
12. Solheim, A. and Thonstad, J., *Model experiments of heat transfer coefficients between bath and side ledge in aluminum cells.* JOM, 1984. **36**(3): p. 51-55.
13. Taylor, M.P., Welch, B.J., and McKibbin, R., *Effect of convective heat transfer and phase change on the stability of aluminium smelting cells.* AIChE Journal, 1986. **32**(9): p. 1459-1465.
14. Taschler, T., *Refractory materials for the copper and lead industry*. in *Tehran International Conference on Refractories*. Tehran, Iran 2004: p. 302-319.
15. Poirier, J., Qafssaoui, F., Ildefonse, J.P., and Bouchetou, M.L., *Analysis and interpretation of refractory micro structures in studies of corrosion mechanisms by liquid oxides.* Journal of the European Ceramic Society, 2008. **28**(8): p. 1557-1568.
16. Malfliet, A., Lotfian, S., Scheunis, L., Petkov, V., Pandelaers, L., Jones, P.T., and Blanpain, B., *Degradation mechanisms and use of refractory linings in copper production processes: A critical review.* Journal of the European Ceramic Society, 2014. **34**(3): p. 849-876.
17. Lee, W.E. and Zhang, S., *Melt corrosion of oxide and oxide-carbon refractories.* International Materials Reviews, 1999. **44**(3): p. 77-104.
18. Lee, W.E. and Zhang, S., *Direct and indirect slag corrosion of oxide and oxide-C refractories*. in *VII International Conference on Molten Slags Fluxes and Salts*. Cape Town, South Africa 2004: p. 309-320.

Chapter 2

Magnesia-chromite bricks

Most refractory materials are based on carbon and 6 oxides: SiO_2, Al_2O_3, Cr_2O_3, MgO, CaO and ZrO_2. Typically, a combination of these components is used to produce refractory bricks. Figure 2.1 gives a schematic overview of the different types of refractory bricks that are commercially used. In this work only magnesia-chromite bricks are considered (highlighted in Figure 2.1). This chapter starts with the production of this type of brick before discussing the reactions during use of the lining and the causes for its eventual failure.

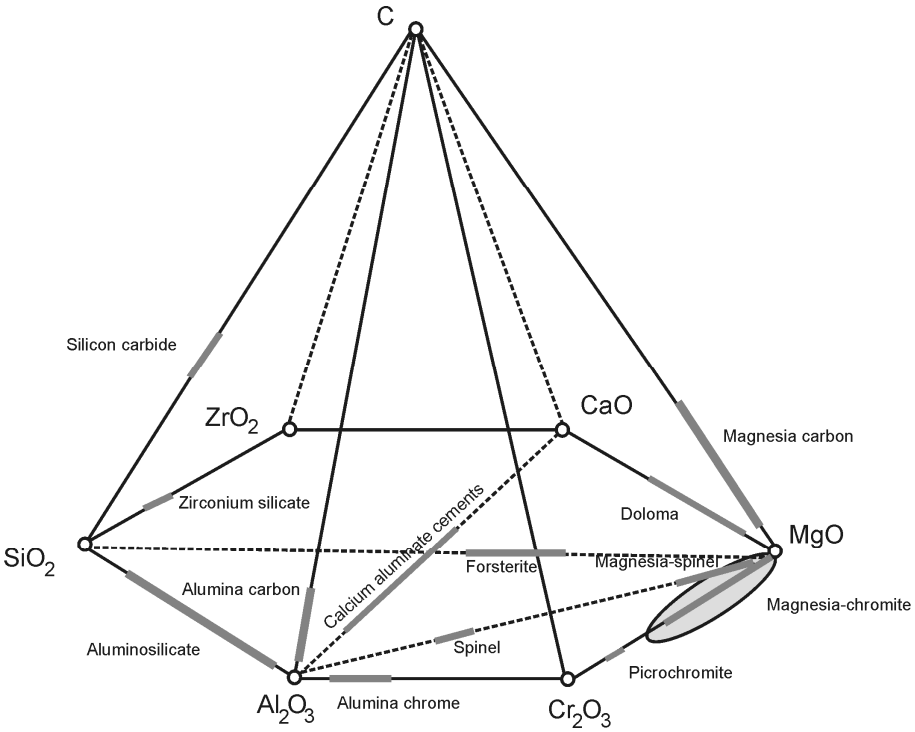

Figure 2.1: Overview of the different compositions used to produce refractory bricks. The composition for magnesia-chromite is highlighted. Based on [1, 2].

2.1 Production of magnesia-chromite bricks

There are several types of magnesia-chromite bricks. The difference lies in (1) the fraction of magnesia and chromite mixed to form the bricks, (2) the size (distribution) of the grains, which controls the porosity of the final product, and (3) the firing temperature. Figure 2.2 gives an overview of the different types of magnesia-chromite bricks and their production route. The production starts with the calcination of magnesite (magnesium carbonate, $MgCO_3$) to form magnesia (MgO) [3-6]. The magnesia is crushed, and the grains are mixed with chromite spinel grains and a binder is added. The mixture is pressed in the desired shape of the bricks and fired to create refractory bricks.

The different firing temperatures and the resulting microstructure they cause are shown in Figure 2.2. When the refractories are fired below 1550 °C the bonding between the periclase and chromite grains is caused by a silica containing phase, typically forsterite (Mg_2SiO_4), due to the relative high amount of impurities (SiO_2 + CaO above 3 wt%). By increasing the firing temperature and reducing the concentration of impurities below 2 wt% a direct bond between the grains is created. A direct bond is defined by Goto and Lee as: ”*a direct attachment of magnesia to chromite without any interrupting film of silicate*” [7]. Further increasing the firing temperature leads to the formation of sintered (2100 °C) or fused grains (2450 °C). After cooling, this material is crushed and mixed with new chromite spinel and fired at 1550-1600 °C to create a direct bond between the different phases.

Depending on the production process of the brick, its microstructure, and thus its properties, differ. With higher firing temperature the resistance of the bricks against chemical corrosion increases due to a larger grain size and thus a lower surface/volume ratio, although the higher temperature requires a higher production cost and also leads to a lower spalling resistance of the bricks [1]. Rebonded fused grain bricks are the most chemically resistant porous brick and, for that reason, the only brick type used in this work.

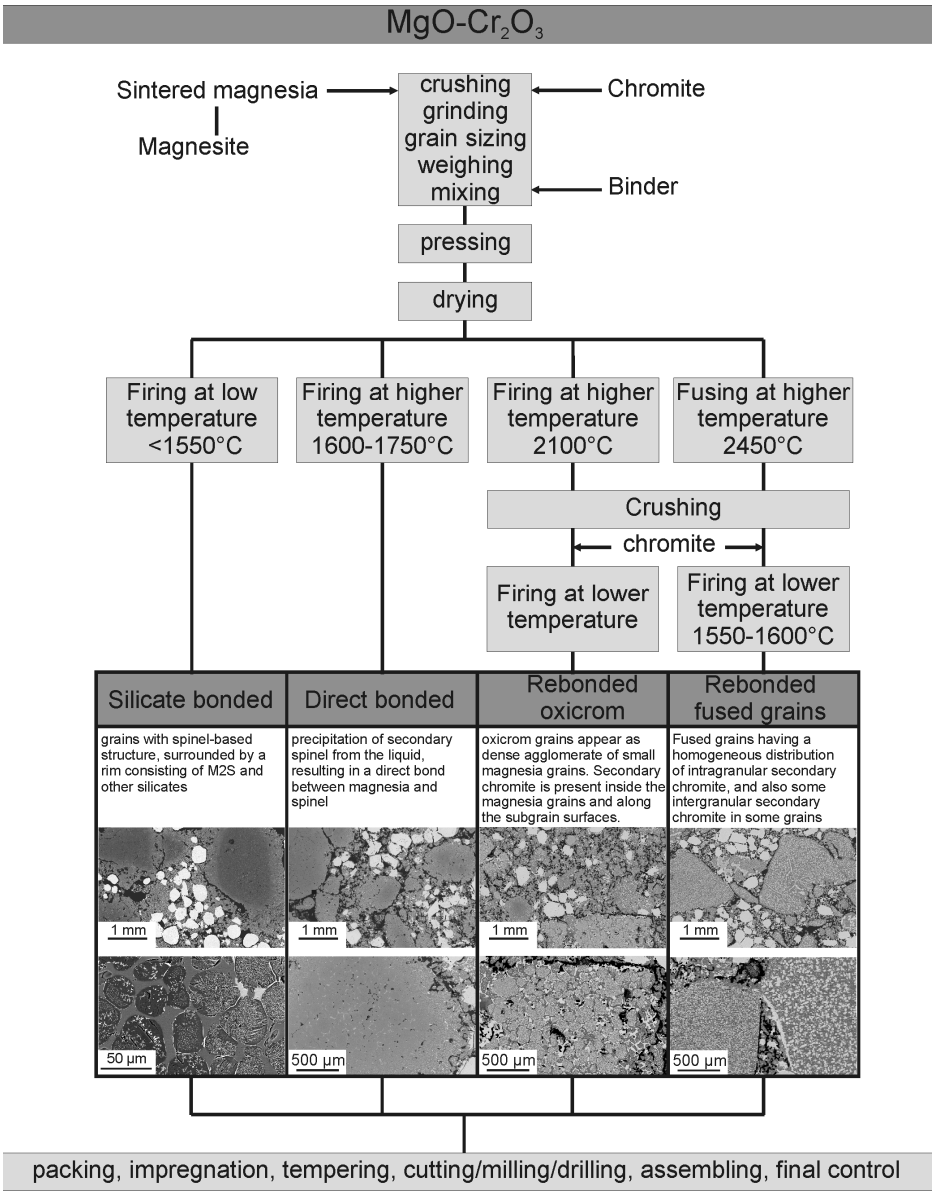

Figure 2.2: Production route and resulting microstructure for the different magnesia-chromite bricks. Based on [8].

The microstructure (Figure 2.3) and bulk and phase's compositions (Table 2.1) of fused grain rebonded magnesia-chromite refractory bricks are discussed and both are linked with the reactions occurring during the production process of the bricks. The final microstructure is shown in Figure 2.3a and consists of (1) large (2-5 mm) fused grains (FG, detailed image in Figure 2.3b), (2) smaller (1 mm) primary chromite grains (PC) and (3) porous refractory matrix of periclase (P) and secondary chromite (SC) (Figure 2.3c). This microstructure is produced in two separate production steps. First, fused grains are produced by melting periclase (MgO) and chrome ores ($Mg(Cr,Al,Fe)_2O_4$) in an electric arc furnace at temperatures to 2400 °C. During cooling of the melt, secondary chromite (SC) (as opposed to primary chromite, which never dissolved into the periclase) precipitates inside the periclase (P) matrix as seen in Figure 2.3b. After cooling, the fused grains are crushed, mixed with new magnesia and chrome ores and in a second production step are sintered at a temperature between 1700 and 1800 °C in order to form a direct bond between the different grains by absorbing part of the chromite into the periclase, forming a solid solution [7, 9-11]. During final cooling, secondary chromite again precipitates out of the periclase solid solution. This occurs either on the edge of the periclase subgrain (type I, SC_I) or inside the periclase subgrains (type II, SC_{II}) (Figure 2.3b). The solubility of the chromite components (Fe, Al and Cr oxides) in periclase differs and is the highest for the iron oxide [12]; hence, more iron oxide is dissolved in the periclase, which upon cooling leads to a higher iron oxide concentration in the formed secondary chromite. This effect can be seen in Table 2.1 by comparing the iron content in the secondary and primary chromite.

The pores (C) are primarily located inside the matrix (Figure 2.3c), making it more susceptible to infiltration by the liquid slag. The pore size distribution for the rebonded fused grain magnesia-chromite brick used in this work is shown in Figure 2.4. Based on this measurement, the majority of the pores have a diameter between 10 µm and 30 µm. Figure 2.3c also shows some impurity phases inside the brick. In the investigated sample only forsterite (F) (Mg_2SiO_4) and monticellite (M) ($MgCaSiO_4$) are detected (Figure 2.3c).

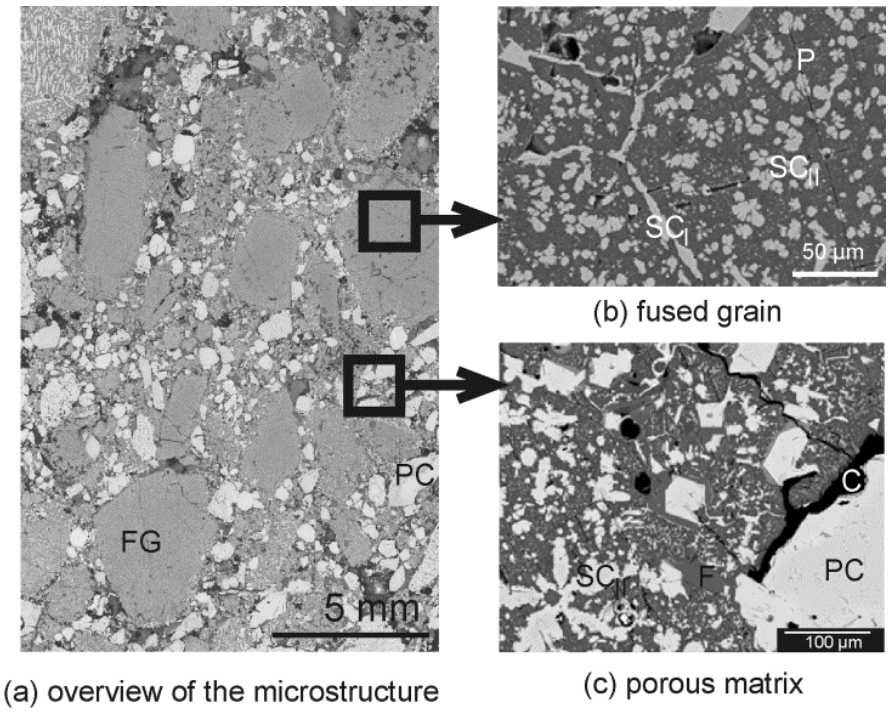

Figure 2.3: a) Microstructure of a fused grain rebonded magnesia-chromite brick. Indicating the 3 main phases: fused grain (FG), primary chromite (PC) and the porous matrix. Detailed SEM-BSE images (b-c) show the presence of periclase (P) and type I and II secondary chromite (SC_I and SC_{II}) inside the fused grains and the matrix. Forsterite (F) impurities are present inside the porous matrix.

Table 2.1: Composition of all detected phases in the refractory sample (determined by quantitative EPMA-WDS) and the bulk composition (determined by standardized XRF).

Phase		Bulk material		Primary chromite (PC)		Secondary chromite (FG) (type I) (SC_I)		Secondary chromite (matrix) (Type II) (SC_{II})		Periclase (P)		Forsterite (F)		Monticellite (M)	
		wt%	mol%	wt%	mol%	wt%	mol%	wt%	mol%	wt%	mol%	wt%	mol%	wt%	mol%
MgO		54.9	80	22.9 ± 0.2	50.2 ± 0.4	23.5 ± 0.2	51.2 ± 0.3[2]	23.8 ± 0.1	51.6 ± 0.1[2]	94.7 ± 0.1	98.6 ± 0.1	57.3 ± 0.2	66.6 ± 0.2	28.5 ± 0.6	36.8 ± 0.7[3]
Al_2O_3		7.9	4.6	17.7 ± 1.6	15.4 ± 1.3	16.8 ± 0.6	14.5 ± 0.3	16.7 ± 0.4	14.3 ± 0.3	0	0	0	0		0
Cr_2O_3		25	9.7	50.4 ± 1.5	29.3 ± 0.9	46.0 ± 0.4	26.6 ± 0.4	46.5 ± 0.8	26.7 ± 0.4	2.6 ± 0.1	0.7 ± 0.1	0	0	0	0
"Fe_2O_3"[1]		9.6	3.5	8.8 ± 2.2	4.9 ± 1.2	13.5 ± 0.8	7.4 ± 0.2	12.8 ± 1.2	7.0 ± 0.7	2.7 ± 0.1	0.7 ± 0.1	0	0	0	0
SiO_2		1.7	1.6	0	0	0	0	0	0	0	0	42.7 ± 0.2	33.4 ± 0.2	38.5 ± 0.5	33.3 ± 0.4
CaO		0.6	0.7	0	0	0	0	0	0	0	0	0	0	31.9 ± 0.4	29.5 ± 0.4

[1] Fe is recalculated to Fe_2O_3 for presentation purposes.

[2] This is higher than the stoichiometric (AB_2O_4 structure) composition, most likely caused by either (1) vacancies in the spinel crystal structure or (2) some interaction with the surrounding periclase during measuring, overestimating the MgO content, due to the limited size of the phase.

[3] This is higher than the stoichiometric composition ($MgCaSiO_4$), most likely an indication of solid solution.

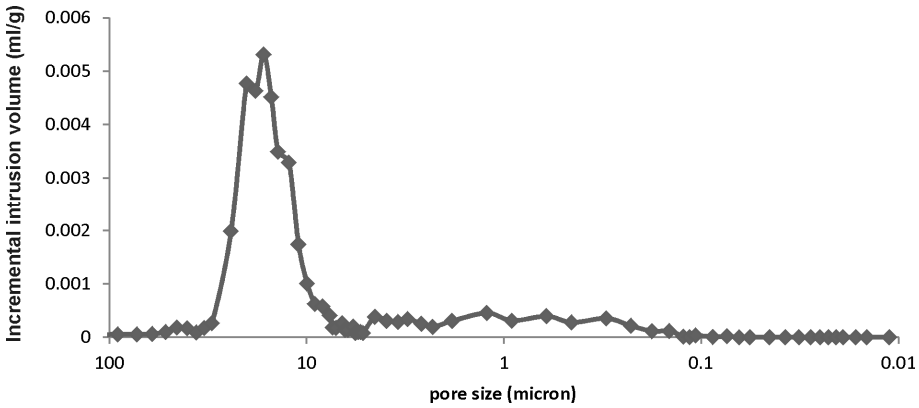

Figure 2.4: Pore size distribution of a rebonded fused grain magnesia-chromite brick obtained using mercury porosimetry.

2.2 Behavior in use

The wear of all refractory linings is caused by either mechanical, thermal or chemical stresses on the lining. When these stresses occur at the same time they can lead to a synergetic effect, accelerating the wear rate.

2.2.1 Thermo-mechanical degradation

The failure of the lining can be due to purely mechanical loads like the movement of the bath during use leading to erosion and impact [13] but mostly it is the combination of thermal and mechanical loads that lead to failure. The expansion of the bricks during the heating of the furnace, for example, can cause internal stresses [14], in turn leading to cracks and eventually the failure of part of the lining when the material can no longer withstand the internal stresses. This type of failure is called spalling. Spalling can also occur during the use of the lining when the temperature in the furnace varies over time leading to internal stresses [15]. Several authors have developed models to predict the failure of the lining based on the material properties of the used brick, the temperature loads in the lining and the design of the furnace [16-21]. The models have been applied to several types of refractory bricks including alumina based, MgO-C and magnesia-chromite. In order to apply the models, it is vital that the properties of the brick, and their temperature dependency, are known. Currently, these models only determine the influence of thermo-mechanical loads on the lining. If the bricks are subjected to chemical stresses, this can result in a change in microstructure and thus also the mechanical properties, which up till now no model has taken into account.

2.2.2 Chemical degradation

All forms of chemical degradation have the same cause: a non-equilibrium situation, which the system tries to overcome by reaction. The specific degradation mechanisms, and thus the wear rate, depend on the process stream in contact with the brick. This can be slag, alloy, matte or gas. In practice the lining's lifetime of non-ferrous smelters is typically limited by either gas or slag degradation. Therefore only the degradation caused by the gas and slag is discussed below.

Gas

A common form of chemical gas attack is caused by sulfur in the gas, which is formed by oxidation of sulfur containing ores in order to produce metals. An example is the production of copper from chalcopyrite ($CuFeS_2$) by oxidation to form FeO, Cu and SO_2 (gas). Below 1050 °C the SO_2 oxidizes to SO_3 in the presence of additional O_2. The SO_3 in turn reacts with CaO and MgO from the refractory bricks to form $CaSO_4$ and $MgSO_4$, leading to a disintegration of the brick structure [22-24].

The used pO_2 in the process also has a significant effect on the degradation of the lining. At very low pO_2 values (10^{-11} atm) decomposition of the primary chromite grains can occur. In particular, the FeO in this phase is susceptible to this reaction [11, 25, 26].

Slag

The chemical degradation caused by liquid slag can be divided into 3 main interactions: (1) dissolution of refractory components into the liquid bath, (2) the formation of new phases and (3) the diffusion of components from the slag into the refractory phases.

Components from the refractory brick dissolve into the liquid slag. This process is called corrosion and is one of the most common chemical degradation mechanisms. The corrosion rate differs per component (MgO, Cr_2O_3, Al_2O_3 and Fe_2O_3) in the brick and depends on the solubility of the components in the liquid slag bath and on the phases in the refractory brick.

Beside the dissolution of refractory components into the liquid bath, components from the bath can also diffuse into the solid refractory phases, forming a new solid solution. The most common example is the diffusion of FeO into the periclase of the refractory bricks leading to the formation of a

magnesio-wustite solid solution [27, 28]. But also other divalent cations form a solid solution with the periclase present, for example NiO [29-32] and CuO [33-35]. The formation of the solid solution results in a volume increase which can result in internal stresses, increasing the spalling risk. The formation of solid solution can also occur for the chromite spinel phase. Because the spinel phase contains both divalent and trivalent cations, many more components can diffuse into it. Examples include FeO, Fe_2O_3, Al_2O_3, ZnO [36], NiO [29-32] and CuO [31, 33].

The reaction between the liquid slag and the refractory bricks can also lead to the formation of new phases. These phases can form at the hot face but also inside the porous structure when the slag infiltrates the open pores.

When they form inside the sample, the new phases lead to densification of the brick. The open pores are replaced by solid phases, changing the thermo-mechanical properties of the brick. This increases the spalling risk of the lining. An example of such a reaction is the formation of forsterite in the copper and lead industry [37] shown in Figure 2.5. The formation of forsterite in the pores of the brick leads to an increase of the volume of the infiltrated part of the lining. When the bricks in the lining are unable to expand, the forsterite formation leads to internal stresses and finally to cracks as can be seen in Figure 2.5.

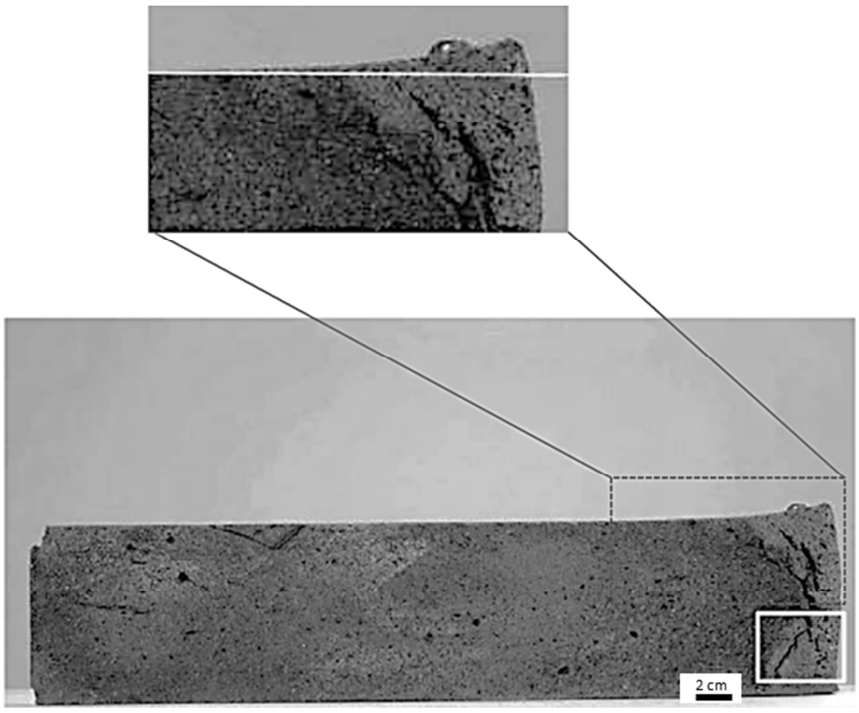

Figure 2.5: Magnesia-chromite brick used in a lead reverberatory furnace. The right side of the brick was exposed to a slag containing exceptionally high SiO_2, resulting in forsterite formation in the brick. The forsterite leads to an expansion seen in the top image. Taken from [37].

2.3 Identification of degradation

In order to prolong the lifetime of the lining it is important to reduce the wear rate. Before any changes to the process or the bricks can be done it is vital to know how the lining fails. In order to investigate this for industrial processes, samples are taken from the lining after its lifetime. This is called post mortem analysis and is typically the first step to improve the lining's lifetime. By identifying the difference in the microstructure before and after use, the causes for the chemical attack can be identified. Thermodynamic data and calculations can then be used to propose possible changes to the process. The effect of the changes is then validated on lab scale before the change is applied on industrial scale.

A post-mortem analysis typically starts with the selection of the bricks from relevant positions in the furnace lining. After this, the brick is visually inspected to identify the presence of cracks in the microstructure. At the

same time positions for further investigation are determined. The microstructure of the selected areas is analyzed by either a light optical microscope or more commonly by a scanning electron microscope (SEM). The latter allows the identification of the phases and their composition by using an EDS (Energy-Dispersive X-ray Spectroscopy) or WDS (Wavelength-Dispersive X-ray Spectroscopy) system.

2.4 Conclusion

Different types of magnesia-chromite bricks exist depending on the firing temperature during their production, all having different thermo-mechanical and chemical properties. Of all porous magnesia-chromite bricks, the fused grain rebonded bricks are the most resistant against chemical degradation. When using these bricks, further improvements of the wear rate are therefore not possible by changing the brick type but will have to consider changes to the process to address the underlying reasons for the failure. The two main causes for failure are chemical and thermo-mechanical degradation. Typically, a combination occurs simultaneous leading to an even faster wear rate. One of the main causes of chemical degradation is attack by the liquid slag. The degradation is controlled by the composition of the liquid slag. Chapter 3 discusses different methods to limit the chemical degradation by changing the slag composition.

References

1. Köffel, M. and Taschler, T., *Refractories for the copper and lead industry*, in *World of Metallurgy*2006. p. 133-143.
2. Lee, W.E. and Rainforth, W.M., *Ceramic microstructures: property control by processing*1994, London: Chapman & Hall.
3. Pike, R.D., *Dead burned magnesia*, 1944,US2348847
4. Pike, R.D., *Production of dead-burned magnesia*, 1949,US2478593
5. Reynolds, J.B. and Amos, C.R., *Process for the production of dead burned refractory magnesia*, 1981,US4243424
6. Bhatti, A., Dollimore, D., and Dyer, A., *Magnesia from seawater: a review.* Clay Minerals, 1984. **19**(5): p. 865-875.
7. Goto, K. and Lee, W.E., *The "Direct bond" in magnesia chromite and magnesia spinel refractories.* Journal of the American Ceramic Society, 1995. **78**(7): p. 1753-1760.
8. Malfliet, A., Lotfian, S., Scheunis, L., Petkov, V., Pandelaers, L., Jones, P.T., and Blanpain, B., *Degradation mechanisms and use of refractory linings in copper production processes: A critical review.* Journal of the European Ceramic Society, 2014. **34**(3): p. 849-876.
9. Jones, P.T., Vleugels, J., Volders, I., Blanpain, B., Van der Biest, O., and Wollants, P., *A study of slag-infiltrated magnesia-chromite refractories using hybrid microwave heating.* Journal of the European Ceramic Society, 2002. **22**(6): p. 903-916.
10. Jones, P.T., Desmet, D., Guo, M., Durinck, D., Verhaeghe, F., Van Dyck, J., Liu, J., Blanpain, B., and Wollants, P., *Using confocal scanning laser microscopy for the in situ study of high-temperature behaviour of complex ceramic materials.* Journal of the European Ceramic Society, 2007. **27**(12): p. 3497-3507.
11. Jones, P.T., Blanpain, B., Wollants, P., Ding, R., and Hallemans, B., *Degradation mechanisms of magnesia-chromite refractories in vacuum-oxygen decarburisation ladles during production of stainless steel.* Ironmaking & Steelmaking, 2000. **27**(3): p. 228-237.
12. Kowalski, M., Spencer, P.J., and Neuschütz, D., *Phase diagrams*, in *Slag Atlas 2nd Edition*, V.D.E. (VDEh), Editor 1995, Verslag Stahleisen GmbH: Düsseldorf. p. 21-215.
13. Huang, A., Gu, H., Zhang, M., Wang, N., Wang, T., and Zou, Y., *Mathematical modeling on erosion characteristics of refining ladle lining with application of purging plug.* Metallurgical and Materials Transactions B, 2013. **44**(3): p. 744-749.

14. Prietl, T., Antrekowitsch, H., Triessnig, A., Studnicka, H., and Filzwieser, A., *The evaluation of refractory linings thermo mechanical properties*. in *European Metallurgical Conference*. 2005: p. 18-21.
15. Damhof, F., Brekelmans, W.A.M., and Geers, M.G.D., *Non-local modeling of thermal shock damage in refractory materials.* Engineering Fracture Mechanics, 2008. **75**(16): p. 4706-4720.
16. Chen, X., Chang, Q.M., Chen, C.J., and Zhang, Y.X., *Simulation of the thermo-mechanical behavior and failure of refractory of converter.* Advanced Materials Research, 2011. **255**: p. 4139-4142.
17. Schmitt, N., Burr, A., Berthaud, Y., and Poirier, J., *Micromechanics applied to the thermal shock behavior of refractory ceramics.* Mechanics of Materials, 2002. **34**(11): p. 725-747.
18. Andreev, K. and Harmuth, H., *FEM simulation of the thermo-mechanical behaviour and failure of refractories—a case study.* Journal of Materials Processing Technology, 2003. **143–144**: p. 72-77.
19. Zabolotsky, A.V., *Thermal crack growth modeling in refractory linings of metallurgical installations.* Int. J. of Mathematical Models and Methods in Applied Sciences, 2011. **5**(3): p. 542-549.
20. Williford, R.E., Johnson, K.I., and Sundaram, S.K., *Modelling of high-chromia refractory spalling in slagging coal gasifiers.* Ceramics International, 2008. **34**(8): p. 2085-2089.
21. Zhang, W., Doynov, N., Wolf, M., Dreibati, O., Ossenbrink, R., and Michailov, V., *Investigation of the thermal shock behavior of ceramic using a combination of experimental testing and FE-simulation methods.* Advanced Engineering Materials, 2013. **15**(6): p. 480-484.
22. Fotoyi, N. and Eric, R., *Interaction of MgO-MgR_2O_4 (R: Al, Cr, Fe) refractories with SO_2-containing gases*. in *Southern African Pyrometallurgy*. Johannesburg 2011: p. 373-388.
23. Barthel, H., *Wear of chrome magnesite bricks in copper smelting furnaces.* Inter-Ceram, 1981. **30**: p. 250-255.
24. Gregurek, D. and Majcenovic, C., *Wear mechanisms of basic brick linings in the non ferrous metals industry – case studies from copper smelting furnaces.* RHI Bulletin, 2003(1): p. 17-21.
25. Guo, M., Parada, S., Smets, S., Jones, P., Van Dyck, J., Blanpain, B., and Wollants, P., *Laboratory study of the interaction mechanisms between magnesia-chromite refractories and Al_2O_3-rich VOD slags*. in *Proceedings of the VIIth International Conference on Molten Slags, Fluxes and Salts*. 2004: p. 327-336.

26. Guo, M., Jones, P.T., Parada, S., Boydens, E., Dyck, J.V., Blanpain, B., and Wollants, P., *Degradation mechanisms of magnesia-chromite refractories by high-alumina stainless steel slags under vacuum conditions.* Journal of the European Ceramic Society, 2006. **26**(16): p. 3831-3843.
27. Jung, I.-H., Decterov, S.A., and Pelton, A.D., *Critical thermodynamic evaluation and optimization of the Fe–Mg–O system.* Journal of Physics and Chemistry of Solids, 2004. **65**(10): p. 1683-1695.
28. Kaur, R.R., Swinbourne, D.R., Wadsley, M.W., and Nexhip, C., *Comparison of ferrous calcium silicate slag and calcium ferrite slag interactions with magnesia-chrome refractories.* Metallurgical and Materials Transactions B-Process Metallurgy and Materials Processing Science, 2011. **42**(3): p. 451-459.
29. Shchekina, T.I., Gramenitskii, E.N., Batanova, A.M., Alfer'eva, Y.O., Sokolov, A.A., Trofimenko, R.A., Pyrikov, A.N., Grigor'ev, B.N., Likhodievskii, A.V., and Us, T.N., *Phase formation processes and structural changes in chromite-periclase refractories used during nickel production.* Refractories and Industrial Ceramics, 2012. **52**(5): p. 363-376.
30. Tereshchenko, D.A., Platonov, A.A., Platonova, G.R., Chaika, E.F., and Maryasev, I.G., *General aspects of periclase-chromite refractory wear during nickel production.* Refractories and Industrial Ceramics, 2011. **52**(3): p. 212-215.
31. Fedorov, M.S., Ertseva, L.N., and Tsymbulov, L.B., *Corrosive interaction between slags high in copper and nickel oxides and periclase, periclase-chromite, and chromite refractories.* Refractories and Industrial Ceramics, 2005. **46**(5): p. 309-314.
32. Gramenitskii, E.N., Shchekina, T.I., Batanova, A.M., Likhodievskii, A.V., Grigor'ev, B.N., and Pyrikov, A.N., *Liquid-phase chemical interaction between chromite-periclase refractories and corrosive media in nickel matte converter technology.* Refractories and Industrial Ceramics, 2005. **46**(5): p. 301-308.
33. Petkov, V., Jones, P.T., Boydens, E., Blanpain, B., and Wollants, P., *Chemical corrosion mechanisms of magnesia-chromite and chrome-free refractory bricks by copper metal and anode slag.* Journal of the European Ceramic Society, 2007. **27**(6): p. 2433-2444.
34. Paranthaman, M., David, K.A., and Lindemer, T.B., *Phase equilibria of the MgO-Cu_2O-CuO system.* Materials Research Bulletin, 1997. **32**(2): p. 165-173.
35. Vorob'eva, K.V. and Perepelitsyn, V.A., *Service of magnesite-chromite refractories in copper-refining furnaces.* Refractories, 1966. **7**(7-8): p. 405-410.

36. Degterov, S., Pelton, A., Jak, E., and Hayes, P., *Experimental study of phase equilibria and thermodynamic optimization of the Fe-Zn-O system.* Metallurgical and Materials Transactions B, 2001. **32**(4): p. 643-657.
37. Gregurek, D., Majcenovic, C., Spanring, A., and Kirschen, M., *Forsterite bursting in magnesia chromite bricks - two case studies from lead and copper smelting furnaces.* RHI Bulletin, 2011(2): p. 49-53.

Chapter 3

Mitigating chemical wear

In this chapter methods to mitigate the chemical wear rate caused by liquid slag are discussed. The wear rate can be controlled by modifying either the slag or the brick composition. The different compositions used as refractory brick were discussed in the previous chapter. In this chapter strategies to limit the refractory degradation by modifying the slag composition are discussed. The effect of slag infiltration on the chemical wear is also discussed together with methods to limit the infiltration depth.

3.1 Viscosity of the slag

The viscosity of the slag system is a vital parameter controlling the lifetime of the refractory. Typically, lower viscosity systems lead to faster wear rates [1]. The lower viscosity makes it easier for the slag to infiltrate the lining, exposing a larger part of the lining to reaction with the aggressive slag. In the copper industry, for example, the use of calcium ferrite slags allows an easier copper production compared to the classic fayalite slag system but the low viscosity of the slag leads to a significant increase in the wear rate of the lining, limiting the industrial use of this type of slag system. As an alternative, a ferrous calcium silicate slag can be used, which due to its higher viscosity, is less aggressive to the refractory lining [2].

3.2 Changing the solubility of refractory components in the slag

The most straightforward method to limit the dissolution of refractory components is to add these components in the slag up to the saturation level of the components [3]. The problem with this approach is that saturation of the liquid is not always possible. For example, when there is no equilibrium between the liquid phase and the refractory phases without the formation of significant amounts of other solid phases. This would mean that saturating the slag with refractory components would result in a partially solid slag, which, for practical reasons, may not be usable in industry. Alternatively, the slag composition can be changed as this controls the solubility of the refractory components in the slag. Yan et al. [4], for example, studied the effect of the pO_2 and Cu_2O concentration on the MgO

solubility in a calcium ferrite slag in order to select conditions that minimize the solubility of MgO and would therefore lead to a longer refractory life.

For most slag systems, existing phase equilibria data can be used to determine the effect of changes in the slag composition on the solubility of the refractory components. The slag system used in this work, PbO-SiO_2-CaO-ZnO-Al_2O_3-Fe_2O_3, has been studied extensively to determine the equilibrium phase relations and their composition [5-9]. The solubility of refractory components has, however, not been studied for the entire system. The MgO solubility of the liquid phase has only been determined for subsystems of the used slag composition: FeO-Fe_2O_3-SiO_2-MgO [10, 11], CaO-Al_2O_3-MgO [12], SiO_2-Al_2O_3-MgO [12] and CaO-MgO-SiO_2 [13]. The only subsystem containing PbO that has been studied together with MgO is PbO-SiO_2-MgO studied by Chen et al. [14]. The experimentally obtained phase diagram is given in Figure 3.1.

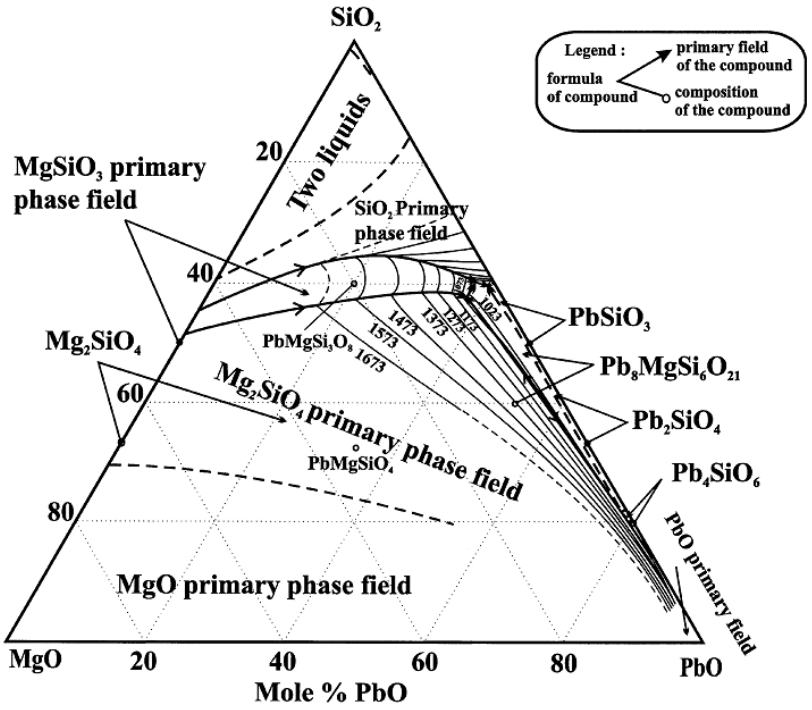

Figure 3.1: PbO-SiO_2-MgO phase diagram in air obtained using phase equilibria experimental data. Taken from [14].

Figure 3.2 gives a detailed view of the PbO-rich region of Figure 3.1. From the liquidus lines in Figure 3.2 it can be seen that the MgO solubility in the liquid decreases with decreasing SiO_2 content. The change in solubility is more pronounced at higher temperatures.

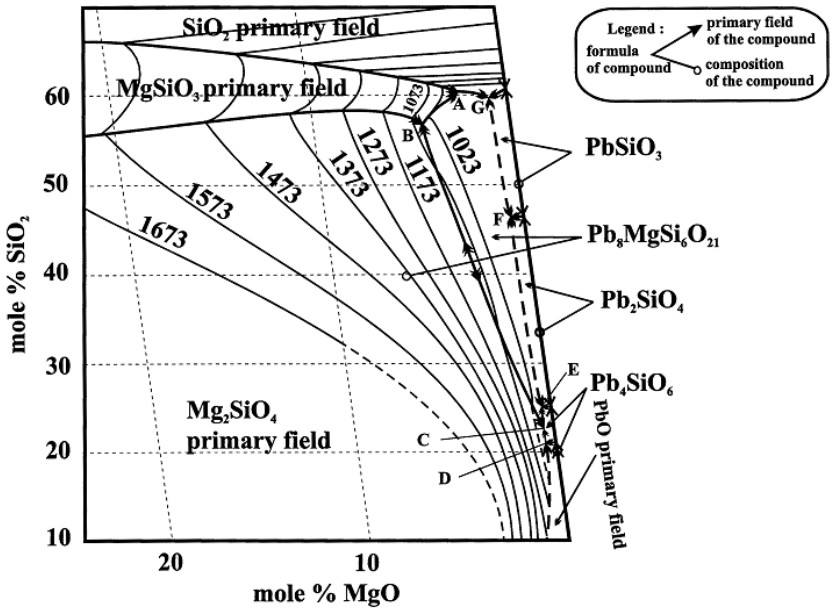

Figure 3.2: Lead rich region from the phase diagram shown in Figure 3.1. Taken from [14].

3.3 Direct-indirect dissolution

Besides the solubility of the refractory components into the liquid slag, the kinetics of the dissolution also control the lifetime of the lining. By forming a solid layer between the refractory phases and the liquid slag the dissolution rate of the former is lowered, leading to a longer lifetime of the lining. This is called indirect dissolution [1, 15]. The continuation of the dissolution process can only take place when the refractory components diffuse through the newly formed solid layer. A process that is significantly slower than the diffusion through the liquid slag, towards the unsaturated bath.

The formation of a new phase depends on the composition of the slag and the refractory brick. Not all newly formed phases, however, lead to a protective layer. Previous research [16, 17] has shown that the formation of a spinel layer between a MgO refractory brick and the liquid slag can significantly reduce the dissolution rate of MgO into the bath. Liu et al. [16] studied the dissolution of MgO particles in a CaO-Al_2O_3-SiO_2-MgO slag using a confocal scanning laser microscope (CSLM) making it possible to visualize the dissolution process at high temperature. The result of their measurements is shown in Figure 3.3. The dissolution causes a reduction in equivalent diameter of the MgO particle. A higher size reduction means a faster dissolution process. Both the solubility and the dissolution rate increase with increasing temperature. For the used slag composition in Figure 3.3, the dissolution is hindered by the formation of a continuous spinel layer between the MgO particle and liquid slag. The effect of this layer on the dissolution process is schematically shown in Figure 3.4. The dissolution of the MgO particle requires the solid state diffusion of MgO through the newly formed spinel layer, a process that is slower than the diffusion through the liquid slag phase.

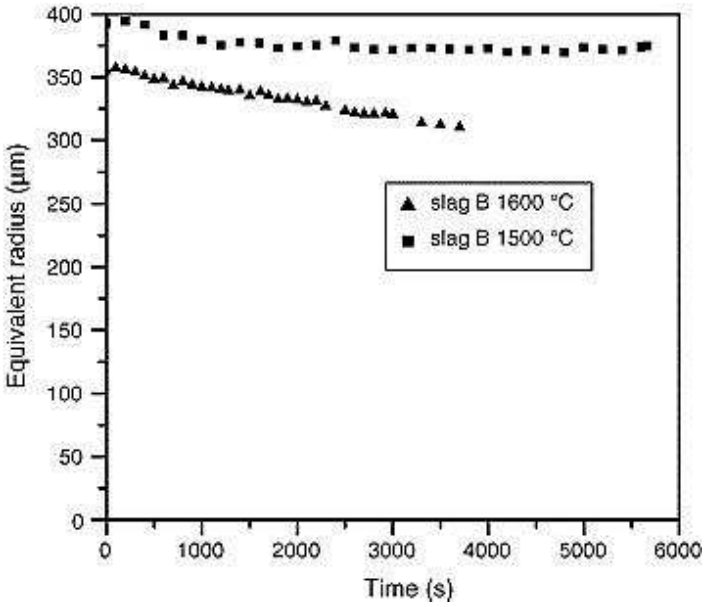

Figure 3.3: Equivalent diameter of a MgO particle in contact with a CaO-Al_2O_3-SiO_2-MgO slag as a function of time. The diameter was determined using a confocal scanning laser microscope, making it possible to determine the area at the experimental temperature during the dissolution of the MgO particle. Taken from [16].

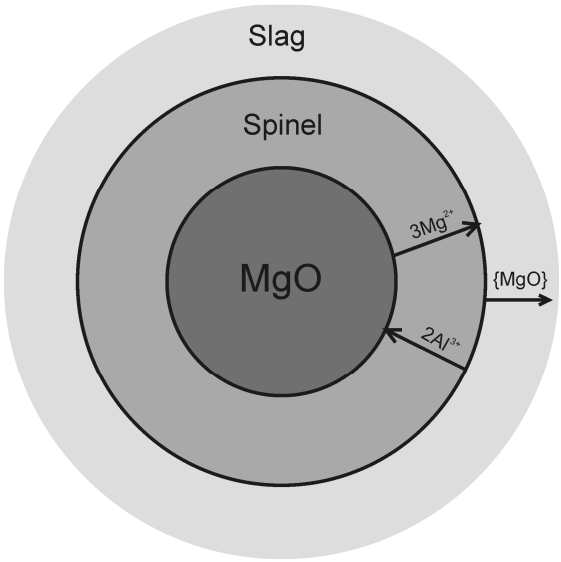

Figure 3.4: Reaction mechanism controlling the dissolution of a MgO particle in CaO-Al_2O_3-SiO_2-MgO slag. The dissolution is controlled by the diffusion of MgO through the newly formed $MgAl_2O_4$ spinel layer. Based on [16].

3.4 Infiltration

The contact between the liquid process phases and the porous refractory lining leads to infiltration into the bricks. In the following the infiltration behavior is discussed in more detail and methods to prevent or limit the infiltration of the liquids are discussed.

3.4.1 Fundamentals of infiltration

The infiltration of the liquid into the open pores of the refractory lining is caused by capillary pressure. In order to model the infiltration behavior of the liquid, the pores are considered to be cylindrical in shape with a constant diameter, as shown in Figure 3.5. Hagen–Poiseuille can be used to describe the infiltration behavior [1, 18]:

$$\frac{dl}{dt} = \frac{r^2 \Delta P}{8\eta l} \tag{3-1}$$

With *l* the infiltration depth, *r* the radius of the open pore, *η* the viscosity of the liquid, *t* the reaction time and *ΔP* the capillary pressure:

$$\Delta P = \frac{2\sigma \cos\theta}{r} \tag{3-2}$$

With σ the surface tension of the liquid slag and ϑ the contact angle between the liquid slag and the refractory. Combining both equations gives the following differential equation:

$$\frac{dl}{dt} = \frac{r\sigma \cos\theta}{4\eta l} \tag{3-3}$$

When the properties of the liquid remain constant during the infiltration equation 3-3 can be solved to:

$$l = \sqrt{\frac{r\sigma \cos\theta t}{2\eta}} \tag{3-4}$$

Based on this equation the infiltration depth increases with the square root of the reaction time.

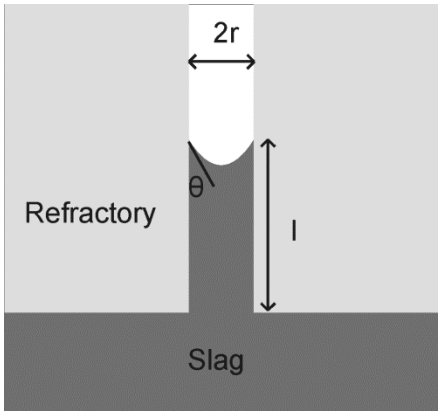

Figure 3.5: Schematic representation of liquid slag infiltration in the pore of a refractory sample. Based on [1, 18].

3.4.2 In-situ measurements

In-situ measurements of the infiltration behavior for a liquid slag have been performed by Mukai et al. [18] using an X-ray transmission device. The result for such a measurement is shown in Figure 3.6, where the slag is seen in black. The slag infiltrates upwards in the MgO refractory sample. The measurement as function of time showed that the infiltration depth initially increases with √t as predicted by equation 3-4. With time, however, the infiltration rate slows down. Mukai et al. explained this by a change in properties due to the changing slag composition during infiltration, which is explained in the next part of this chapter.

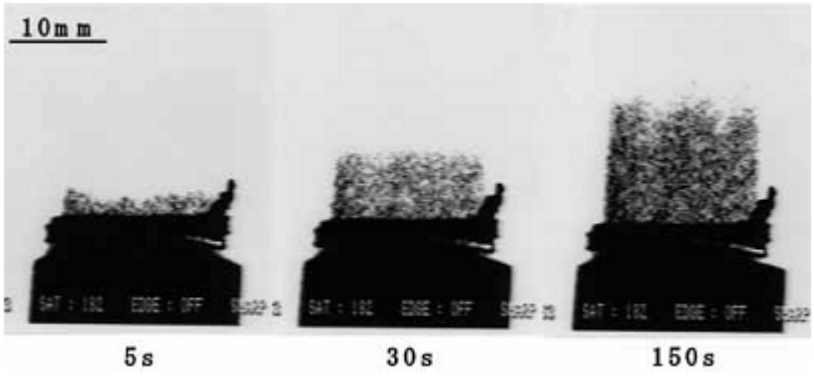

Figure 3.6: In-situ measurement of slag infiltration into a MgO refractory sample using an X-ray transmission device. Taken from [18].

3.4.3 Changes in slag composition

The chemical degradation of refractory bricks by liquid slag has been discussed in Chapter 2 , showing that the interaction can be classified into (1) dissolution of the refractory phases into the slag, (2) the formation of new solid phases and (3) the formation of a solid solution with the existing refractory phases. All of these interactions lead to a change in slag composition; the first by adding components to the slag while the latter two mechanisms selectively remove specific components from the liquid. When these reactions occur at the same time as the slag infiltration into the refractory brick, they lead to a slag composition which changes with position. For example, the composition of the SiO_2-FeO-CaO slag used in the in situ experiments in 3.4.2 changes due to the formation of an MgO-FeO solid solution during infiltration. The selective removal of FeO means that the SiO_2 content of the slag increases with infiltration depth, which in turn leads to a higher viscosity of the liquid, slowing down the infiltration. This effect causes the deviation from the theoretical √t increase of the infiltration depth for longer reaction times reported by Mukai et al. [18].

3.4.4 Predicting the slag changes

Thermodynamic calculations can be used to model the infiltration of liquid slag into the porous refractory lining and predict which phases are formed as well as their composition [19]. In order to do this Berjonneau et al. [20] defined a parameter (A) as:

$$A = \frac{R}{S+R} \tag{3-5}$$

with R the refractory amount and S the slag amount.

Figure 3.7 shows the change in the relative amount of slag and refractory phases when the reaction rate varies between 0 (only slag) and 1 (only refractory). By performing thermodynamic equilibrium calculations for different values of A between 0 and 1, the reaction in the bath and the porous brick is simulated. The result of such a calculation is given in Figure 3.8. At the hot face of the sample, a limited amount of refractory is in contact with a large amount of slag. The phase formation and slag composition at the hot face can thus be predicted using the low A results from Figure 3.8. The value of the slag composition at the formation of the first solid phase can be used to predict the slag composition at the hot face and determine which refractory components dissolve into the bath and to what extent. It also predicts which phase will form at the interface between

the slag and the refractory brick. Both of these insights are essential in order to modify the slag composition to slow down the dissolution process. For example, by adding refractory components to the bath composition and preventing the dissolution of the brick or by changing the slag composition to form a specific phase to form a protective layer at the interface of the brick.

For higher values of A, Figure 3.8 predicts the phase formation and slag composition inside the sample. This method, however, only takes the variation in porosity into account, as only the relative amount of slag and refractory is varied, assuming a higher porosity near the hot face due to previous (partial) dissolution of the refractory. It does not consider the selective removal of components from the liquid during infiltration, which, as discussed in section 3.4.3 of this chapter, is one of the dominant effects controlling the reactions inside a refractory sample.

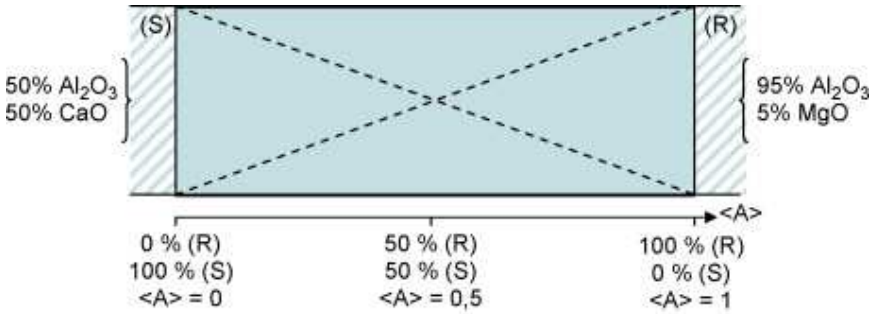

Figure 3.7: Schematic representation of the modeling method. The model uses thermodynamic equilibrium calculations between a synthetic slag and refractory sample varying the composition between both. The dotted lines indicate the decrease (increase) in the amount of slag (refractory). The effect on the parameter A is also shown. Taken from [20].

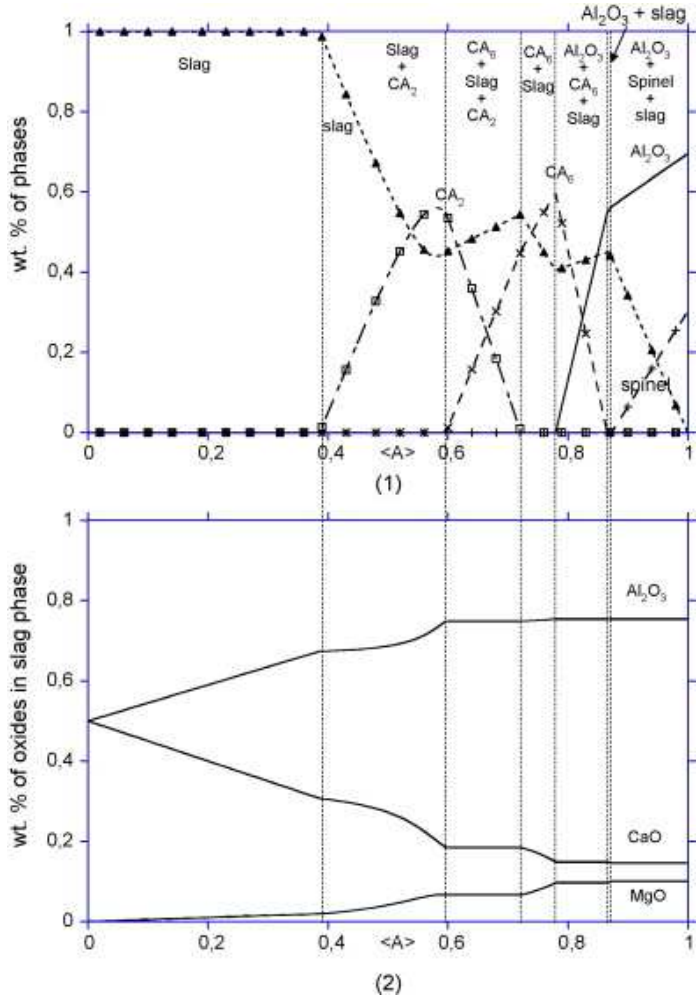

Figure 3.8: Results from the calculation method shown in Figure 3.7 between a synthetic slag with a composition of 50 wt% Al_2O_3 and 50 wt% CaO and a refractory with a composition of 95 wt% Al_2O_3 and 5 wt% MgO. The results indicate the phase fraction for different values of A as well as the composition of the liquid phase. Taken from [20].

In order to overcome this problem, a modified modelling method has been developed by Besmann [21] and Luz et al. [22], schematically shown in Figure 3.9. A series of thermodynamic equilibrium calculations is performed in which a limited amount of the average refractory composition is added to a large amount of slag. For the first calculation the bath composition is used but for each new calculation step the result of the slag composition from the previous calculation is used as a starting point. This method gives

the same results as the previous method when predicting the solubility in the slag and the formation of the first solid phase. The difference lies in the predictions inside the sample. Because the slag composition changes for each new calculation the selective removal of components can be taken into account.

The model predicts which components are dissolved or removed from the slag, to what extent and in which sequence this occurs. It is, however, unable to link a specific composition to a specific distance from the hot face. One of the main assumptions of the model is that the infiltration rate is sufficiently slow compared to the reaction rate to already allow some reaction, and thus change in slag composition, during the infiltration of the liquid. The validity of this assumption depends on the specific slag systems used and is not necessarily true for very fast infiltration of slags. A final limitation of the model is the assumption that the change in slag composition only occurs during the initial infiltration. The movement of the bath during the lining's lifetime can still lead to additional supply of new components by convection and inside the sample the difference in composition of the liquid over the sample can result in diffusion inside the pores. Both these effects result in a changing slag composition after infiltration and these effects are not taken into account in the model.

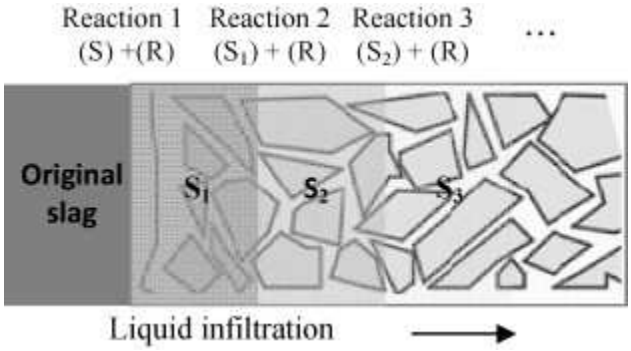

Figure 3.9: Modelling of slag infiltration taking into account the change of the slag composition. In each calculation the slag composition obtained from the previous equilibrium calculation is used. Taken from [22].

3.4.5 Methods to stop infiltration

The infiltration of liquid slag into the porous refractory lining has a significant effect on the degradation and, thus, on the lifetime of the reactor. By infiltration the reaction surface between the liquid slag and the refractory phases increases, leading to faster chemical corrosion of the lining. The reactions in the interior of the lining can also lead to new degradation mechanisms, limiting the lining's lifetime. For example, the formation of new phases can lead to a volume expansion and the internal stresses in turn can lead to spalling of a part of the lining [23]. Due to the detrimental effect of slag infiltration on the lifetime of the refractory lining several methods have been studied trying to stop the infiltration. An overview is given below.

Brick production

Already during the production process the infiltration behavior of the slag can be controlled. From equation 3-4 it is clear that the infiltration behavior depends on the size of the open pores and the contact angle between the slag and the refractory phases. Both can be controlled during the production process. By selecting the size distribution of the grains before firing, the open pore size can be controlled, leading to a limited infiltration behavior. The contact angle between the slag and the refractory phases differs for the chromite and periclase phases. During the production process, the amount of both phases can be modified to increase the amount of the phase limiting the infiltration of the liquid.

Even after the firing of the brick the pore size can still be reduced. Deng et al. [24] used vacuum impregnation of the open pores in magnesia-chromite bricks using Cr_2O_3 precursor sol and $MgCr_2O_4$ spinel precursor sol to reduce the median pore size diameter from 22.03 micron (untreated brick) to 14.75 micron (Cr_2O_3 precursor sol) and 13.31 micron ($MgCr_2O_4$ spinel precursor sol). The effect of the reduced pore size on infiltration of a copper convertor (fayalite type) slag was studied; the results are shown in Figure 3.10. The reduction in pore size clearly leads to a reduction in the slag penetration depth.

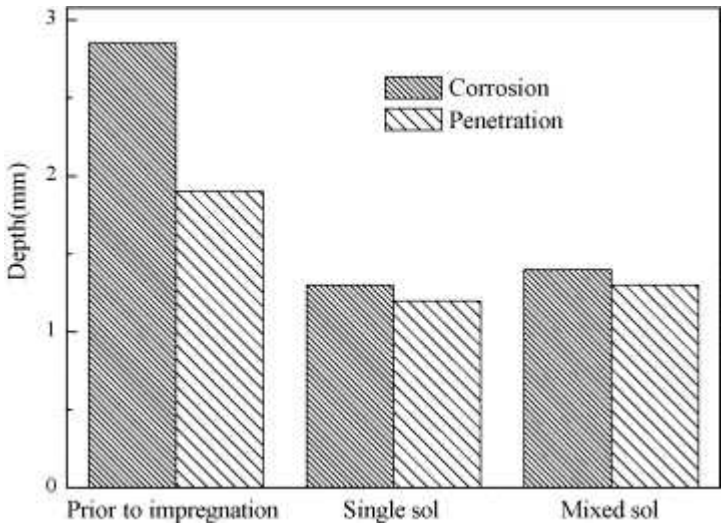

Figure 3.10: Effect of the impregnation of the open pores of a magnesia-chromite brick with Cr_2O_3 precursor sol (single sol) and $MgCr_2O_4$ spinel precursor sol (mixed sol) on the penetration by and chemical corrosion caused by a fayalite slag from a copper convertor after 3 h at 1600 °C. Taken from [24].

Pretreatment of the brick

The infiltration of the slag is only possible due to the open pores in the refractory bricks. Several authors [25, 26] have therefore tried to create a completely dense surface layer on the bricks, thereby keeping the beneficial properties of a porous refractory lining, while at the same time preventing the infiltration and chemical degradation in the refractory lining. In order to get this dense layer, the surface of the porous brick is melted using a laser, which, after solidification leads to the formation of dense layer. The large temperature difference between the top layer and the rest of the brick can, however, result in internal stresses and cracks [27, 28], leading to slag infiltration or spalling of the dense layer. In order to mitigate this effect Bradley et al. [29] have used the setup shown in Figure 3.11 which heats the surrounding of the melted part of the lining to prevent internal stresses resulting into a complete dense layer without cracks.

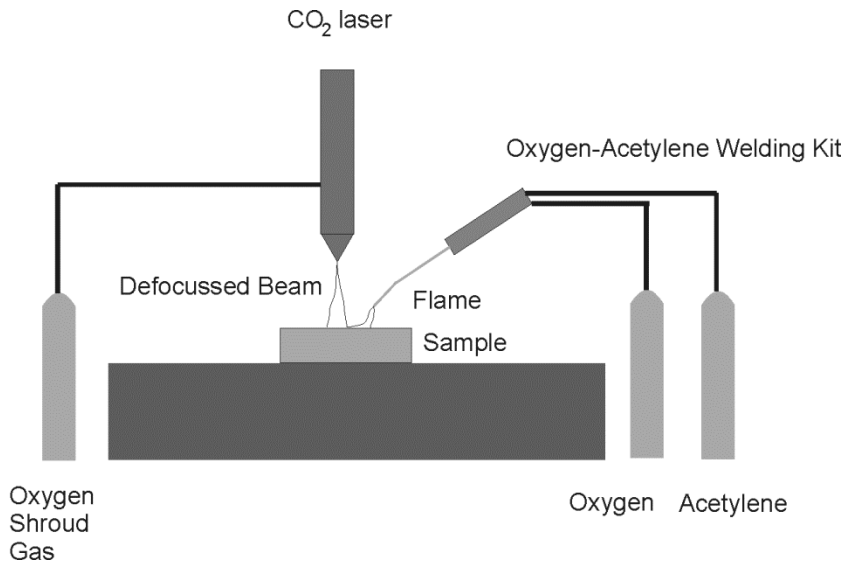

Figure 3.11: Schematic representation of the setup used to pretreat refractory bricks by melting the surface. Based on [29].

Reactions during the lifetime of the lining

The reaction between the slag and the refractory itself can limit or even stop the infiltration. As mentioned in section 3.4.3, the reaction during infiltration changes the slag composition inside the sample. This can lead to a change in slag properties like the viscosity or the liquidus temperature when specific components are removed from the infiltrating liquid. The system studied by Mukai et al. [18], for example, resulted in an increase in the SiO_2 content of the slag with infiltration depth. The resulting increase in viscosity slowed down any further infiltration while the increase of the liquidus temperature of the slag caused the slag to eventually freeze in the sample.

The formation of new phases can seal off the open pores and thus stop the infiltration of the liquid. A well-known mechanism in the steel industry [30], leading to the sealing of the open pores, occurs when MgO-C bricks are heated to the typical working temperature for the steel industry, usually 1700 °C. At this temperature the carbon reduces the MgO to form Mg and CO, both are gases at the working temperature. When this gas mixture exits the porous lining it can come into contact with a locally higher pO_2, either in the gas phase or in the slag. The reaction with oxygen again creates solid MgO, forming a layer at the hot face of the lining. When this layer seals the

interior of the brick from the surroundings, the reaction between MgO and C inside the lining reaches an equilibrium state, preventing further oxidation of carbon. If part of the layer fails, the gas will start to flow through it again, reforming the sealing layer at all holes, thus resulting in a self-healing mechanism.

The closing of the open pores can also be caused by the formation of new phases due to the reaction between slag and refractory, preventing further slag infiltration into the brick. Kaneko et al. [31] for example showed that the infiltration of a synthetic Al_2O_3-SiO_2-FeO-CaO-MgO-Na_2O-K_2O slag was hindered by the formation of a sealing $FeCr_2O_4$ layer on top of a Cr_2O_3-Al_2O_3 refractory brick formed by reaction between the refractory brick and the FeO from the liquid slag.

3.5 Conclusions

Modification of the slag composition can directly influence refractory wear by changing either the slag viscosity, the solubility of refractory components or the kinetics of the dissolution process. The first method unfortunately also influences the properties of the liquid bath, which has a direct influence on the production process. For the same reason the modification of the slag bath is undesirable if it results in the formation of significant amounts of solid phases. The most promising method is therefore the modification of the slag composition to form a protective layer at the bath refractory interface. In Chapter 4 this method is applied to a PbO-based slag.

The liquid slag infiltrates into the open pores of the refractory brick under the influence of capillary forces. This leads to an increase in the reaction surface between the slag and the refractory sample, accelerating the chemical corrosion. The reaction can also change the slag composition inside the sample due to reactions between the liquid and the refractory phases during the infiltration.

Several methods to slow down or prevent deep infiltration were discussed in this chapter. However, they have some limitations. The modification of the brick properties, like the pore size and the used phases, can change the infiltration behavior of the slag but only up to a point. For slag systems that fully infiltrate even the smallest pores, it is unlikely that changing the brick production process will lead to significant changes in the infiltration

behavior of the slag or the wear rate of the brick. Pretreatment of the brick to form a dense layer at the surface is an expensive alternative currently only applied to alumina-based refractories. Once (part of) the dense layer fails, the slag will be able to infiltrate into the porous part of the bricks and the infiltration will continue anyway.

The most promising approach is the use of reactions between the slag and the refractory sample. This would be self-healing as even after failure of part of the lining, the slag will just start reacting again when it infiltrates the newly exposed brick, leading to the same mechanisms that halted the infiltration in the first place.

Up to now this method has only been used for slag systems that infiltrate the pores relatively slowly, allowing adequate time for reaction, to form phases that seal off the lining or changes in slag composition that prevent further infiltration. Whether or not this approach can also be used for fast infiltrating slag systems still needs to be validated, which is discussed in Chapter 6 of this text.

References

1. Lee, W. and Zhang, S., *Melt corrosion of oxide and oxide–carbon refractories.* International Materials Reviews, 1999. **44**(3): p. 77-104.
2. Kaur, R.R., Swinbourne, D.R., Wadsley, M.W., and Nexhip, C., *Comparison of ferrous calcium silicate slag and calcium ferrite slag interactions with magnesia-chrome refractories.* Metallurgical and Materials Transactions B-Process Metallurgy and Materials Processing Science, 2011. **42**(3): p. 451-459.
3. Jansson, S., Brabie, V., and Bohlin, L., *Corrosion mechanism and kinetic behaviour of refractory materials in contact with CaO-Al_2O_3-MgO-SiO_2 slags*. in *VII International Conference on Molten Slags Fluxes and Salts. The Southern African Institute of Mining and Metallurgy, Johannesburg*. 2004: p. 341-347.
4. Yan, S., Sun, S., and Jahanshahi, S., *Reactions of dense MgO with calcium ferrite-based slags at 1573 K.* Metallurgical and Materials Transactions B-Process Metallurgy and Materials Processing Science, 2005. **36**(5): p. 651-656.
5. Jak, E., Degterov, S., Zhao, B., Pelton, A., and Hayes, P., *Coupled experimental and thermodynamic modelling study of the system PbO-ZnO-FeO-Fe_2O_3-CaO-SiO_2-Al_2O_3 for lead and zinc smelting*. in *Zinc and Lead Processing*. 1998: p. 313-333.
6. Jak, E. and Hayes, P.C., *The effect of the CaO/SiO_2 ratio on the phase equilibria in the ZnO-"Fe_2O_3"-(PbO+CaO+SiO_2) system in air: CaO/SiO_2=0.1, $PbO/(CaO+SiO_2)$=6.2, and CaO/SiO_2=0.6, $PbO/(CaO+SiO_2)$=4.3.* Metallurgical and Materials Transactions B-Process Metallurgy and Materials Processing Science, 2003. **34**(4): p. 369-382.
7. Jak, E. and Hayes, P.C., *Experimental study of phase equilibria in the PbO-ZnO-"Fe_2O_3"-CaO-SiO_2 system in air for high lead smelting slags (CaO/SiO_2=0.35 and $PbO/(CaO+SiO_2)$=5.0 by weight).* Metallurgical and Materials Transactions B-Process Metallurgy and Materials Processing Science, 2002. **33**(6): p. 817-825.
8. Jak, E. and Hayes, P.C., *Experimental liquidus in the PbO-ZnO-"Fe_2O_3"-(CaO+SiO_2) system in air, with CaO/SiO_2=0.35 and $PbO/(CaO+SiO_2)$=3.2.* Metallurgical and Materials Transactions B-

Process Metallurgy and Materials Processing Science, 2002. **33**(6): p. 851-863.

9. Jak, E., Hayes, P.C., Degterov, S., Pelton, A.D., and Wu, P., *Thermodynamic optimization of the systems PbO-SiO_2, PbO-ZnO, ZnO-SiO_2 and PbO-ZnO-SiO_2.* Metallurgical and Materials Transactions B, 1997. **28**(6): p. 1011-1018.
10. Decterov, S.A., Jung, I.H., and Pelton, A.D., *Thermodynamic modeling of the FeO–Fe_2O_3–MgO–SiO_2 system.* Journal of the American Ceramic Society, 2002. **85**(12): p. 2903-2910.
11. Jung, I.-H., Decterov, S., and Pelton, A., *Critical thermodynamic evaluation and optimization of the FeO-Fe_2O_3-MgO-SiO_2 system.* Metallurgical and Materials Transactions B, 2004. **35**(5): p. 877-889.
12. Jung, I.-H., Decterov, S., and Pelton, A., *Critical thermodynamic evaluation and optimization of the MgO-Al_2O_3, CaO-MgO-Al_2O_3, and MgO-Al_2O_3-SiO_2 Systems.* Journal of Phase Equilibria and Diffusion, 2004. **25**(4): p. 329-345.
13. Huang, W., Hillert, M., and Wang, X., *Thermodynamic assessment of the CaO-MgO-SiO_2 system.* Metallurgical and Materials Transactions A, 1995. **26**(9): p. 2293-2310.
14. Chen, S., Zhao, B., Jak, E., and Hayes, P.C., *Experimental study of phase equilibria in the PbO-MgO-SiO_2 system.* Metallurgical and Materials Transactions B-Process Metallurgy and Materials Processing Science, 2001. **32**(1): p. 11-16.
15. Lee, W.E. and Zhang, S., *Direct and indirect slag corrosion of oxide and oxide-C refractories*. in *VII International Conference on Molten Slags Fluxes and Salts*. Cape Town, South Africa 2004: p. 309-320.
16. Liu, J., Guo, M., Jones, P.T., Verhaeghe, F., Blanpain, B., and Wollants, P., *In situ observation of the direct and indirect dissolution of MgO particles in CaO-Al_2O_3-SiO_2-based slags.* Journal of the European Ceramic Society, 2007. **27**(4): p. 1961-1972.
17. Nightingale, S.A., Monaghan, B.J., and Brooks, G.A., *Degradation of MgO refractory in CaO-SiO_2-MgO-FeO_x and CaO-SiO_2-Al_2O_3-MgO-FeO_x slags under forced convection.* Metallurgical and Materials Transactions B, 2005. **36**(4): p. 453-461.
18. Mukai, K., Tao, Z., Goto, K., Li, Z., and Takashima, T., *In-situ observation of slag penetration into MgO refractory.* Scandinavian Journal of Metallurgy, 2002. **31**(1): p. 68-78.
19. Lee, W.E., Argent, B.B., and Zhang, S.W., *Complex phase equilibria in refractories design and use.* Journal of the American Ceramic Society, 2002. **85**(12): p. 2911-2918.
20. Berjonneau, J., Prigent, P., and Poirier, J., *The development of a thermodynamic model for Al_2O_3–MgO refractory castable corrosion*

by secondary metallurgy steel ladle slags. Ceramics International, 2009. **35**(2): p. 623-635.

21. Besmann, T.M., *Thermochemical modeling of refractory corrosion in slagging coal gasifiers.* Calphad, 2008. **32**(3): p. 466-469.
22. Luz, A.P., Martinez, A.G.T., Braulio, M.A.L., and Pandolfelli, V.C., *Thermodynamic evaluation of spinel containing refractory castables corrosion by secondary metallurgy slag.* Ceramics International, 2011. **37**(4): p. 1191-1201.
23. Petkov, V., Jones, P.T., and Blanpain, B., *Optimisation of an anode furnace refractory lining using distinct magnesia-chromite refractory types.* World of Metallurgy 2007. **60**(4): p. 255-264.
24. Deng, Y.Y., Wang, H.Z., and Zhao, H.Z., *Influence of chrome-bearing sols vacuum impregnation on the properties of magnesia-chrome refractory.* Ceramics International, 2008. **34**(3): p. 573-580.
25. Lawrence, J. and Li, L., *Surface treatment of an Al_2O_3-based refractory with CO_2 and high power diode lasers for improved mechanical and chemical resistance characteristics.* Surface and Coatings Technology, 2003. **162**(1): p. 93-100.
26. Bradley, L., Li, L., and Stott, F.H., *Surface modification of alumina-based refractories using a xenon arc lamp.* Applied Surface Science, 2000. **154–155**: p. 675-681.
27. Li, J.F., Li, L., and Stott, F.H., *Thermal stresses and their implication on cracking during laser melting of ceramic materials.* Acta Materialia, 2004. **52**(14): p. 4385-4398.
28. Triantafyllidis, D., Li, L., and Stott, F.H., *Surface treatment of alumina-based ceramics using combined laser sources.* Applied Surface Science, 2002. **186**(1–4): p. 140-144.
29. Bradley, L., Li, L., and Stott, F., *Flame-assisted laser surface treatment of refractory materials for crack-free densification.* Materials Science and Engineering: A, 2000. **278**(1): p. 204-212.
30. Watanabe, A., Takahashi, H., and Nakatani, F., *Mechanism of dense magnesia layer formation near the surface of magnesia-carbon brick.* Journal of the American Ceramic Society, 1986. **69**(9): p. C-213-C-214.
31. Kaneko, T.K., Thomas, H., Bennett, J.P., and Sridhar, S., *Synthetic coal slag infiltration into varying refractory materials.* Journal of the American Ceramic Society, 2012. **95**(10): p. 3325-3333.

Chapter 4 Slag engineering for PbO slags

4.1 Introduction

The literature review in Chapter 2 showed that chemical degradation by liquid slag is one of the main causes of refractory wear. One of the mechanisms of chemical wear is dissolution of refractory components in the liquid slag bath. This is most severe at the hot face of the samples, where the brick is constantly in contact with unsaturated slag due to the movement of the bath. The first goal of this chapter is to determine the chemical degradation mechanisms of a magnesia-chromite brick when it is in contact with a PbO-containing slag.

The second goal of this chapter is to determine if the slag composition can be modified to slow down the dissolution at the hot face as suggested in Chapter 3 . A spinel-saturated slag will be used to determine if this will lead to the formation of a sealing layer at the hot face. Finally, the effect of a protective layer on the degradation that occurs will be determined.

These goals are achieved by comparing the degradation for refractory samples in contact with two different slags: one leading to contact between the liquid slag and the refractory phases and the second resulting in the formation of a protective layer. To get the best possible insights into the reaction between the slag and the refractory sample, the interaction is tested on lab scale using synthetic systems allowing optimal control of the conditions during the experiment.

4.2 Materials and methods

Lab scale experiments with two different slags are performed. The selection of the used slag composition in each experiment is made using Figure 4.1. It gives the results of thermodynamic calculations, using FactSage 6.4 and its FTOxid database, by varying the ratio of Fe_2O_3 and ZnO for fixed concentrations of PbO, SiO_2, CaO and Al_2O_3. The first slag composition is selected without the addition of Fe_2O_3 to the system. This composition is completely liquid at the experimental temperature. The second slag is selected to ensure the formation of a solid $(Zn,Fe)(Fe,Al)_2O_4$ spinel phase together with the liquid phase, making it possible to determine if the

presence of this spinel phase leads to the formation of a protective spinel layer at the hot face of the refractory sample. The experiments are performed in an alumina crucible. The first slag shown in Figure 4.1, however, still has a high solubility of Al_2O_3. Al_2O_3 is therefore added to this slag to limit the crucible dissolution, while still staying in the fully liquid region. The used slag compositions are given in Table 4.1.

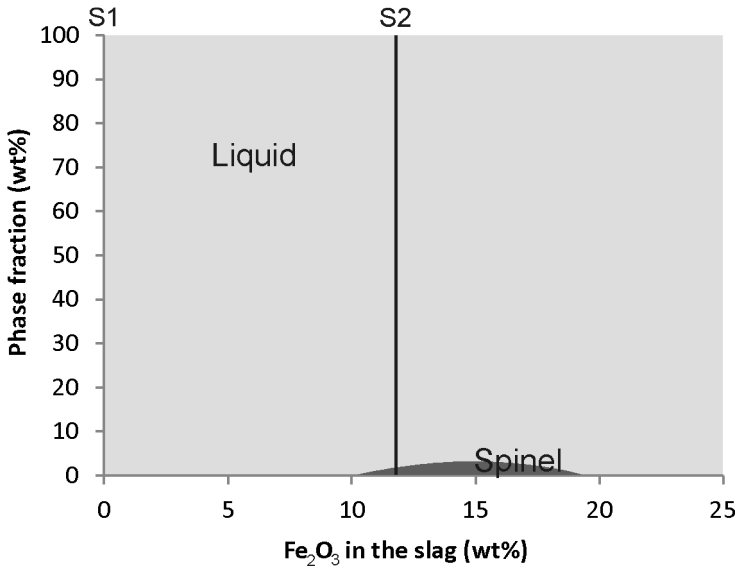

Figure 4.1: Equilibrium phase composition at 1300 °C and pO2=0.21 atm for a slag with 58.2 wt% PbO, 14.6 SiO_2, 0.9 wt% CaO and 2.9 wt% Al_2O_3. The remaining 23.4 wt% is the combination of Fe_2O_3 and ZnO. The amount of Fe_2O_3 is varied between 0 and 23.4 wt% while ZnO shows the opposite trend (from 23.4 to 0 wt%).

Table 4.1: Composition of the bulk slag (wt%).

Slag	PbO	SiO_2	CaO	ZnO	Fe_2O_3	Al_2O_3
S1	55.2	13.8	0.9	22.1	0.0	8.0
S2	58.2	14.6	0.9	11.7	11.7	2.9

The experimental setup used during the experiments is schematically shown in Figure 4.2. Firstly, different pure oxide powders are mixed in the desired ratio shown in Table 4.1. The mixture with a total weight of 1.5 kg is then added to a 1 liter alumina crucible and heated in an induction furnace at a rate of 600 °C/hour to 1300 °C. The refractory sample is heated in the same furnace with the alumina crucible but is only submerged when the slag has reached the desired experimental temperature. After 3 hour reaction time, the refractory sample is removed from the furnace and quenched in water to preserve the microstructure and the composition of the different phases.

After the experiment the sample is cut using a diamond saw. The position of the cut is shown in Figure 5.1. The sample was ground using SiC and polished. After polishing, the microstructure of the sample is analyzed using a fully quantitative electron probe micro-analyzer with a wavelength-dispersive spectroscopy (EPMA-WDS, JEOL JXA-8530F) system operated using an acceleration voltage of 15 kV and a probe current of 15 nA. The following standards were used for the measurements: pyrope, fluorite, periclase, willemite, galena, chromium oxide and haematite.

4.3 Results

An overview of the bath-refractory interface for both slag systems is shown in Figure 4.2 and Figure 4.3. Both show the presence of the same phases: the fused grain from the refractory sample, the liquid from the bath and solid spinel phases present in the liquid bath. To understand the difference in reaction caused by both slags, and thus the degradation mechanisms leading to failure, detailed images of the microstructure for each phase in the microstructure are analyzed and discussed below.

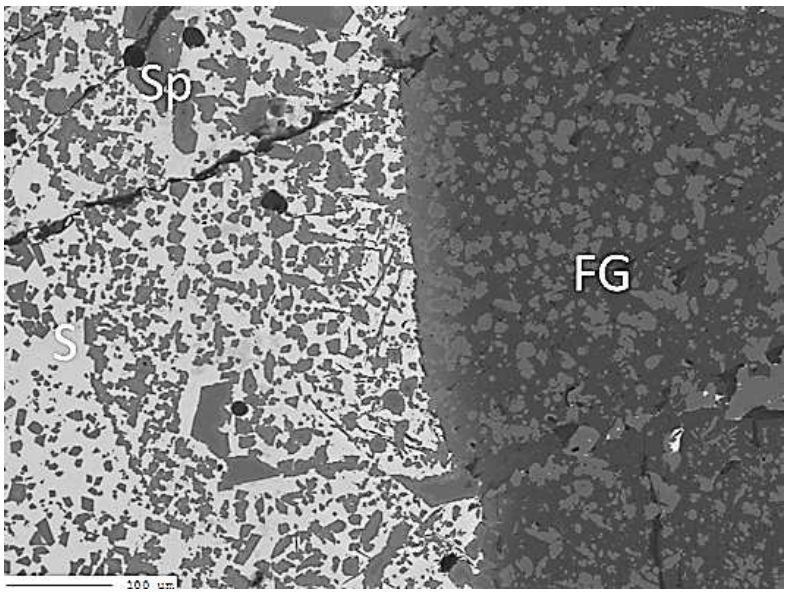

Figure 4.2: SEM-BSE image of the hot face of the refractory sample after 3h reaction time with the S1 slag. With S: slag, Sp: spinel and FG: fused grain.

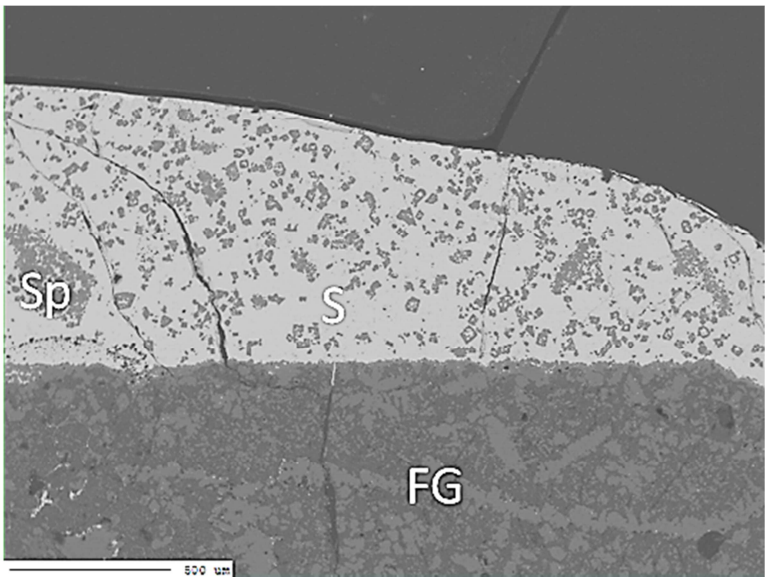

Figure 4.3: SEM-BSE image of the hot face of the refractory sample after 3h reaction time with the S2 slag. With S: slag, Sp: spinel and FG: fused grain.

4.3.1 Slag S1

The slag composition S1 was selected to ensure a contact between a fully liquid slag and the refractory sample. As no Fe_2O_3 is added to this slag, insufficient trivalent cations are present to form a protective spinel layer at the interface with the refractory sample. A BSE (backscattered electrons) image of the microstructure of the sample after the experiment is shown in Figure 4.2. The bath is investigated in more detail in Figure 4.4, showing that it consists of an amorphous phase which was most likely liquid during the experiment and several spinel particles in this liquid. The composition of these phases is analyzed using a linescan where the chemical composition is determined every micrometer along a line, starting in the liquid phase and going over the spinel particle. The results are shown in Figure 4.5. The chemical composition of the rim of the spinel particle differs from the center. The center of the particle has the same chemical composition as a secondary chromite particle from the fused grain. The rim, on the other hand, has a composition enriched in Al_2O_3 and also contains ZnO as a new component. The ZnO appears deeper in the spinel particle than the Al_2O_3 enrichment.

The interface between the bath and the refractory sample, called the hot face, is studied for both of the main phases present in the sample: fused grain and primary chromite grains. Figure 4.6 shows the interface between the bath and the fused grain. The line scan in Figure 4.7 shows the diffusion of ZnO from the slag into the periclase of the fused grain. Also the secondary chromite present in the fused grains is measured in the linescan and contains ZnO.

The last phase analyzed for this sample is a primary chromite grain at the hot face. The microstructure is shown in Figure 4.8, while the chemical composition as a function of position is shown in Figure 4.9. As for the spinel particles present in the bath, the spinel composition again differs for the center and the rim in the primary chromite. The rim is enriched in Al_2O_3 and contains ZnO as a new component. The ZnO also diffuses deeper into the chromite spinel than the Al_2O_3 enrichment.

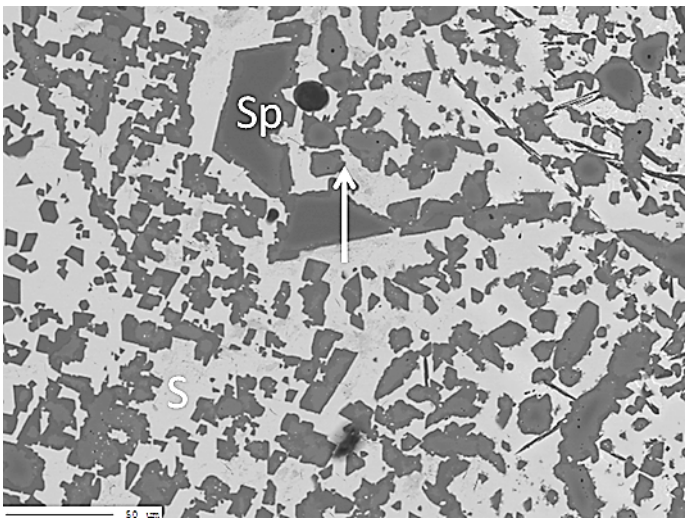

Figure 4.4: Detailed SEM-BSE image of the microstructure of the bath after reaction with slag S1, showing the spinel phases (Sp) in a glass phase which was liquid slag (S) at high temperature. The arrow indicates the position of a linescan, measuring the chemical composition over the different phases.

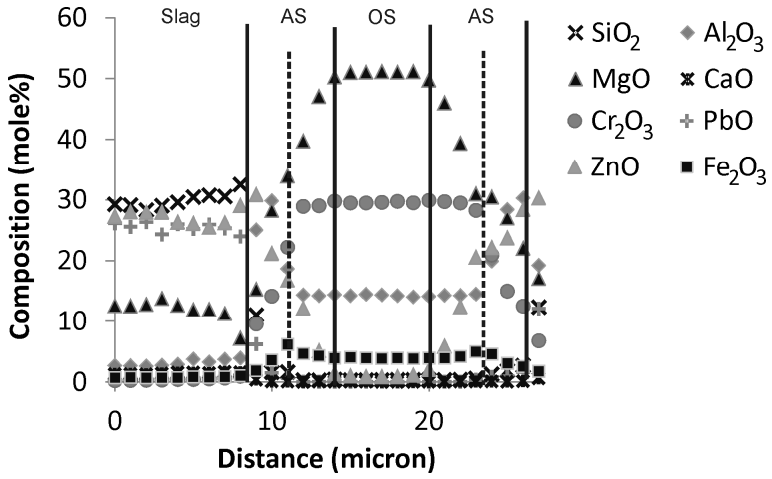

Figure 4.5: Chemical composition along the arrow indicated in Figure 4.4. The full lines indicate the transition between the different phases: slag, the original spinel structure (OS) and the attacked part of the spinel (AS). The dotted line givens the transition between the attacked part of the spinel enriched in Al_2O_3 and the part having the same Al_2O_3 content as the original spinel.

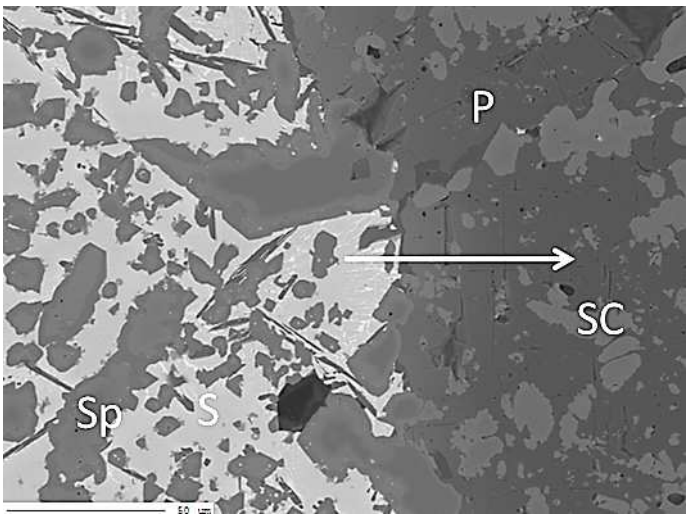

Figure 4.6: Detailed SEM-BSE image of the microstructure at the interface between the bath and a fused grain from the refractory sample after reaction with slag S1, showing the spinel phases (Sp) in a glass phase which was liquid slag (S) at high temperature and the fused grain consisting of periclase (P) and secondary chromite (SC). The arrow indicates the position of a linescan, measuring the chemical composition over the different phases.

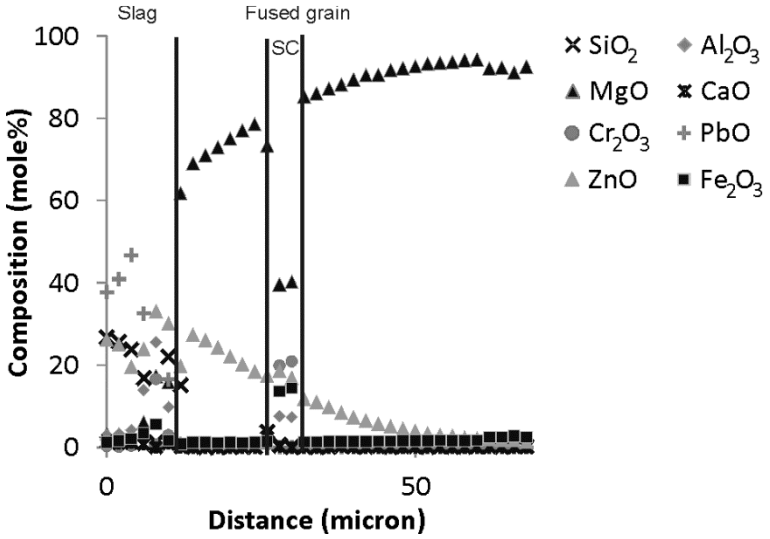

Figure 4.7: Chemical composition along the arrow indicated in Figure 4.6. The full lines indicate the transition between the different phases. The linescan also measures a secondary chromite particle (SC).

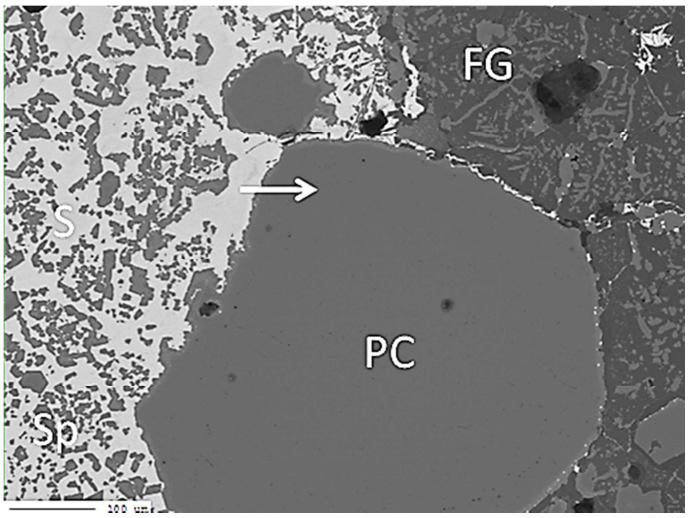

Figure 4.8: Detailed SEM-BSE image of the microstructure at the interface between the bath and a primary chromite spinel from the refractory sample after reaction with slag S1, showing the spinel phases (Sp) in a glass phase which was liquid slag (S) at high temperature and the fused grain (FG) and primary chromite (PC) of the refractory. The arrow indicates the position of a linescan, measuring the chemical composition over the different phases.

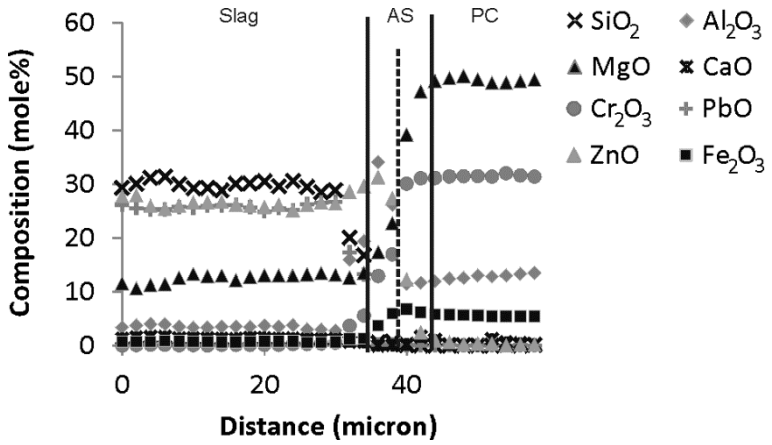

Figure 4.9: Chemical composition along the arrow indicated in Figure 4.8. The full lines indicate the transition between the different phases: slag, the original primary chromite spinel (PC) and the attacked part of the spinel (AS). The dotted line givens the transition between the attacked part of the spinel enriched in Al_2O_3 and the part having the same Al_2O_3 content as the primary chromite.

4.3.2 Slag S2

Slag S2 has been saturated in spinel components to determine if this will lead to the formation of a protective spinel layer at the hot face of the sample. The microstructure after reaction for the slag S2 is given in Figure 4.3. It shows the same phases as for the first slag (Figure 4.2): the fused grain for the refractory sample, an amorphous phase which was liquid at high temperature and the spinel particles in the liquid phase. The difference with the first slag is the formation of a spinel layer between the bath and the refractory sample. The same analyses as for the first slag are performed: a detailed view of the microstructure and chemical composition of the different phases.

Figure 4.10 shows a detailed view of the microstructure of the bath. A linescan of the chemical variation over the spinel particle in the bath shows that the spinel particle has a very homogeneous composition, consisting mostly out of ZnO, Al_2O_3 and Fe_2O_3.

At the interface between the fused grain and the liquid bath, Figure 4.12 shows the formation of a solid spinel layer on top of the fused grain. The chemical composition over this layer, shown in Figure 4.13, shows that the composition of this spinel phase is similar to that of the spinel particles in the bath. The main difference between both is the diffusion profile in MgO over the spinel layer, going down the periclase of the refractory sample to the liquid bath. ZnO also shows a diffusion profile but has the opposite trend as the MgO.

The interaction between a primary chromite grain and the slag S2 is shown in Figure 4.14 and Figure 4.15. The rim of the chromite spinel has a different composition than its center. Specifically the presence of ZnO and enrichment in Fe_2O_3 are noted.

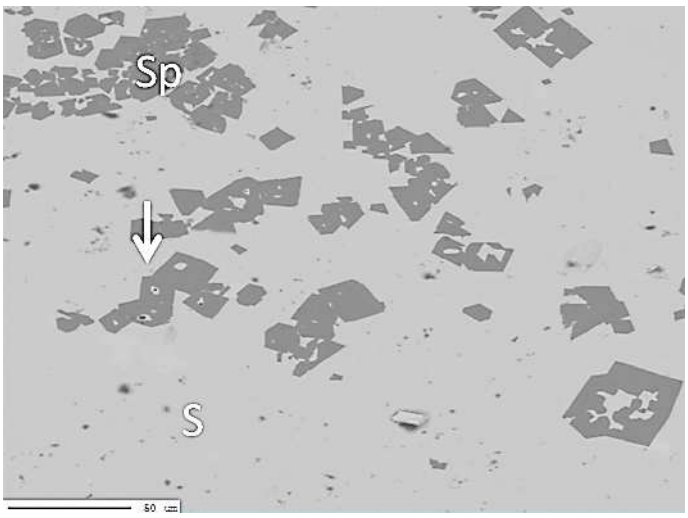

Figure 4.10: Detailed SEM-BSE image of the microstructure of the bath of slag S2, showing the spinel phases (Sp) in a glass phase which was liquid slag (S) at high temperature. The arrow indicates the position of a linescan, measuring the chemical composition over the different phases.

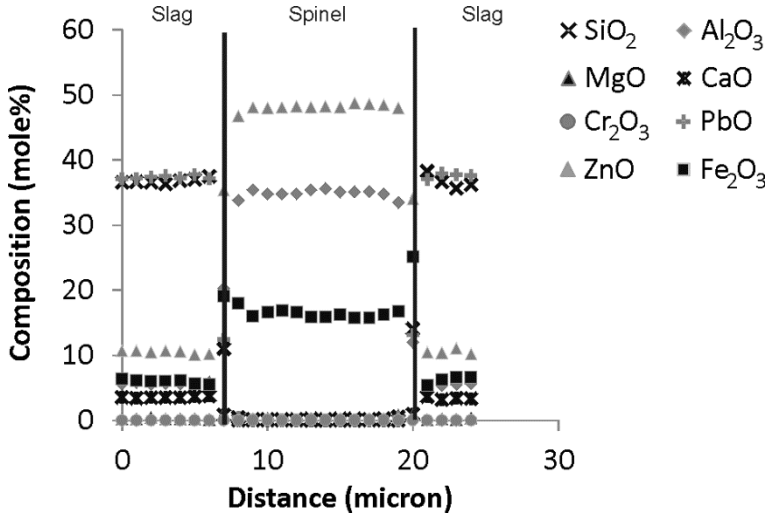

Figure 4.11: Chemical composition along the arrow indicated in Figure 4.10. The lines indicate the transition between the different phases: slag and spinel.

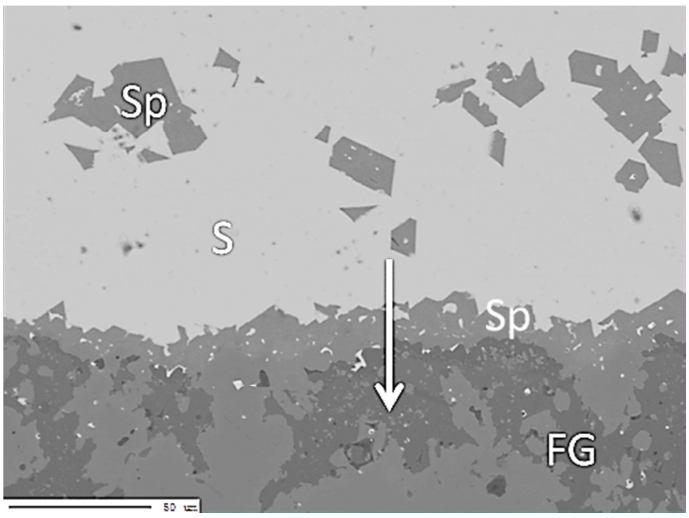

Figure 4.12: Detailed SEM-BSE image of the microstructure at the interface between the bath and a fused grain from the refractory sample after reaction with slag S2, showing the spinel phases (Sp) in a glass phase which was liquid slag (S) at high temperature and the fused grain. The arrow indicates the position of a linescan, measuring the chemical composition over the different phases.

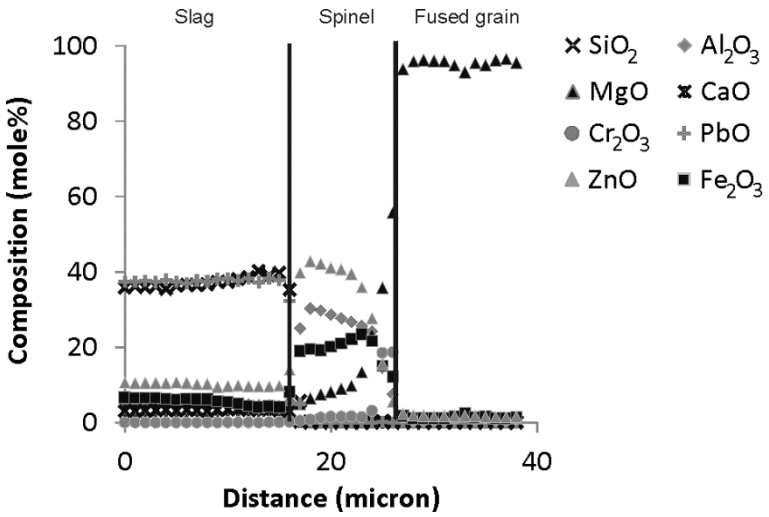

Figure 4.13: Chemical composition along the arrow indicated in Figure 4.12. The lines indicate the transition between the different phases: slag, spinel and fused grain.

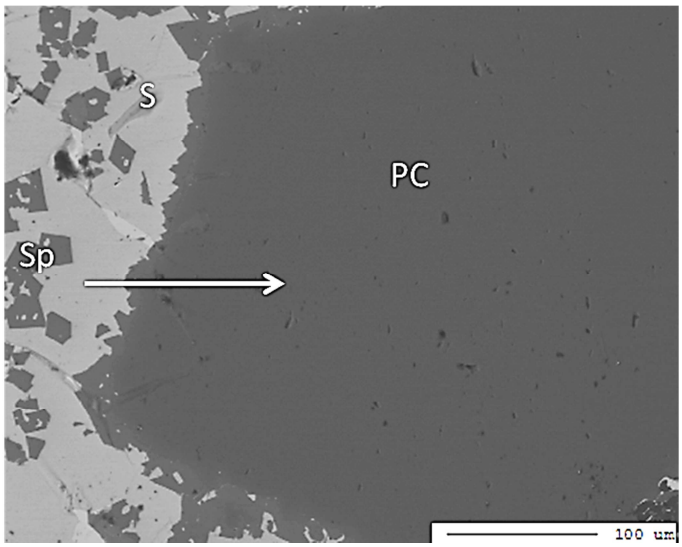

Figure 4.14: Detailed SEM-BSE image of the microstructure at the interface between the bath and a primary chromite spinel from the refractory sample after reaction with slag S2, showing the spinel phases (Sp) in a glass phase which was liquid slag (S) at high temperature and a primary chromite (PC) grain of the refractory. The arrow indicates the position of a linescan, measuring the chemical composition over the different phases.

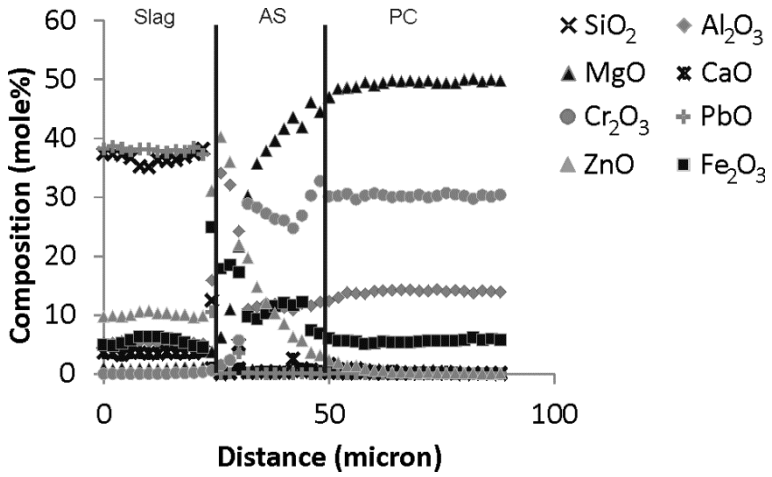

Figure 4.15: Chemical composition along the arrow indicated in Figure 4.14. The lines indicate the transition between the different phases: slag, the original primary chromite spinel (PC) and the attacked part of the spinel (AS).

4.4 Discussion

The degradation of the refractory in contact with slag S1 is primarily caused by dissolution of MgO from the refractory into the liquid bath. The result is that the periclase matrix of the fused grains disappears. The secondary chromite spinel particles, that are originally present inside the periclase, now come into contact with the bath, where they start to react with the liquid slag. The result of this reaction is formation of the spinel rim with a different composition as shown in Figure 4.5. The enrichment in Al_2O_3 and ZnO is due to the following reaction:

$$Al_2O_{3,slag}+ZnO_{slag}+Mg[Cr,Al,Fe]_2O_{4refractory} \rightarrow [Zn,Mg][Al,Cr,Fe]_2O_4 \quad (4.1)$$

The ZnO is found deeper inside the secondary spinel phase than the Al_2O_3 enrichment and is most likely caused by the fact that ZnO can diffuse through the periclase matrix (as seen in Figure 4.7), already leading to some ZnO presence in the spinel before it comes into contact with the bath.

Although the slag S2 also has spinel particles inside the liquid at the hot face of the sample, it is in this case not an indication of MgO dissolution. The spinel phases have a different composition than the secondary spinel grains. Most noteworthy is the lack of chromium in these phases as this also is not detected in the liquid it is unlikely that these spinel grains are reacted secondary chromite spinel particles. They are an equilibrium phase formed in the slag. This is further supported by the homogeneous composition of these phases and the predicted presence of spinel phases according to Figure 4.1.

Because the slag is spinel saturated, the addition of components forming this phase, in this case MgO dissolving from the refractory sample, will result in the formation of new spinel particles. This is the reason that the slag leads to the formation of a complete sealing layer at the interface between the refractory sample and the liquid bath. The presence of this protective spinel layer completely changes the dissolution mechanisms for MgO. As seen in Figure 4.13 the MgO has to diffuse through the spinel layer before it can dissolve into the liquid bath. The result is a much slower chemical degradation for the second slag compared to the first slag. This is further supported by the difference in MgO content of the slag. Slag S1 contains 12 mole % MgO after reaction while slag S2 contains less than 1 mole % MgO.

4.5 Conclusion

This chapter shows that for PbO-containing slag systems it is possible to reduce the chemical wear rate by the modification of the slag composition. The saturation of the slag in spinel components results in the formation of a protective layer between the refractory sample and the slag bath at the hot face. This layer slows down the MgO dissolution from the refractory sample in the liquid bath, which was identified as the main chemical degradation mechanism when the slag is in direct contact with the refractory. Because the MgO has to diffuse through the protective spinel layer the wear rate decreases, leading to a longer refractory lifetime.

Chapter 5 The influence of slag compositional changes on the chemical degradation of magnesia-chromite refractories exposed to PbO-based non-ferrous slag saturated in spinel

L. Scheunis[1], M. Campforts[2], P.T. Jones[1], B. Blanpain[1] and A. Malfliet[1]

Journal of the European Ceramic Society, 35(1), 347-355, 2015

[1]Department of Materials Engineering, KU Leuven, Kasteelpark Arenberg 44, BE-3001 Leuven, Belgium

[2]Research & Development, Umicore, Watertorenstraat 33, BE-2250 Olen, Belgium

DOI: 10.1016/j.jeurceramsoc.2014.08.017

Contribution Lennart Scheunis: Lennart Scheunis performed the experiments, analyzed the samples, interpreted the results and wrote the paper. The contribution of the co-authors consisted in discussion of the results and reviewing of the paper before final publication.

Abstract

In non-ferrous metallurgy the refractory life is application dependent, typically going from several months up to 2 years or more. Slag engineering is widely used to reduce the dissolution rate of a refractory lining by forming a solid protection layer at the slag-lining interface, thereby increasing the lining's lifetime. The non-ferrous slag in this paper is engineered to form a protective spinel layer. This phase, however, only forms near and at the slag-lining interface, while deeper inside the sample forsterite grains are detected, resulting in direct contact between the still unsaturated slag and the magnesia-chromite refractory phases. At this position the MgO dissolution increases by a factor 3-4 compared with the slag-refractory interface, attacking the bonding between grains and decreasing the brick's mechanical strength. As this happens deeper inside the sample, the spalling risk increases. Strategies to simultaneously reduce refractory dissolution and spalling are discussed.

5.1 Introduction

Ceramic magnesia-chromite refractory bricks are commonly used in non-ferrous smelting furnace linings because of their high melting point, good mechanical properties at elevated temperatures and their ability to withstand aggressive conditions [1-10]. Despite these properties, lining wear still occurs due to the combination of chemical, mechanical and thermal stresses, eventually requiring a replacement of the lining. Slag engineering is a common method used in industry to decrease the chemical degradation rate and thus to prolong the lining lifetime [4]. Two methods are typically used: (1) the bath composition can be saturated in the refractory components [11] or (2) the composition of the bath can be chosen to ensure the formation of a protective layer after reaction with the lining [12]. The first method reduces the thermodynamic driving force for dissolution, while the second creates a kinetic barrier for the dissolution as the refractory components have to diffuse through this newly formed solid layer.

In this paper the second approach is studied, focusing on how the formation of these protective phases, and thus the refractory dissolution, changes along the depth of a porous lining that has been infiltrated with liquid slag. Porous linings are widely used in pyrometallurgical reactors, especially batch processes as they are subjected to large changes in operating temperatures, to ensure that the lining is able to withstand the

thermal and mechanical loads. This, however, comes at the cost of an accelerated chemical degradation, as the slag can infiltrate the porous brick, reacting with a larger part of the lining. The extent of the infiltration depends on the viscosity and wetting behavior of the slag system, and thus, for a given operating temperature, on its composition. PbO based, non-ferrous slag systems, for example, are known to easily and deeply infiltrate the refractory lining [13]. Other components are added to this slag to ensure the formation of new phases: alumina [9, 12] and iron oxide [14] because these components are known to form spinel phases [15-17] (of the type $(Mg,Fe^{2+})O.[Cr,Al,Fe^{3+}]_2O_3$), which in turn can lead to the indirect dissolution of the lining. Also SiO_2 is added as this component can lead to the formation of a second new phase (forsterite, $2MgO.SiO_2$ [18]), but not always forms a protective layer [13].

5.2 Experimental procedure

Constant temperature experiments were performed using standard static finger tests (see Figure 5.1) for different reaction times. The materials used consist of a commercially available fused grain rebonded magnesia-chromite brick and a synthetic $PbO\text{-}SiO_2\text{-}Al_2O_3\text{-}Fe_2O_3\text{-}CaO$ slag. Magnesia-chromite bricks are commonly used in both copper and lead smelters [2, 3]. A detailed description of the microstructure and the composition of all present phases for the used refractory sample can be found in Scheunis et al. [13]. The phase equilibria of a $PbO\text{-}SiO_2\text{-}Al_2O_3\text{-}Fe_2O_3\text{-}CaO$ slag have been extensively studied and the system has been optimized in FactSage [19]. Such a slag forms during the 2 stage production of lead from sulfur containing ores. First the ores are oxidized in contact with air to form the slag, which in a second stage is reduced to form Pb [16]. The used composition in this paper is chosen to ensure both a deep infiltration into the refractory as well as the formation of two different phases (forsterite and spinel) after reaction with the MgO from the brick. The slag is saturated in corundum ($(Al,Fe)_2O_3$) in order to limit the dissolution of the alumina crucible. The composition of the bath at the start of the experiment, determined using standardized XRF (X-ray fluorescence), is 47.5 wt% PbO, 11.9 wt% SiO_2, 21.2 wt% Fe_2O_3, 16.3 wt% Al_2O_3 and 0.8 wt% CaO. The properties of this slag are given in Table 5.1.

Prior to the experiment the refractory samples are cut in a bar shape (20x15x100 mm). The slag is produced by mixing different pure oxides powders in the desired ratio. The total weight of the mixture is 1.5 kg. It is

heated in open air at a rate of 600 °C/hour in a 1 liter Al_2O_3 crucible using an induction furnace until a temperature of 1300 °C is reached. At the desired temperature, the refractory finger, which is heated together with the crucible, is partially submerged into the liquid slag bath. After the required reaction time the sample is taken out of the bath and quenched in water in order to preserve the high temperature microstructure and composition in the best possible way. Three different reaction times are tested: 15 min, 1 hour and 3 hours.

After the test the finger is cut using a diamond saw. The section is made parallel and 1 cm below the slag bath line (see Figure 5.1). Before this section is analyzed it was embedded in an epoxy resin and polished. After coating the sample with a conducting carbon layer, both its microstructure and the composition of the different phases are analyzed using a fully quantitative EPMA-WDS (JEOL JXA-8530F) system operated using an acceleration voltage of 15 kV and a probe current of 15 nA. The oxygen content is not measured directly; instead the oxidation state of the element was selected a priori. Although both Fe^{2+} and Fe^{3+} can be present, only "Fe_2O_3" was selected for presentation purposes because the experiments are performed under a pO_2 of 0.21 making Fe^{3+} the most likely form of iron.

Table 5.1: Properties of the used slag calculated using FactSage [20, 21] with a pO_2=0.21.

Liquidus temperature	1425 °C
Solidus temperature	725 °C
Primary phase	spinel
Phases present at 1300 °C	Liquid + corundum
Viscosity liquid fraction at 1300 °C	0.409 Pa.s

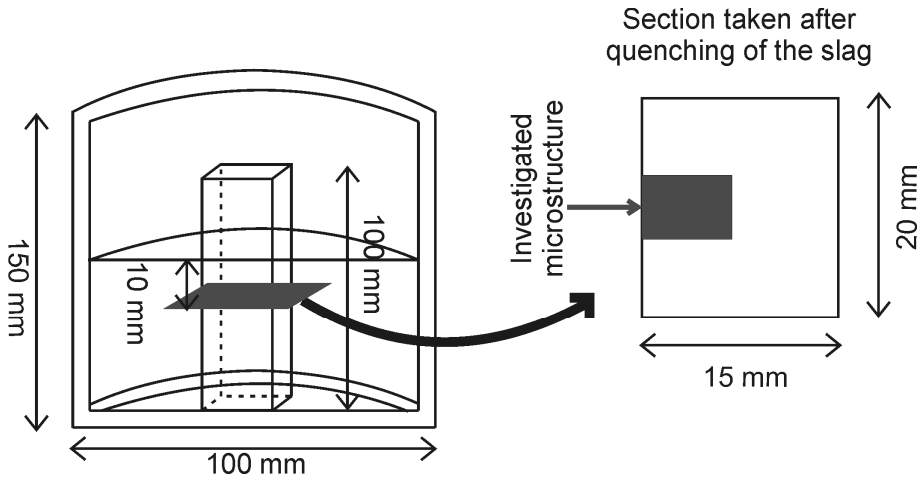

Figure 5.1: Schematic representation of the experimental procedure showing the high temperature experimental setup, removal of the sample and the position of the investigated microstructure.

5.3 Results

5.3.1 Microstructure

An overview image of the microstructure of the quenched sample after 15 min reaction time is shown in Figure 5.2. Besides the primary chromite (PC) and the fused grains (FG) present in the original microstructure, a new liquid phase (L) (appearing as the white phase) is observed, which penetrates the porous refractory sample under the influence of capillary forces. Despite the limited reaction time, the sample is already infiltrated right down to the center of the sample, indicating that the PbO-based slag infiltrates rapidly. As the sample after 15 min is already fully infiltrated, no additional infiltration will occur after 15 min and the difference between the different reaction times (15 min, 1h and 3h) lies in the changes in microstructure and slag composition, discussed in the rest of the paper.

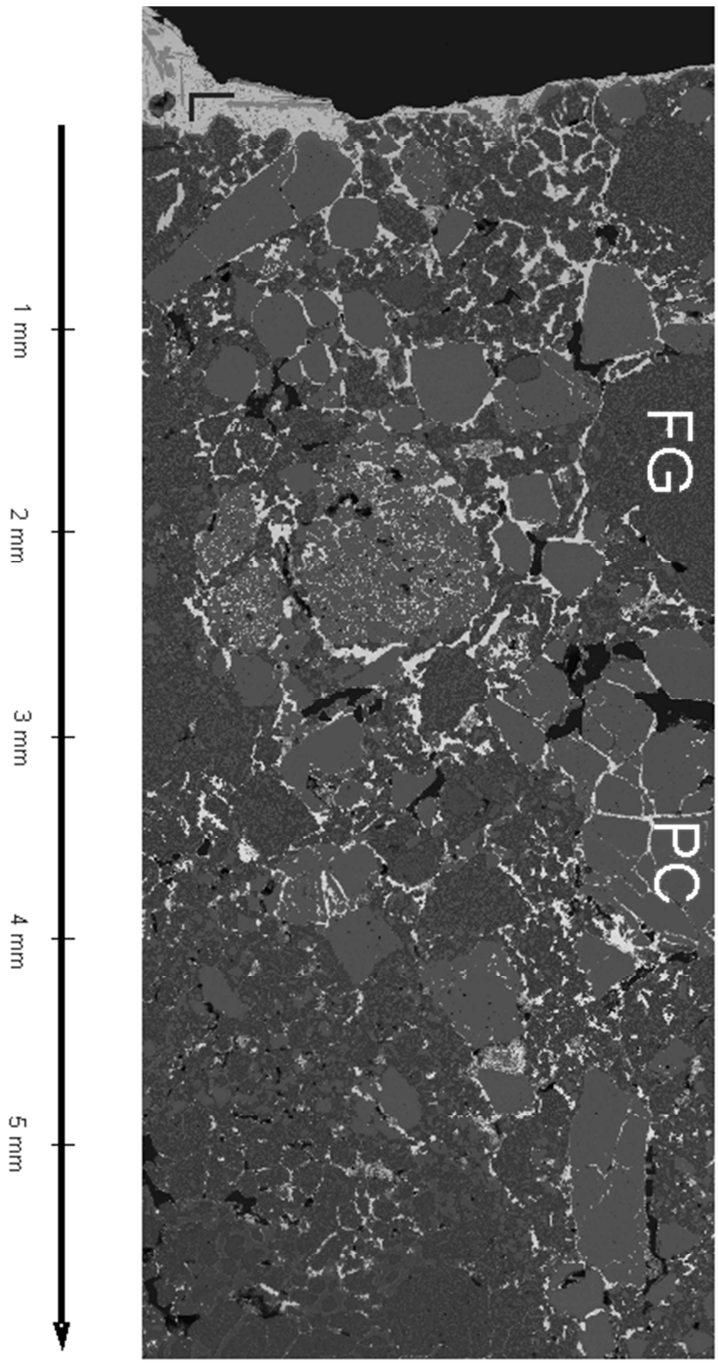

Figure 5.2: BSE overview image of the microstructure after 15 min reaction time. With L: liquid; PC: primary chromite; FG: fused grain.

Figure 5.3 shows a high magnification image of the interface between the refractory sample and the liquid slag bath, where a new spinel layer is observed on top of the original fused grain microstructure. To study the formation mechanism of this new spinel layer in more detail, compositional line scans are performed from the liquid bath along the newly-formed spinel layer to the original fused grains for the 3 tested times. The results are shown in Figure 5.4. The positions for the line scan measurements are chosen on the largest grains, as far away from the open pores as possible, to limit the effect of liquid motion, caused by slag infiltration into the pores, on the growth of the new layers. In addition, only positions where the liquid-refractory interface runs parallel with the sample surface have been measured, making it possible to assume one-dimensional growth of the new spinel phases.

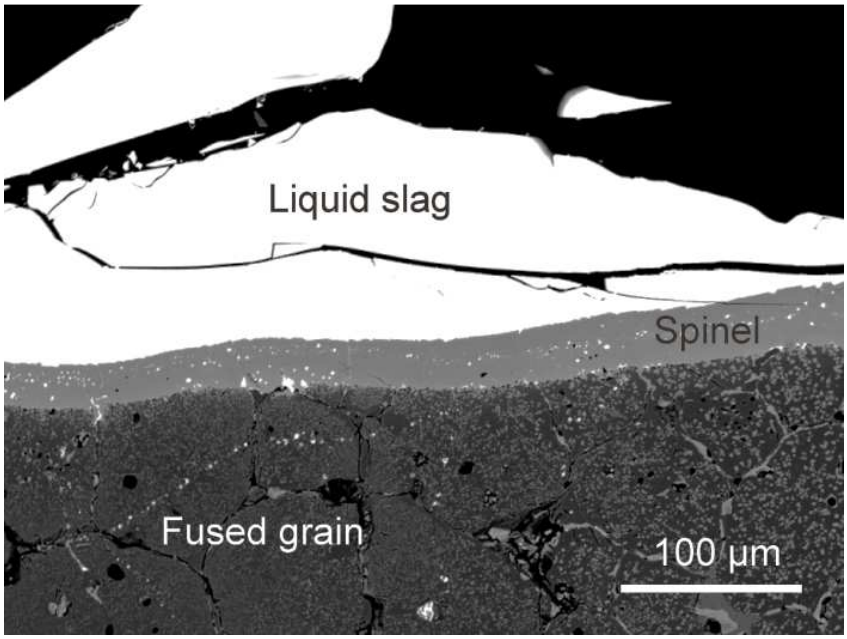

Figure 5.3: Microstructure image of the interface between the sample and the liquid slag after 3 hours reaction time. A spinel layer is observed on the interface between the refractory material and the slag.

For all measurements seen in Figure 5.4, three different phases can be distinguished: (1) the liquid slag, (2) the new spinel layer and (3) the original fused grain. The slag can be identified as it is the only phase containing PbO and SiO_2, while the periclase matrix of the fused grain consists of almost pure MgO. The transition between the different phases is shown by vertical lines in Figure 5.4, showing that the thickness of the new layer increases with time. This is also shown in Figure 5.6 where the thickness of the new spinel layer as a function of time is given, indicating an increase with √t. The growth rate (k), defined as $\Delta x^2/2t$, is thus 290.5 $\mu m^2/h$.

Figure 5.4 shows a decreasing Al_2O_3 concentration inside the new spinel layer from the liquid slag towards the fused grain in the refractory sample, while at the same time the MgO concentration increases. The "Fe_2O_3" concentration also decreases towards the original refractory, leveling off with time. Finally, Cr_2O_3 is detected in the interior of the new spinel phases, but only locally.

Figure 5.5 shows the interaction between the slag and a chromite spinel grain, the second main phase in the original refractory sample. The same behavior for MgO and Al_2O_3 can be seen for the new spinel forming on top of the original primary chromite grain compared to the one forming on top of the original fused grain. The main difference is the presence of Cr_2O_3 throughout the entire new spinel phase, increasing from the slag towards the chromite spinel grain.

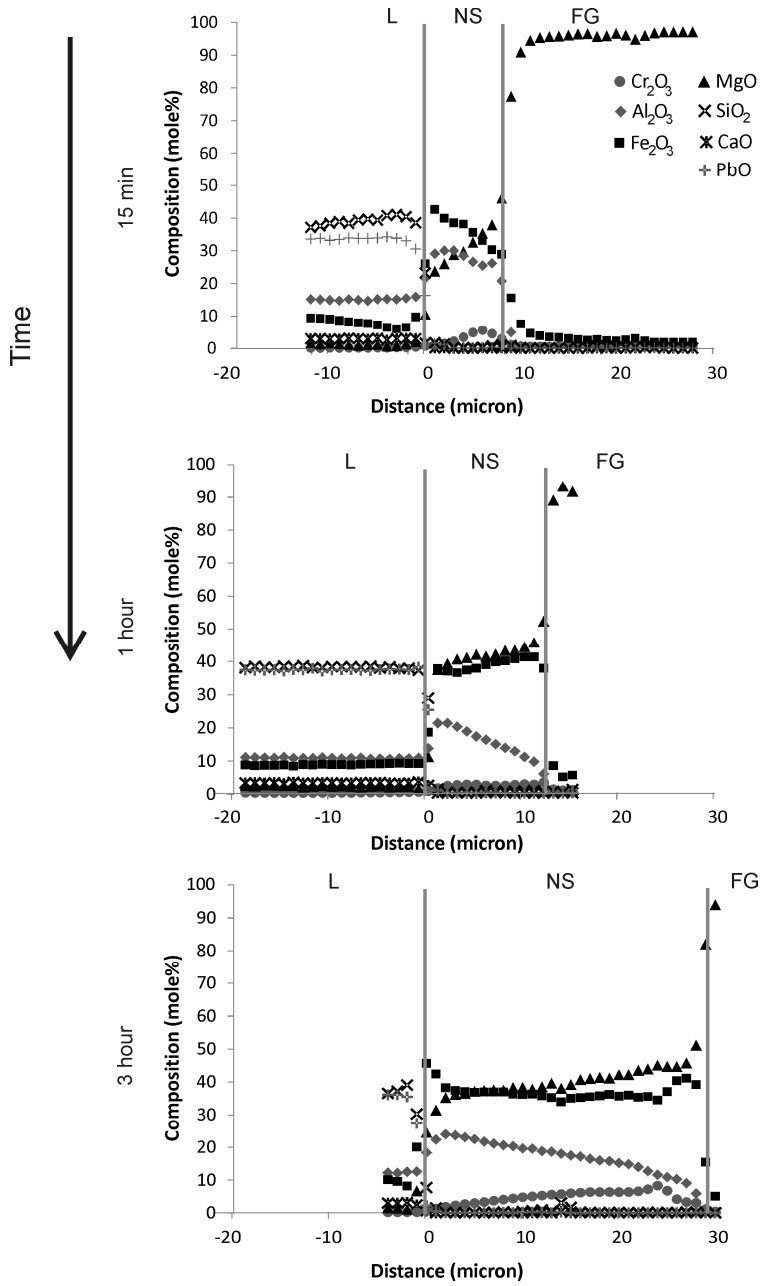

Figure 5.4: Line scans showing the compositional variation as a function of distance over the spinel layer (NS) growing at the hot face between the liquid (L) and the fused grains (FG) for 3 different reaction times.

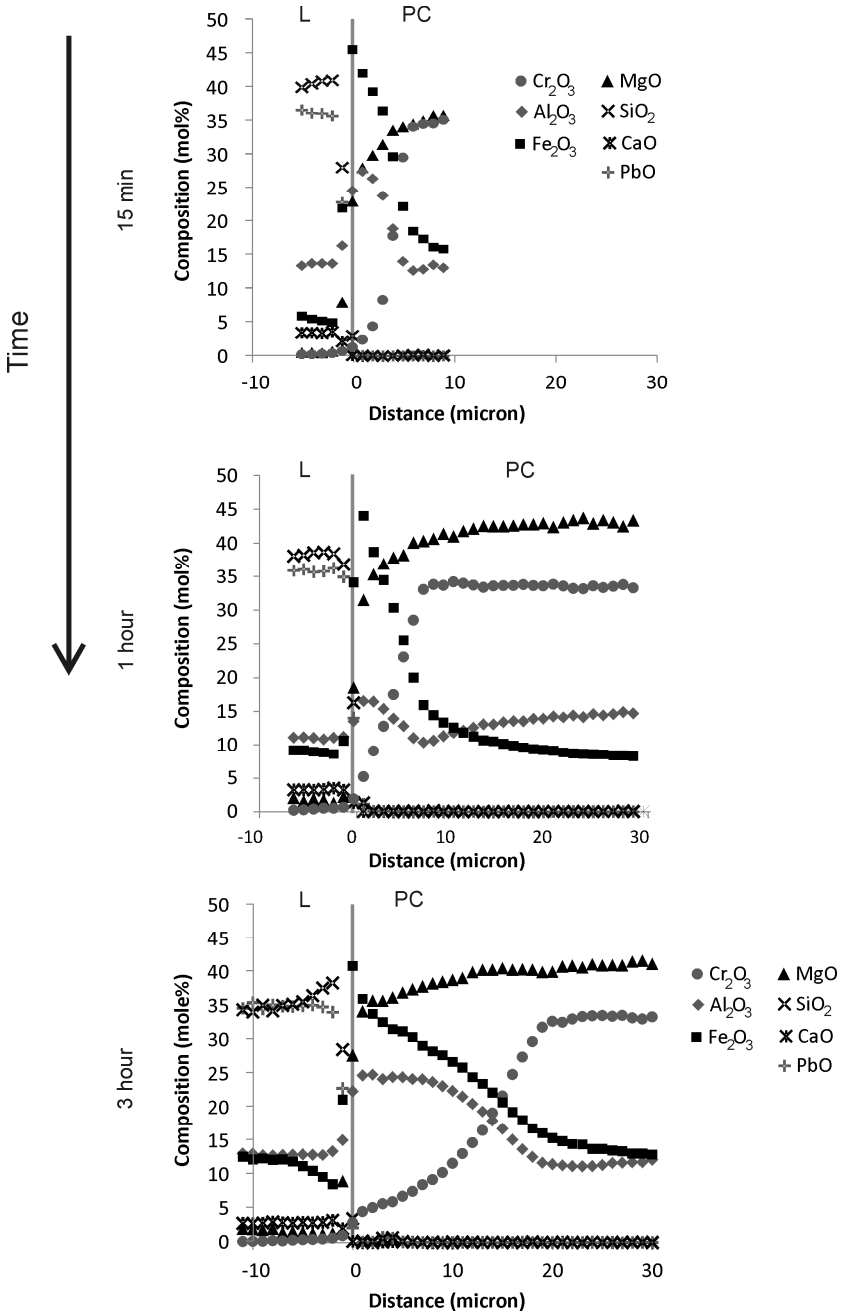

Figure 5.5: Line scan showing the compositional variation as a function of distance between the liquid slag (L) and a primary chromite spinel grain (PC) after 3 different reaction times.

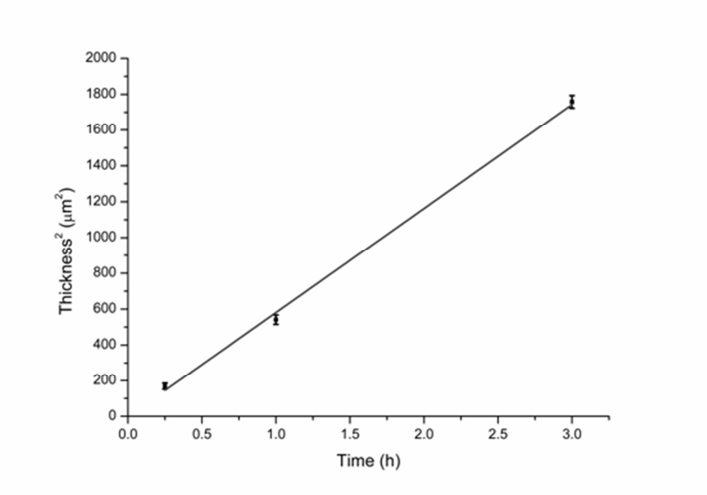

Figure 5.6: Thickness variation of the new spinel layer as a function of the reaction time. The average thickness and the 95% confidence interval are shown for each reaction time (each based on at least 150 measurements). A linear fit of the average thickness values is shown with the following equation: $\Delta x^2=581t$ ($R^2 = 0.998$).

Figure 5.7 shows detailed images of the microstructure at different depths from the refractory/slag interface for all three reaction times. Near the surface with the bath (0.5 mm), the new spinel (NS), also seen at the interface with the bath, forms a dense layer covering the entire original microstructure for all reaction times, while towards the center (3 mm), forsterite (F) is found as separate grains in all samples. At intermediate positions (1 and 2 mm) both the spinel and forsterite are present and the new spinel layer no longer covers the entire original microstructure. The forsterite grains grow with time, as seen at 3 mm from the bath/refractory interface.

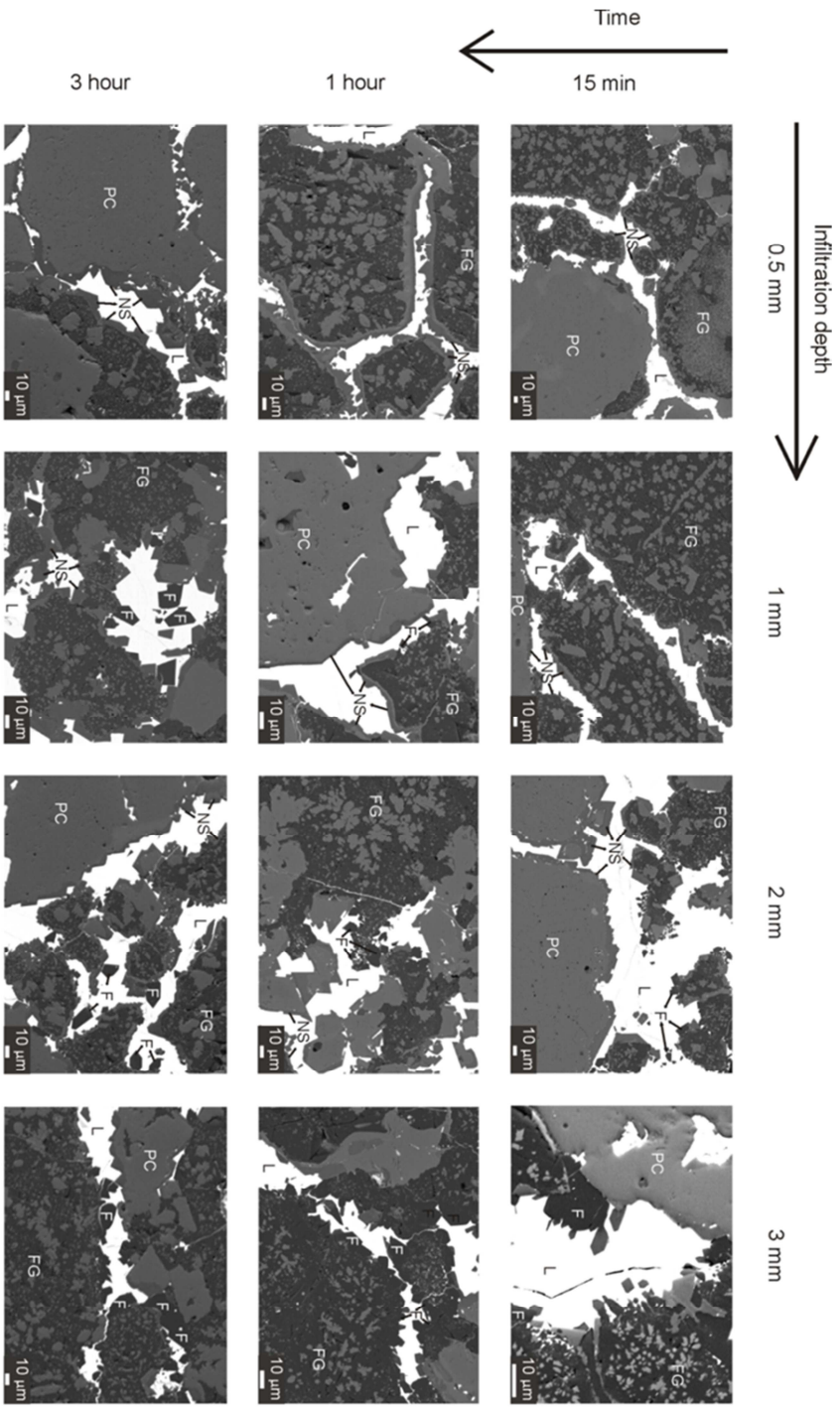

Figure 5.7: Overview of the microstructure at different positions in the samples for the 3 tested times.

5.3.2 Composition of the slag inside the sample

Figure 5.8 shows the variation of the composition of the liquid as a function of both distance and time. The results are all given in mole% to facilitate the analyses. Due to the increase in the PbO content of the slag and the high molecular weight of this component, the weight fraction of other (lighter) components automatically decreases. This can lead to wrong conclusions as it appears that components are (partially) removed from the slag, while in fact additional dissolution occurs. When the results are calculated to mole fractions, this problem is avoided. Figure 5.8 shows that the PbO content of the liquid increases while the SiO_2 content decreases with infiltration depth. This decrease, respectively increase, is, however, not uniformly distributed and can be divided into 3 main parts. In the first part (1), closest to the liquid bath, the concentration in PbO and SiO_2 remains relatively constant over time, although a slight decrease in SiO_2 and increase in PbO with distance can be seen. Deeper inside the sample, (2) the silica content decreases while the PbO concentration increases with depth. Finally, (3) in the center of the sample, the concentration for both remains constant again, albeit different from the concentration in zone 1. The composition in zones 1 and 3 does not change with time, only the position at which they occur varies over time.

Besides PbO and SiO_2, the two main components in the slag, Figure 5.8 also shows the variation in Al_2O_3 and MgO. The Al_2O_3 concentration shows a continuous drop with distance in zones 1 and 2, while the MgO concentration increases in zone 1 from near zero at the interface to a maximum value of 8-10 mole%, before decreasing again in zone 2. Both the Al_2O_3 and MgO concentrations reach a constant value in zone 3; 2-4 mole% for Al_2O_3 and 0-1 mole% for MgO.

Finally, "Fe_2O_3", Cr_2O_3 and CaO are also present inside the infiltrated slag. The iron content shows a drop at the hot face and remains constant at a value of about 6 mole% throughout the sample. The CaO content has a value between 4 and 6 mole% in zone 1 and 2, starting to drop at the end of zone 2 and reaching a constant value in zone 3 around 2 mole%. Cr_2O_3 is not detected in zones 1 and 2, but its concentration increases to about 2 mole% in zone 3.

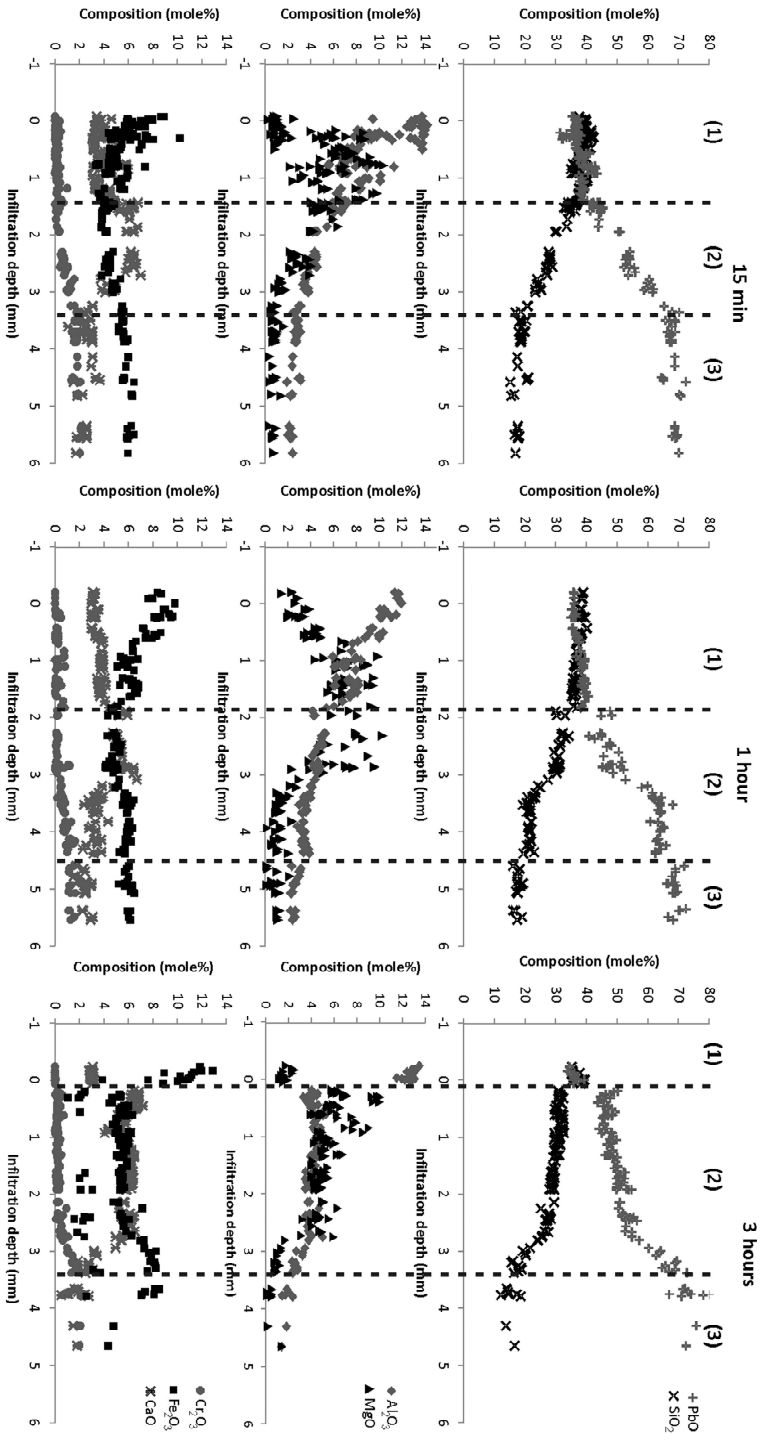

Figure 5.8: Composition of the liquid phase as a function of infiltration depth for different reaction times (measured using EMPA-WDS).

5.4 Discussion

According to Figure 5.3 and Figure 5.7 the new spinel forms in the first 2 mm of the samples. Figure 5.8 shows that at the same positions there is a drop in the Al_2O_3 and "Fe_2O_3" content of the infiltrating slag. The reaction forming these new spinel layers can thus be written as:

$$MgO_{refr} + Al_2O_{3\ slag} + "Fe_2O_3"_{slag} \rightarrow (Mg,Fe)\ [Al,Fe]_2O_4 \quad (5\text{-}1a)$$

$$MgO_{refr} + Cr_2O_{3\ refr} + Al_2O_{3\ slag,refr} + "Fe_2O_3"_{slag,refr} \rightarrow (Mg,Fe)\ [Al,Fe,Cr]_2O_4 \quad (5\text{-}1b)$$

This is further supported by the line scan results in Figure 5.4-5 where MgO, Al_2O_3, Cr_2O_3 and "Fe_2O_3" are the only components present in the new layer.

The spinel layer growing on top of the fused grain shows an MgO concentration gradient decreasing from the fused grain to the liquid bath, while Al_2O_3 shows the opposite trend. The growth rate of the spinel layer thus appears to be controlled by the counterdiffusion of MgO and Al_2O_3. The formation mechanism of a spinel layer forming on the outside of a pure MgO grain has been studied for the MgO-Al_2O_3 [22, 23], MgO-Fe_2O_3 [22] and MgO-Cr_2O_3 [24] systems, using only pure oxides. For all these systems the spinel layers grow by solid state diffusion of the cations through the newly-formed solid spinel layer. Nightingale and Monaghan [25] showed that the same mechanism also holds when MgO reacts with liquid slag by studying the formation of a $MgAl_2O_4$ spinel between pure MgO and a synthetic CaO-Al_2O_3-SiO_2 slag, identifying the diffusion of Mg^{2+} and Al^{3+} through the spinel layer as the mechanism for additional growth. The spinel phase grows on both the MgO/spinel and spinel/Al_2O_3 (or slag) interfaces. The fused grains of the refractory, however, contain secondary chromite particles, with a different composition than the new spinel layer, which get incorporated into the growing layer. The most noteworthy difference is the presence of Cr_2O_3, which could explain why locally Cr_2O_3 is detected inside the new spinel layer.

Compared with the layers forming on the fused grains those forming on the original primary chromite systematically have Cr_2O_3 as an additional component. This component is known to diffuse much slower than Al_2O_3 [26] and therefore leads to a slow, continuous decrease in Cr_2O_3 from the chromite spinel towards the liquid bath, as seen in Figure 5.4. Because Cr_2O_3 takes the positions of Fe_2O_3 and Al_2O_3 in the new spinel phase, the

composition of the latter 2 components decreases towards the original chromite spinel.

The thickness variation for the new spinel layer as a function of time is fitted in Figure 5.6 according to a $\sqrt{t}$ dependency, typical for diffusion-controlled growth of a phase, thereby confirming the diffusion-controlled formation mechanism for the spinel layers suggested in the literature [22-25]. The obtained growth rate (k=290.5 $\mu m^2/h$) is, however, 50 times larger than the values in the literature [25, 27, 28] for the growth rate of an $MgAl_2O_4$ spinel.

The new spinel phase $(Mg,Fe)[Al,Fe]_2O_4$ is not pure $MgAl_2O_4$ but can be regarded as a combination of $MgAl_2O_4$ and magnetite (Fe_3O_4). Dieckmann and Schmalzried [29] studied the self-diffusion coefficient for Fe in magnetite (Fe_3O_4) and found a variation of several orders of magnitude as a function of pO_2, due to the creation of vacancies in the spinel lattice by the oxidation of Fe^{2+} to Fe^{3+}. At room temperature magnetite is an inverse spinel [30, 31] but at higher temperatures Fe^{2+} and Fe^{3+} cations are randomly distributed between both the tetrahedral and octahedral sublattices. The vacancies most likely also have this distribution over both sublattices [32]. This leads to an increased mobility for all the cations and can explain why the experimental growth rate of the $[Mg,Fe][Al,Fe]_2O_4$ spinel is so much higher compared to a pure $MgAl_2O_4$ spinel.

Due to the formation of new spinel layers, the concentration of spinel forming components (Al_2O_3, "Fe_2O_3") in the slag decreases with infiltration depth (see Figure 5.8), until the formation of new spinel is no longer possible. At this point forsterite becomes the dominant new phase. The formation of this phase requires the removal of silica from the bath, explaining the decrease in this component seen in Figure 5.8 in zone 2.

$$2MgO_{refr} + SiO_{2\ slag} \rightarrow Mg_2SiO_{4\ refr} \qquad (5.2)$$

The dissolution rate of the refractory into the liquid bath is closely related to the phase formation. At the interface with the bath, the spinel acts as a protective layer slowing dissolution of MgO into the liquid slag. The diffusion profile in Figure 5.4 shows that MgO has to diffuse through the solid spinel layer before it can be dissolved in the liquid bath. The removal of "Fe_2O_3" and Al_2O_3 from the slag at the hot face means that insufficient driving force is available for new spinel formation to create a continuous protective layer inside the sample (see Figure 5.7, 1 mm). The MgO then makes direct contact with the slag, significantly increasing the dissolution of

MgO, as seen in Figure 5.8, zone 1. Deeper inside the sample (zone 2 in Figure 5.8), the MgO content decreases again, despite direct contact between the slag and periclase. The reason for this is the removal of SiO_2 by forsterite formation, which, according to the PbO-SiO_2-MgO phase diagram, [18], lowers the MgO solubility. At the end of zone 2, the CaO concentration in the slag also decreases, because the formed forsterite also contains some CaO.

When Al_2O_3, "Fe_2O_3", SiO_2 and CaO react with the refractory to form new phases, the slag gets enriched in PbO. The Cr_2O_3 concentration in the slag also increases towards the center of the sample, indicating that the chromite phase is attacked, as Cr_2O_3 is only present in this phase. The Cr_2O_3 increase only occurs in zone 3, together with a SiO_2 drop, which would suggest that the removal of SiO_2 increases the Cr_2O_3 solubility for high PbO slag systems. To validate this hypothesis, thermodynamic calculations are performed using the FactSage FTOxid database [21] to predict the effect of SiO_2 removal on the Cr_2O_3 solubility of a Cr_2O_3 saturated slag. The results are shown in Figure 5.9 together with the experimental data shown in Figure 5.8 rescaled to only PbO-SiO_2-Cr_2O_3. Figure 5.9 shows that for both the calculations and the measured data the Cr_2O_3 solubility increases with a decreasing SiO_2 content. The effect of other components (in this case Al_2O_3) in the slag decreases the Cr_2O_3 solubility, but does not change the increasing trend for the Cr_2O_3 solubility with decreasing SiO_2 content in the slag.

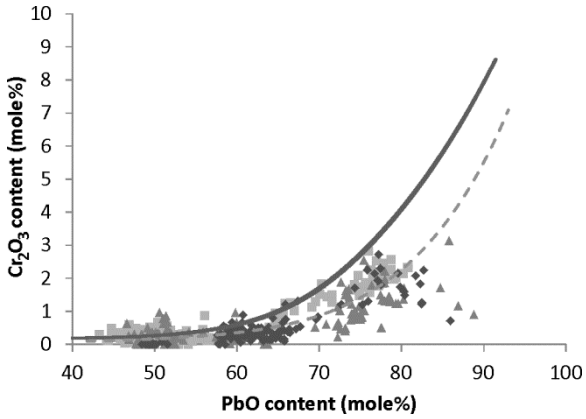

Figure 5.9: Cr_2O_3 solubility in a PbO-SiO_2-Cr_2O_3 slag at 1300 °C and pO_2=0.21 calculated using FactSage (full line) and with 10 mole% Al_2O_3 added to the liquid slag (dotted line). The experimental data given in Figure 5.8 are also shown, rescaled to only PbO, SiO_2 and Cr_2O_3 to compare with the calculations. (with ■: 15 min ▲: 1h and ♦:3h reaction time).

5.5 Effect on the overall degradation of a refractory lining

The experimental results indicate that the formation of a protective spinel layer near the hot face lowers the dissolution of MgO from the refractory into the liquid slag bath. Figure 5.10 gives a conceptual description of how the formation of such a protective layer can affect the overall degradation in a refractory lining. The original refractory sample (Figure 5.10a) consists of different grains which are sintered together with open pores between them. The bonds between the different grains give the refractory bricks their mechanical strength. When such a brick comes into contact with liquid slag (Figure 5.10b), the refractory components start to dissolve into the slag. This dissolution is typically the fastest at the hot face as the lining is in contact with a large amount of slag, constantly being replaced by fresh, unsaturated liquid by the movement of the bath. Deeper inside the sample the infiltrated liquid is saturated by the previous reactions and no further dissolution occurs. By forming a protective layer at the hot face (Figure 5.10c), the MgO dissolution at the hot face decreases and is shifted to the interior of the lining where the movement of the bath is less pronounced and, furthermore, the amount of liquid slag in contact with the refractory phases is significantly lower, reducing the chemical attack. The main disadvantage of MgO dissolution inside the sample is that the attack of the

bonding between the grains now occurs much deeper in the sample, resulting in a locally weakened structure of the lining. When this part is no longer able to withstand the applied mechanical or thermal loads, an entire part of the lining, including the protective spinel layer, may spall off and the cycle can start again on the newly exposed part of the lining.

For SiO_2 containing systems, forsterite bursting [33] is a common cause of spalling. It is caused by internal stresses after formation of forsterite phases. When forsterite forms near the hot face (Figure 5.10d), the part of the lining affected by spalling is limited. Deeper in the sample, the liquid is typically depleted in SiO_2 and no more forsterite is formed there. When a protective spinel layer forms near the hot face (Figure 5.10e), the SiO_2 cannot react with the refractory grains near the hot face and is transported deeper into the refractory with the infiltrating liquid slag. Forsterite therefore forms much deeper inside the lining, when the protective layer no longer forms. In this case, the internal stresses caused by the forsterite can lead to the spalling of a much larger part of the lining.

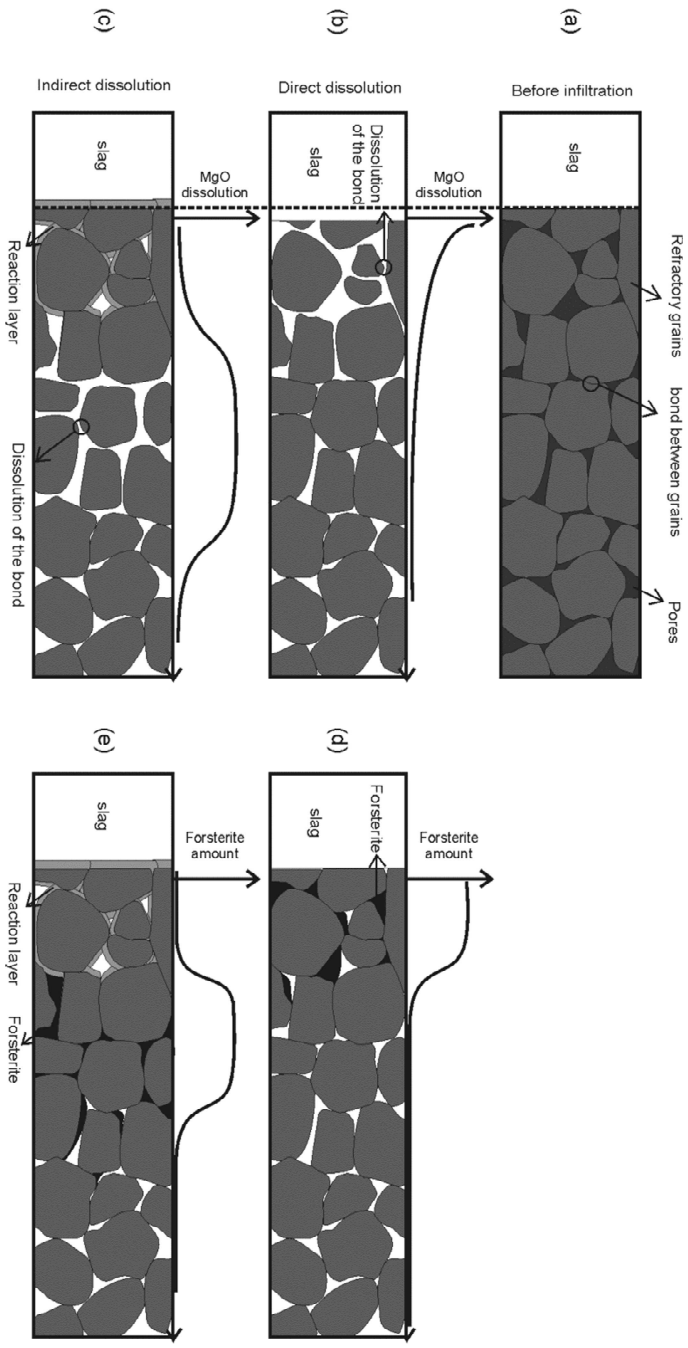

Figure 5.10: Conceptual description of the effect of a protective reaction layer on the dissolution of the refractory grains (b-c) and on the formation of a second phase (forsterite in this case, d-e).

A possible way to minimize the overall degradation is further slag engineering to limit the MgO dissolution. The easiest way to do this is to saturate the slag in MgO. However, the MgO solubility will depend on the slag composition, which in turn (as seen from the experimental results) changes throughout the brick. If too much MgO is added to the slag bath, it will start reacting with the Al_2O_3 and "Fe_2O_3" components, forming spinel phases in the slag, which could be undesirable as they increase slag viscosity.

Alternatively, external cooling can be applied to the lining. The resulting temperature gradient lowers the growth rate of the spinel layer inside the sample, slowing down the removal of spinel forming components from the infiltrating liquid. This would mean that a (thinner) protective layer forms in a larger part of the lining. Direct contact between the refractory phases and the infiltrating liquid, therefore, occurs deeper inside the sample at a lower temperature and, thus, at a lower solubility of the refractory components into the liquid slag, reducing the spalling risk. This effect can be further enhanced by combining it with slag engineering: by modifying the slag to limit iron (or other multivalent) cations inside the spinel layer, the vacancy concentration (and thus the growth rate) will decrease, allowing even more spinel forming components to be transported into the interior of the lining.

5.6 Conclusions

In this paper the interaction between a magnesia-chromite refractory sample and a synthetic PbO-SiO_2-Fe_2O_3-Al_2O_3-CaO non-ferrous slag is studied using constant temperature finger experiments at 1300 °C for 3 different reaction times. The main conclusions are:

- During the infiltration of the liquid slag into the porous refractory sample, the reaction between the slag and the refractory leads to formation of new interfacial layers, corroborating the importance of local equilibria with respect to refractory wear [34]. In the studied samples two different types were formed: a forsterite and a spinel layer. The spinel forms closest to the hot face while the forsterite is present deeper inside the brick.

- The slag compositional evolution is closely related to the phase formation and therefore also changes with position. Near the hot face the spinel formation requires Al_2O_3 and "Fe_2O_3" thereby

removing them from the slag. When insufficient Al_2O_3 and "Fe_2O_3" remain in the infiltrating slag to form new spinel layers, forsterite is formed decreasing the SiO_2 content of the slag. The removal of Al_2O_3, "Fe_2O_3" and SiO_2 from the slag results in a PbO-enriched slag in the center of the sample.

- A spinel layer forms at the interface between the slag and the refractory sample, leading to indirect dissolution of the refractory lining as the MgO has to diffuse through the solid spinel layer to dissolve into the slag, slowing down the lining wear.

- Dissolution of MgO from the refractory phases is significantly higher inside the lining than at the interface with the bath because the continuous protective spinel layer no longer forms. The MgO concentration in the slag decreases again further inside the lining as the MgO solubility decreases with the SiO_2 concentration.

- The Cr_2O_3 dissolution from the chromite spinel phases only occurs deep inside the sample when the slag contains primarily PbO.

- The formation of a protective spinel layer on top of the refractory phases slows down the dissolution of MgO into the liquid bath but at the same time increases the risk of spalling by weakening the structure of the refractory deeper inside the lining, which can lead to failure during thermo-mechanical loads. There are two main reasons for the loss of mechanical strength: (1) dissolution of the bond between the different refractory grains and/or (2) internal stresses caused by formation of new phases inside the lining. Engineering the slag to minimize the refractory wear rate, therefore, not only has to consider the dissolution rate at the hot face, which can be reduced by the formation of a protective layer, but also needs to consider the effect this has on the spalling behavior of the lining.

5.7 Acknowledgement

This research was supported by the Agency for Innovation by Science and Technology in Flanders and by Umicore (IWT Baekeland mandate 100700). The authors also like to thank Saskia Bodvin, Mieke Van Dingenen and Jef Vets from Umicore for their help with the planning and execution of the experimental part. We also gratefully acknowledge support for the FEG-EPMA measurements from the Hercules Foundation (project ZW09-09).

References

1. Barthel, H., *Wear of chrome magnesite bricks in copper smelting furnaces.* Inter-Ceram, 1981. **30**: p. 250-255.
2. Köffel, M. and Taschler, T., *Refractories for the copper and lead industry.* World of Metallurgy, 2006. **59**(3): p. 133-142.
3. Taschler, T., *Refractory materials for the copper and lead industry*. in *Tehran International Conference on Refractories*. Tehran, Iran 2004: p. 302-319.
4. Malfliet, A., Lotfian, S., Scheunis, L., Petkov, V., Pandelaers, L., Jones, P.T., and Blanpain, B., *Degradation mechanisms and use of refractory linings in copper production processes: A critical review.* Journal of the European Ceramic Society, 2014. **34**(3): p. 849-876.
5. Petkov, V., Jones, P.T., Boydens, E., Blanpain, B., and Wollants, P., *Chemical corrosion mechanisms of magnesia-chromite and chrome-free refractory bricks by copper metal and anode slag.* Journal of the European Ceramic Society, 2007. **27**(6): p. 2433-2444.
6. Jones, P.T., Blanpain, B., Wollants, P., Ding, R., and Hallemans, B., *Degradation mechanisms of magnesia-chromite refractories in vacuum-oxygen decarburisation ladles during production of stainless steel.* Ironmaking & Steelmaking, 2000. **27**(3): p. 228-237.
7. Jones, P.T., Desmet, D., Guo, M., Durinck, D., Verhaeghe, F., Van Dyck, J., Liu, J., Blanpain, B., and Wollants, P., *Using confocal scanning laser microscopy for the in situ study of high-temperature behaviour of complex ceramic materials.* Journal of the European Ceramic Society, 2007. **27**(12): p. 3497-3507.
8. Jones, P.T., Vleugels, J., Volders, I., Blanpain, B., Van der Biest, O., and Wollants, P., *A study of slag-infiltrated magnesia-chromite refractories using hybrid microwave heating.* Journal of the European Ceramic Society, 2002. **22**(6): p. 903-916.
9. Guo, M., Jones, P.T., Parada, S., Boydens, E., Dyck, J.V., Blanpain, B., and Wollants, P., *Degradation mechanisms of magnesia-chromite refractories by high-alumina stainless steel slags under vacuum conditions.* Journal of the European Ceramic Society, 2006. **26**(16): p. 3831-3843.
10. Lee, W.E. and Zhang, S., *Melt corrosion of oxide and oxide-carbon refractories.* International Materials Reviews, 1999. **44**(3): p. 77-104.

11. Van Ende, M.-A., Guo, M., Jones, P.T., Blanpain, B., and Wollants, P., *Degradation of MgO-C refractories by MnO-rich stainless steel slags.* Ceramics International, 2009. **35**(6): p. 2203-2212.
12. Liu, J., Guo, M., Jones, P.T., Verhaeghe, F., Blanpain, B., and Wollants, P., *In situ observation of the direct and indirect dissolution of MgO particles in CaO-Al_2O_3-SiO_2-based slags.* Journal of the European Ceramic Society, 2007. **27**(4): p. 1961-1972.
13. Scheunis, L., Fallah Mehrjardi, A., Campforts, M., Jones, P.T., Blanpain, B., and Jak, E., *The effect of phase formation during use on the chemical corrosion of magnesia–chromite refractories in contact with a non-ferrous PbO–SiO_2 based slag.* Journal of the European Ceramic Society, 2014. **34**(6): p. 1599-1610.
14. Yan, S., Sun, S., and Jahanshahi, S., *Reactions of dense MgO with calcium ferrite-based slags at 1573 K.* Metallurgical and Materials Transactions B-Process Metallurgy and Materials Processing Science, 2005. **36**(5): p. 651-656.
15. Jak, E. and Hayes, P.C., *The effect of the CaO/SiO_2 ratio on the phase equilibria in the ZnO-"Fe_2O_3"-(PbO+CaO+SiO_2) system in air: CaO/SiO_2=0.1, $PbO/(CaO+SiO_2)$=6.2, and CaO/SiO_2=0.6, $PbO/(CaO+SiO_2)$=4.3.* Metallurgical and Materials Transactions B-Process Metallurgy and Materials Processing Science, 2003. **34**(4): p. 369-382.
16. Jak, E. and Hayes, P.C., *Experimental study of phase equilibria in the PbO-ZnO-"Fe_2O_3"-CaO-SiO_2 system in air for high lead smelting slags (CaO/SiO_2=0.35 and $PbO/(CaO+SiO_2)$=5.0 by weight).* Metallurgical and Materials Transactions B-Process Metallurgy and Materials Processing Science, 2002. **33**(6): p. 817-825.
17. Jak, E. and Hayes, P.C., *Experimental liquidus in the PbO-ZnO-"Fe_2O_3"-(CaO+SiO_2) system in air, with CaO/SiO_2=0.35 and $PbO/(CaO+SiO_2)$=3.2.* Metallurgical and Materials Transactions B-Process Metallurgy and Materials Processing Science, 2002. **33**(6): p. 851-863.
18. Chen, S., Zhao, B., Jak, E., and Hayes, P.C., *Experimental study of phase equilibria in the PbO-MgO-SiO_2 system.* Metallurgical and Materials Transactions B-Process Metallurgy and Materials Processing Science, 2001. **32**(1): p. 11-16.
19. Jak, E., Degterov, S., Zhao, B., Pelton, A., and Hayes, P., *Coupled experimental and thermodynamic modelling study of the system PbO-ZnO-FeO-Fe_2O_3-CaO-SiO_2-Al_2O_3 for lead and zinc smelting*. in *Zinc and Lead Processing*. 1998: p. 313-333.

20. Bale, C.W., Chartrand, P., Degterov, S.A., Eriksson, G., Hack, K., Ben Mahfoud, R., Melancon, J., Pelton, A.D., and Petersen, S., *FactSage thermochemical software and databases.* Calphad-Computer Coupling of Phase Diagrams and Thermochemistry, 2002. **26**(2): p. 189-228.
21. Bale, C.W., Belisle, E., Chartrand, P., Decterov, S.A., Eriksson, G., Hack, K., Jung, I.H., Kang, Y.B., Melancon, J., Pelton, A.D., Robelin, C., and Petersen, S., *FactSage thermochemical software and databases - recent developments.* Calphad-Computer Coupling of Phase Diagrams and Thermochemistry, 2009. **33**(2): p. 295-311.
22. Carter, R.E., *Mechanism of solid-state reaction between magnesium oxide and aluminium oxide and between magnesium oxide and ferric oxide.* Journal of the American Ceramic Society, 1961. **44**(3): p. 116-120.
23. Sako, E.Y., Braulio, M.A.L., Zinngrebe, E., van der Laan, S.R., and Pandolfelli, V.C., *Fundamentals and applications on in situ spinel formation mechanisms in Al_2O_3-MgO refractory castables.* Ceramics International, 2012. **38**(3): p. 2243-2251.
24. Nagata, K., Nishiwaki, R., Nakamura, Y., and Maruyama, T., *Kinetic mechanisms of the formations of $MgCr_2O_4$ and $FeCr_2O_4$ spinels from their metal-oxides.* Solid State Ionics, 1991. **49**: p. 161-166.
25. Nightingale, S.A. and Monaghan, B.J., *Kinetics of spinel formation and growth during dissolution of MgO in CaO-Al_2O_3-SiO_2 slag.* Metallurgical and Materials Transactions B-Process Metallurgy and Materials Processing Science, 2008. **39**(5): p. 643-648.
26. Suzuki, A.M., Yasuda, A., and Ozawa, K., *Cr and Al diffusion in chromite spinel: experimental determination and its implication for diffusion creep.* Physics and Chemistry of Minerals, 2008. **35**(8): p. 433-445.
27. Zhang, P., Debroy, T., and Seetharaman, S., *Interdiffusion in the MgO-Al_2O_3 spinel with or without some dopants.* Metallurgical and Materials Transactions a-Physical Metallurgy and Materials Science, 1996. **27**(8): p. 2105-2114.
28. Whitney, W.P. and Stubican, V.S., *Interdiffusion studies in system MgO-Al_2O_3.* Journal of Physics and Chemistry of Solids, 1971. **32**(2): p. 305-312.
29. Dieckmann, R. and Schmalzried, H., *Defects and cation diffusion in magnetite .1.* Berichte Der Bunsen-Gesellschaft-Physical Chemistry Chemical Physics, 1977. **81**(3): p. 344-347.
30. Shull, C.G., Wollan, E.O., and Koehler, W.C., *Neutron scattering and polarization by ferromagnetic materials.* Physical Review, 1951. **84**(5): p. 912-921.

31. Verwey, E.J., Haayman, P.W., and Romeijn, F.C., *Physical properties and cation arrangement of oxides with spinel structures II Electronic conductivity.* The Journal of Chemical Physics, 1947. **15**(4): p. 181-187.
32. Dieckmann, R. and Schmalzried, H., *Defects and cation diffusion in magnetite (II).* Berichte Der Bunsen-Gesellschaft-Physical Chemistry Chemical Physics, 1977. **81**(4): p. 414-419.
33. Gregurek, D., Majcenovic, C., Spanring, A., and Kirschen, M., *Forsterite bursting in magnesia chromite bricks - two case studies from lead and copper smelting furnaces.* RHI Bulletin, 2011(2): p. 49-53.
34. Lee, W.E., Argent, B.B., and Zhang, S.W., *Complex phase equilibria in refractories design and use.* Journal of the American Ceramic Society, 2002. **85**(12): p. 2911-2918.

Chapter 6 The effect of phase formation during use on the chemical corrosion of magnesia-chromite refractories in contact with a non-ferrous $PbO-SiO_2$ based slag

L. Scheunis[1], A. Fallah-Mehrjardi[2], M. Campforts[3], P.T. Jones[1], B. Blanpain[1] and E. Jak[2]

Journal of the European Ceramic Society, 34 (6), 1599-1610, 2014

[1] Department of Materials Engineering, KU Leuven, Kasteelpark Arenberg 44, Box 2450, 3001 Heverlee, Belgium

[2] Pyrometallurgy Research Centre, School of Engineering, The University of Queensland, Brisbane, Queensland, Australia

[3] Research & Development, Umicore, Kasteelstraat 7, 2250 Olen, Belgium

DOI: 10.1016/j.jeurceramsoc.2013.12.026

Contribution Lennart Scheunis: Lennart Scheunis performed the experiments, analyzed the samples, interpreted the results and wrote the paper. The contribution of the co-authors consisted in discussion of the results and reviewing of the paper before final publication.

Abstract

One of the main factors limiting the lining lifetime in pyrometallurgical smelters is continuous refractory oxides dissolution in the slag bath. The overall wear is accelerated when the slag infiltrates the porous brick and the dissolution thus occurs in a larger part of the lining. This work investigates the possibility of preventing deep infiltration by sealing off the pores with newly formed phases. Static finger tests at constant temperature (1200 °C) were performed in contact with a synthetic non-ferrous PbO-SiO_2-MgO slag showing the formation of forsterite (Mg_2SiO_4) throughout the refractory sample by the reaction between SiO_2 (slag) and MgO (refractory). This phase grows with time, eventually sealing off the pores near the interface with the bath. The phase grows too slow to prevent full infiltration of the refractory but creates an equilibrium state in the sealed off part of the sample ceasing the chemical corrosion in that part of the sample.

6.1 Introduction

Because of their high hot strength and good resistance against chemical corrosion, ceramic magnesia-chromite refractories are commonly used to line furnaces in both the non-ferrous and the ferrous industry. Despite these good properties the bricks still suffer from wear caused by the combination of high temperatures, mechanical loads and direct contact with the aggressive process liquids and gasses. The wear rate of the lining in contact with the liquid slag is typically the highest. Knowledge of this refractory-slag interaction is therefore indispensable in controlling and improving the overall furnace lifetime. The latter strongly determines the feasibility and cost effectiveness of pyrometallurgical processes. For that reason previous refractory research focused on the development of new bricks [1] and the comparison between these bricks [2] under different conditions in order to select the optimal lining for a wide variety of processes. This reduces the wear of the lining and increases its lifetime, reducing the production losses during downtime, leading to more cost and energy efficient processes.

The chemical degradation of the lining caused by the liquid slag is typically the most severe and can lead to a loss of structural integrity of the brick, making it more susceptible to thermal shock, mechanical stresses and erosion (for example washing away of refractory grains after the bonding with the rest of the brick dissolves). Chemical degradation consists of: (1)

the dissolution of the refractory components into the liquid slag [3], (2) the diffusion of slag components into the refractory phases [2-5] and (3) the formation of new phases [4, 6]. The latter is especially undesirable if the newly-formed phase leads to a volume expansion or densification of the brick (either during formation or during temperature variations of the furnace), both leading to a detrimental change in mechanical properties of the brick and therefore increasing the overall corrosion rate. The formation of these new phases can, however, also be positive if the new phase forms a protective layer between the refractory phases and the slag, causing the dissolution of the lining to slow down as the refractory components have to diffuse through the new solid layer. This effect is called indirect dissolution [7]. Examples are the formation of forsterite (Mg_2SiO_4) [2, 8] (for silica containing systems) and spinel ($Mg(Al,Fe,Cr)_2O_4$) phases (for alumina [7] and iron oxide [9] containing systems). Another example is the formation of a dense MgO layer on top of the MgO-C refractories in steel convertors, formed by reduction of the MgO (by the carbon) inside the refractory followed by diffusion of the newly formed Mg gas towards the refractory-slag interface where it is oxidized, forming this dense MgO layer protecting the refractory against further infiltration of the liquid slag [3].

Chemical attack is not limited to the bath-lining interface but, under the influence of capillary forces, also occurs deep inside most of the porous refractory bricks, significantly increasing the part of the lining in contact with the aggressive liquid [3, 4, 10, 11]. This leads to additional degradation inside the brick and thus lowers the lifetime of the lining. Several methods are used to limit this undesirable slag infiltration, which, for the following overview, are classified into 3 main categories: (1) modification to the brick production process, (2) an additional pretreatment step of the bricks and (3) modifications/reactions during use in the pyrometallurgical process. Examples of the first category are: changing the overall composition [12], the raw materials used [13] and/or the firing temperature during production [14], thereby modifying the porosity and the wetting properties of the slag-brick system, which in turn directly determine the infiltration behavior of the slag. Alternatively the bricks can be pretreated (second category), for example by laser melting of the surface [15, 16], which after cooling, results in a dense surface layer, preventing infiltration. Deng et al. [17] used vacuum impregnation with Cr_2O_3 or $MgCr_2O_4$ sols and subsequent firing of the brick as a method to lower the pore size and change the wetting properties (as more chrome rich phases are present at the surface

of the pores), thereby slowing down the slag infiltration. Finally, the process itself (third category) can be modified to reduce infiltration. For example, industrial furnaces often apply external cooling of the lining [18, 19], thereby freezing the liquid in the brick before deep infiltration occurs; however, this can apply additional thermo-mechanical stresses on the lining. The reactions between the infiltrating slag and the refractory phases can slow down or even prevent further infiltration by either changing the liquid composition (making it more viscous) [20] or by the formation of new phases [21], blocking the pores. As mentioned earlier, these new phases can be undesirable if they lead to internal stresses during thermal cycling but can, alternatively, be a sound way to limit chemical degradation for those linings where thermal cycling during industrial operation is minimal. In such a process chemical corrosion is typically the dominant degradation mechanism, as thermal wear (due to the thermal expansion mismatch between the new phases and the original refractory phases) will be limited.

Unlike the other categories, category 3 is self-healing and does not require expensive changes to the brick production processes (higher firing temperature, different resources and/or more production steps). Within this category only the formation of new phases can be applied to all slag systems, even those where the slag viscosity decreases during reaction with the brick and infiltration will thus not stop by itself. For these reasons this work focuses solely on the formation mechanisms and effects of solid phases formed during use of the lining. Up to now the formation of these phases has only been studied for high viscous slag systems which have a slow slag infiltration rate, giving the slag sufficient time to react with the refractory phases. This insures that the slag can reach a (local) equilibrium state before infiltrating deeper into the sample, leading to a position dependent slag composition inside the brick. The effect of the reaction (new phases, different viscosity) influences the future infiltration behavior, making it possible to prevent full infiltration of the sample. This reaction mechanism does not necessarily hold for fast infiltrating slag systems as the infiltration can be faster than the phase formation. To investigate this, a fast infiltrating (lead silicate) slag system is used in this study to determine: (1) if the newly formed phases grow fast enough to stop infiltration, (2) if the liquid composition is still controlled by local equilibrium despite the limited reaction time and (3) if the formation mechanism of these blocking phases differs from that of slowly infiltrating slag systems. To do this at a fundamental level, the slag system, which in industrial systems can be very complex, is simplified to its most basic form: (1) the value metal oxide

(PbO), (2) flux (SiO_2) and (3) refractory component dissolving into the slag (MgO). The silica will be removed by reaction with the brick, decreasing the slag viscosity with infiltration depth, accelerating the infiltration by the reaction. An additional advantage of this system is the availability of experimental phase equilibria data [22] of this ternary system, making it possible to compare the results with equilibrium data.

6.2 Experimental procedure

Constant temperature experiments were performed using standard static finger tests (see Figure 6.1) for different reaction times. The materials used consist of a commercially available fused grain rebonded magnesia-chromite brick and a synthetic PbO-SiO_2-MgO slag. Prior to the experiment the refractory samples are cut in a bar shape (20x15x100 mm). The slag is produced by mixing different pure oxides powders (Alfa Aesar, purity level of 99.9 wt%) in the desired ratio (54 mol% PbO, 41 mol% SiO_2 and 5 mol% MgO). This slag composition was selected to ensure adequate SiO_2 for reaction while at the same time ensuring that the viscosity stays sufficiently low, promoting easy infiltration of the sample. The total weight of the mixture is 0.5 kg. It is heated in open air at a rate of 150 °C/hour in a 1/4 liter MgO crucible using a muffle furnace until a temperature of 1200 °C is reached. At the desired temperature, the refractory finger, which is heated together with the crucible, is partially submerged into the liquid slag bath. After the required reaction time the sample is taken out of the bath and quenched in water in order to preserve the high temperature microstructure in the best possible way. The time interval between removal of the refractory finger from the hot bath till submergence into the cold quenching water was approximately 2-3 seconds. Two different reaction times are tested: 15 min and 18 hours. The sample after 15 min is used to determine if the phase growth can stop full infiltration of the sample, while after 18 hours the effect that additional phase growth has on the degradation inside the sample can be studied.

After the test the finger is cut using a diamond saw. The section is made parallel to the bath line, more specifically 1 cm below the slag bath (see Figure 6.1). Before this section is analyzed it was embedded in an epoxy resin and polished. After coating the sample with a conducting carbon layer, both its microstructure and the composition of the different phases are analyzed using a full quantitative electron probe X-ray microanalysis EPMA-WDS JEOL 8200L (JEOL is a trade mark of Japan Electron Optics Ltd.,

Tokyo). It was operated using an acceleration voltage of 15 kV and a probe current of 15 nA. The oxygen content is not measured directly; instead the oxidation state of the element was selected a priori. Both Fe^{2+} and Fe^{3+} are always present in the phases, all Fe was recalculated to Fe_2O_3 for presentation purposes only.

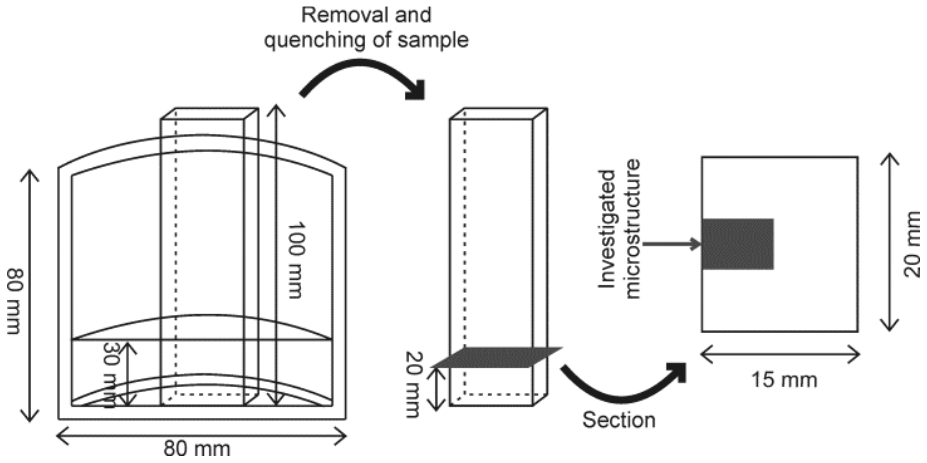

Figure 6.1: Schematic representation of the experimental procedure showing the high temperature experiment, removal of the sample and the position of the investigated microstructure.

6.3 Results and discussion

6.3.1 Reacted brick

Microstructure

The microstructure of the samples obtained after reaction with the slag is investigated. The position of the section and the investigated part of the sample are indicated in Figure 6.1. An overview and detailed images of the microstructure for both tested times are given in Figure 6.2.

In the overview images (Figure 6.3a-b) the original refractory phases are still present: fused magnesia-chromite grains (FG) and primary chromite spinel grains (PC). The figure also shows a high PbO-containing liquid phase (L), seen in white. After removing the sample from the liquid bath at the

end of the experiment, a thin layer of slag remains in contact with the sample, seen on the left of the sections. The liquid is also present inside the sample, filling the pores originally present in the sample. The cracks (C), seen in black, are formed either by (1) thermal shock during quenching, (2) mechanical load during sample preparation or (3) were closed off from the slag during infiltration.

Comparison of Figures 6.2a and b indicates that the amount of the liquid phase in the refractory sample decreases with time and distance. In order to quantify this difference, the volume fraction of the liquid phase as a function of infiltration depth is evaluated using an image analysis program, especially developed for this purpose in Matlab, which separates the phases based on their SEM-BSE brightness: the image is divided into several rectangular sections along the infiltration direction with each rectangle having a size of 200 micron and covering the entire width of the image. In each section the slag volume fraction is determined by dividing the number of pixels of the slag phase by the number of pixels of all phases (not including the cracks and pores). The result of this analysis, performed on an 8x6 mm section, is shown in Figure 6.3, indicating that the liquid fraction in the brick after 15 minutes varies around 4.5 vol%. The detected variation is primarily caused by the local microstructure. If there are large grains, 1-5 mm in size, (that are not infiltrated) present in a given section the liquid fraction is locally lower. The result for the 18 hour sample indicates that at a distance of around 1 mm from the interface with the bath the liquid fraction drops to about 1%. The part further away from the slag-refractory interface, however, has a liquid fraction of 4-4.5 vol% similar to the 15 minutes sample.

To identify the underlying reason for the local drop in liquid fraction, detailed images of the microstructures for both samples are shown in Figures 6.2c-f. For each sample 2 positions are shown. The first position is chosen to be equal to the location where the liquid fraction falls to its minimum value in Figure 6.3 (1 mm behind hot face). The second location is chosen where the liquid fraction of both the 15 min and 18 hours samples become equal again (4.5-5 mm behind hot face).

The microstructure after both reaction times shows two new phases: (1) a high PbO-containing liquid phase (L) and (2) forsterite (F)(Mg_2SiO_4) formed by the reaction between silica from the infiltrating liquid and the periclase (MgO) from the refractory sample. The difference in the microstructures of

both samples is in the quantity and morphology of these phases. After 15 min reaction time (Figures 6.2c-d), small (1-5 µm) forsterite grains are present throughout the sample in contact with large quantities of liquid. After 18 hours, larger (±20 µm) forsterite grains are detected, indicating that this phase grows with time. At this time there is also a clear position dependency in the forsterite grain size. At a distance of 5 mm from the hot face (Figure 6.2f); forsterite is present as separate grains in contact with significant amounts of liquid. At 1 mm from the hot face (Figure 6.2e) the liquid is only present in limited amounts. In addition, the forsterite is more abundantly and the grains are much larger (±20 µm), filling up the pores originally present in the brick.

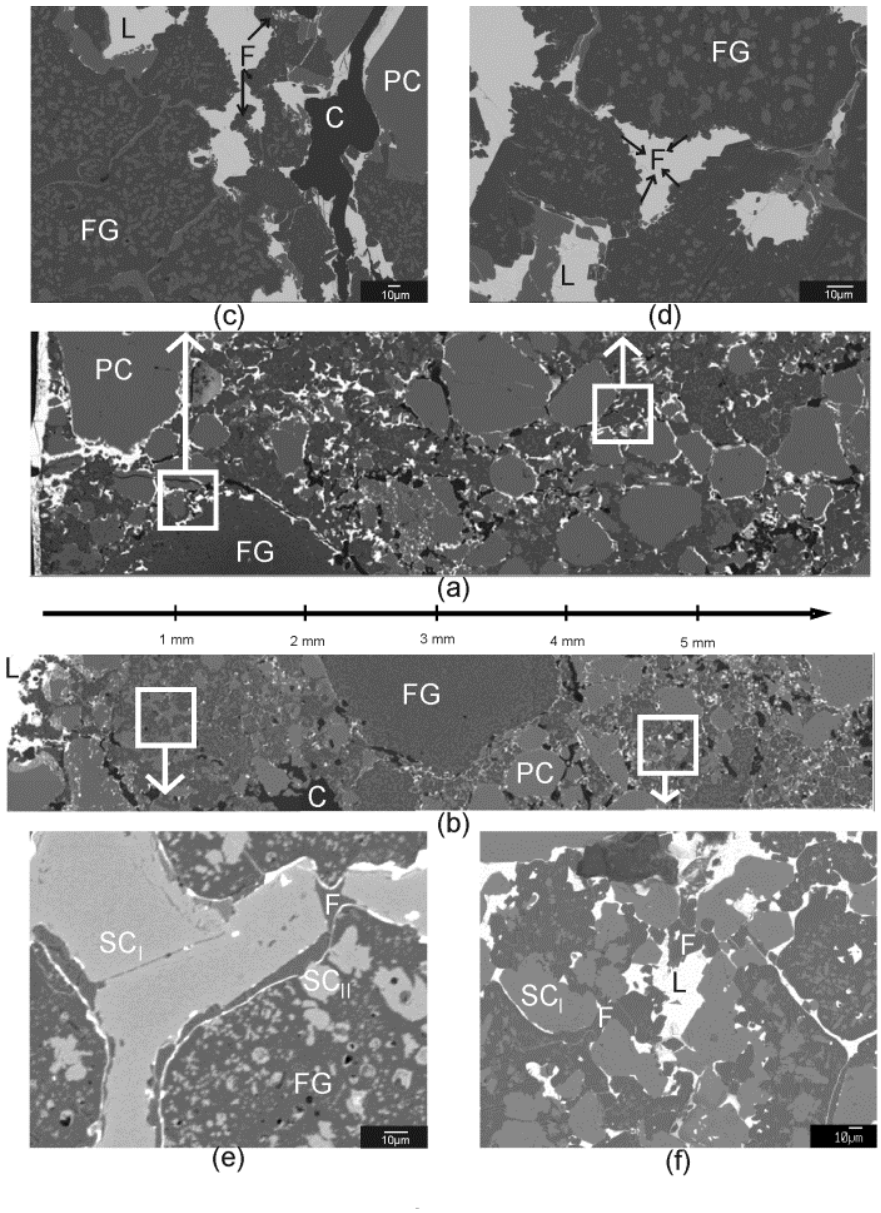

Figure 6.2: Microstructure of the tested samples, showing an overview after 15 min (a) and 18 hour (b) at the position indicated in Figure 6.1. Detailed images of the microstructure at the highlighted areas are given in c-f. With L: liquid during experiment; F: forsterite; SC_I: secondary chromite type I, SC_{II}; secondary chromite type II, PC: primary chromite, FG: fused grain and C: cracks and pores.

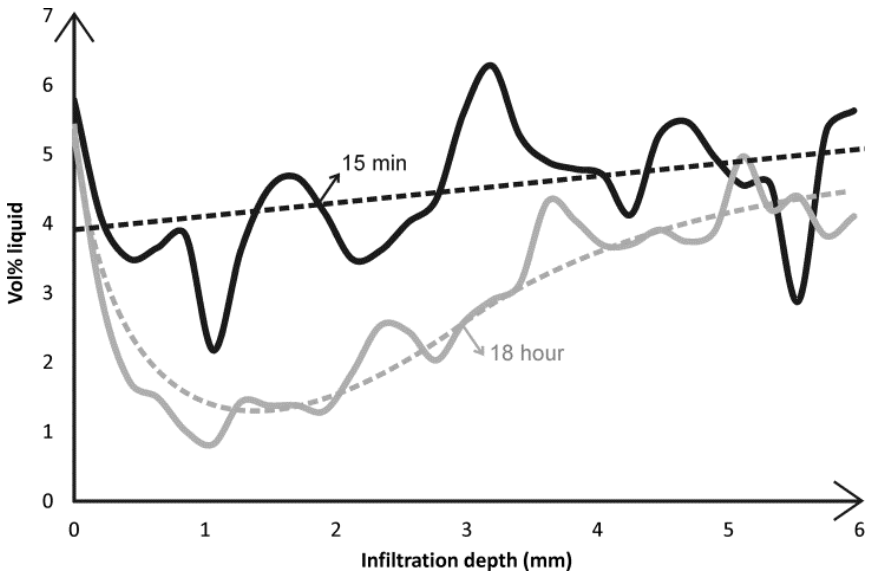

Figure 6.3: Variation in the fraction of high PbO liquid present in the refractory as a function of the distance from the slag-refractory interface obtained from image analyses of the microstructure for both the 15 min and 18 hour samples (full lines). The trend lines for both samples are indicated as the dotted lines.

Composition

The composition of the infiltrating liquid phase is measured at different positions across the sample (see Table 6.1 and Figure 6.4-6.5). Figure 6.4 shows the variation of the liquid composition with depth inside the sample for the main components (PbO, SiO_2 and MgO). The same data are given in Table 6.1 as the averages for different parts along the infiltration direction. These data are projected on the PbO-SiO_2-MgO ternary phase diagram in Figure 6.5. The position of the liquidus line at the testing temperature (1200°C) is determined using phase equilibria experimental results reported by Chen et al. [22].

Figure 6.4 shows a decrease in SiO_2 and MgO content of the liquid phase with infiltration depth for both samples, while at the same time the PbO concentration increases. Figure 6.5 shows that the liquid compositions follow the 1200°C liquidus line, indicating that the liquid composition at different positions follows local equilibrium. The silica removal is due to the formation of forsterite (Mg_2SiO_4) detected in Figure 6.2. As seen in Figure 6.5, phase equilibria dictate that the PbO content of the liquid phase

increases while the MgO content decreases if silica is removed from the liquid phase.

The variation of the liquid composition with distance is different for the different reaction times. After 15 min the decline is continuous, while after 18 hours the liquid composition only changes over a small part of the brick. At the same position the liquid fraction seen in Figure 6.3 drops by the formation of forsterite blockages, separating the sample into 2 parts. In the part where the pore is still in contact with the bath, the composition of the liquid phase becomes homogeneous, close to the bath composition. The second part of the pore is physically separated from the bath and the liquid already inside the brick reaches a composition in equilibrium with the refractory material seen in Figure 6.5 for the 18h sample at a position > 2 mm.

Table 6.1: Average composition of the liquid phase for different positions in the sample after 15 min and 18 hour reaction time.

	15 min reaction time						
Position (mm)	MgO	SiO_2	CaO	Cr_2O_3	Al_2O_3	"Fe_2O_3"[1]	PbO
bath	8.6	39.6	0.2	0.2	0.3	0.3	50.7
0--0.25	6.9	36.4	1.0	0.4	0.9	0.9	53.4
0.25--0.5	5.5	30.7	3.1	0.5	1.7	2.1	56.4
0.5--1	3.7	25.8	3.4	0.8	1.6	2.5	62.1
1--2	2.7	24.7	3.1	0.7	1.5	2.4	64.9
2--3	2.9	27.5	4.5	0.6	1.9	2.5	60.2
3--4	2.4	26.0	3.8	0.7	1.9	2.6	62.7
4--5	1.4	23.2	3.5	0.8	1.9	3.4	65.8
5--6	1.1	18.3	2.6	1.2	1.8	4.2	71.0
6--7	0.8	17.7	2.3	1.6	1.9	4.8	70.8
7--8	0.7	8.5	1.2	1.5	1.0	4.0	83.0

	18 hour reaction time						
Position (mm)	MgO	SiO_2	CaO	Cr_2O_3	Al_2O_3	"Fe_2O_3"[1]	PbO
bath	10.2	39.6	0.0	0.3	0.3	0.1	49.3
0--0.25	8.7	40.0	0.1	0.5	0.6	0.2	49.8
0.25--0.5	7.1	38.1	0.3	0.7	0.8	0.5	52.3
0.5--1	5.9	34.4	0.5	1.2	2.0	1.3	54.7
1--2	1.5	16.6	1.0	2.8	1.3	2.4	74.5
2--3	0.5	5.1	0.4	5.1	0.5	5.5	82.7
3--4	0.6	5.3	1.1	3.6	0.5	6.7	82.3
4--5	0.4	4.8	0.5	4.9	0.4	4.5	84.4
5--6	0.6	7.1	1.0	4.0	0.8	6.3	80.3
6--7	0.5	6.3	0.6	3.8	0.5	4.8	83.4

[1] Fe is recalculated to Fe_2O_3 for presentation purpose

The slight deviation of the points from the liquidus line may be due to either (1) imperfect quenching of the sample, due to its large size, (2) the effect of the minor components (especially CaO), which up till now has been neglected or (3) limited size of the measurement areas in the sample (1-5 micron), leading to some interaction with the surrounding phases.

Table 6.1 shows the liquid composition at different positions throughout the sample. Besides the components present in the bath (PbO, SiO_2 and MgO) some refractory components (Cr_2O_3, Fe_2O_3, Al_2O_3 and CaO) also dissolve into the liquid during infiltration. The solubility of spinel components (especially iron and chromium) increases with time and with the PbO content of the liquid. The CaO content of the liquid, on the other hand, decreases with time. This CaO is dissolved into the liquid out of the monticellite phase. After 15 min it is quite high (around 3-4 mol% inside the sample) while after 18 hours it decreases to less than 1 mol%. With time a large amount of forsterite formed and measurements indicate that this phase inside the sample contains some CaO (0.5-2 mol%) explaining the decrease in CaO content of the liquid with time. At the hot face the

forsterite contains no CaO (less than 0.01 mol%). The large variation in CaO content of the liquid slag and the newly formed forsterite inside the sample is due to the random distribution of the CaO-containing monticellite phases in the unreacted sample. Where these phases were present, the slag dissolved more CaO and the newly-formed forsterite therefore also has a higher CaO concentration.

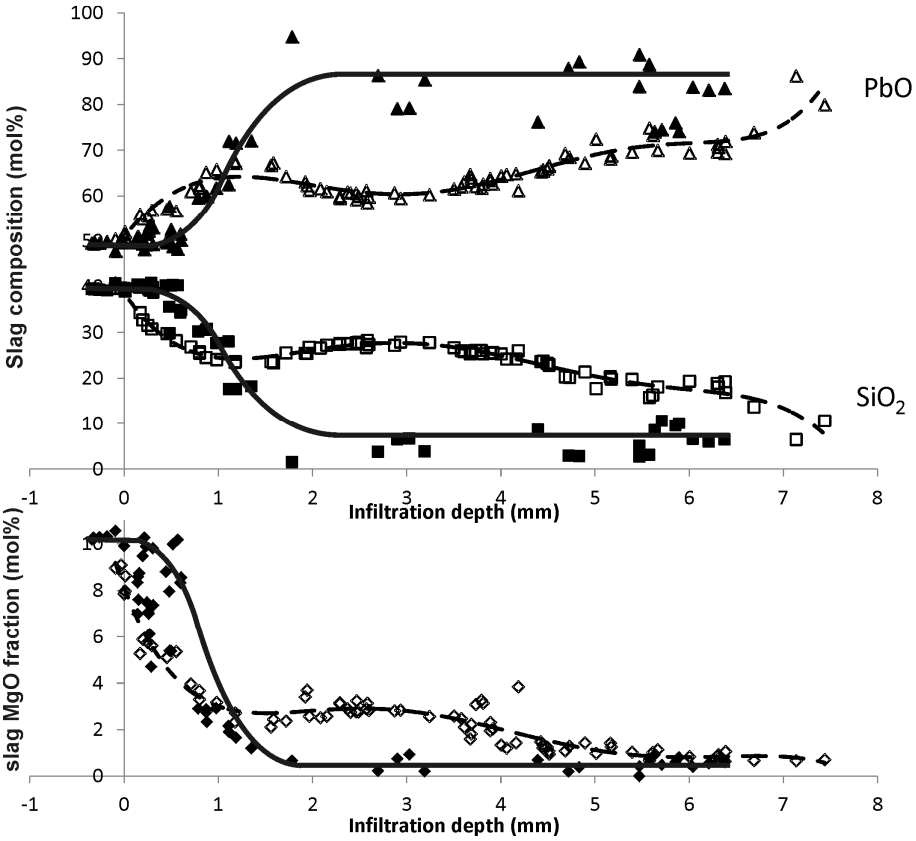

Figure 6.4: Composition of the liquid phase as a function of infiltration depth after 15 min (open markers and dotted trend lines) and 18 hours (closed markers and full trend lines).

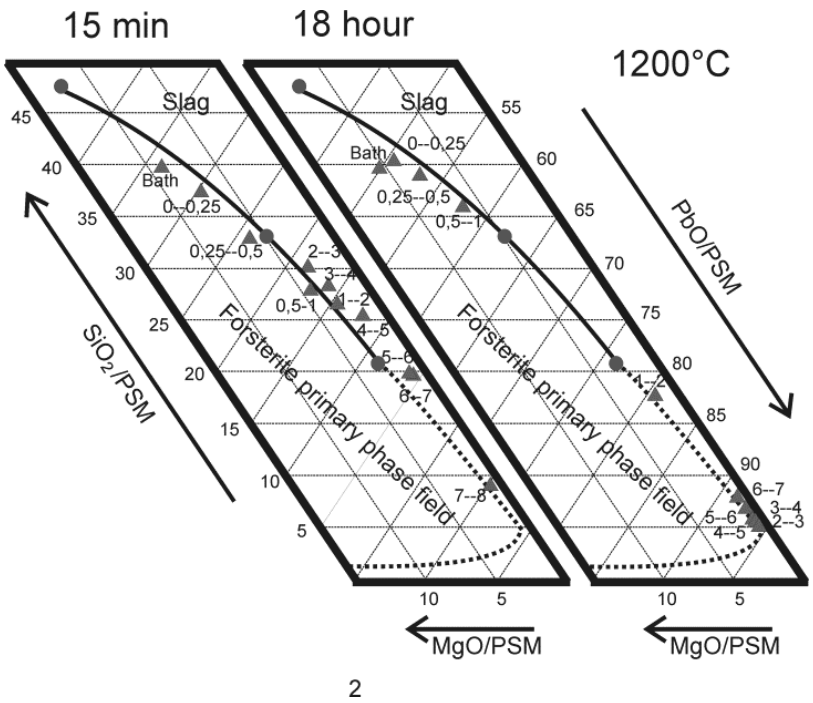

2

Figure 6.5: PbO-SiO_2-MgO phase diagram (in mol%) containing the measured composition of the infiltrated liquid at different depths (in mm) after 15 min and 18 hour for the values are given in Table 6.1. The 1200°C liquidus line is determined based on the phase equilibria results (●) obtained from Chen et al [22].

6.3.2 Slag-refractory interaction

A conceptual description of the formation of new phases during slag-refractory interaction is developed based on the presented results and schematically illustrated in Figure 6.6. To obtain a generalized description, that could also hold for more complex systems, a classification is introduced for the different time stages and zones inside the lining as well as for the different components and phases (see Table 6.2). In the following section this generalized description is used to describe the parameters controlling the growth of these new phases and how this formation in turn influences the slag composition and the liquid fraction inside the brick both as a function of time and of position.

Table 6.2: Summary of the different time stages during reaction, the components, zones and different phases present in both the slag and the refractory.

		Description	Example
Components	C_1	Slag component not reacting with the refractory	PbO
	C_2	Slag component reacting with the refractory forming new phases	SiO_2, MgO
	C_3	Refractory component dissolving into the slag	CaO, Al_2O_3, Fe_2O_3, Cr_2O_3
	C_4	Refractory component reacting with the slag to form new phases	MgO
Phases	P_1	Original refractory phases	Periclase, chromite, forsterite, monticellite
	P_2	New phases formed from slag and refractory components	Forsterite
Stages	t_0	Refractory before exposure to slag	Figure 2.3
	t_1	Initial penetration of the liquid and the initial reaction into the refractory	15 min sample
	t_2	First blockage occurs, separating part of the brick from the slag bath	/
	t_3	More blockages occur. The part of the brick connected to the slag bath decreases	18 hour sample
Zones	I	Liquid channel in contact with the bath. Supply and removal of components by diffusion and convection. The composition of the liquid in the channel is close to the liquid bath composition.	/
	II	Liquid channel in contact with the bath. Supply and removal of components only by diffusion. The composition of the liquid in the channel is noticeably different from the liquid bath	15 min sample (entire sample) 18hour sample (< 0.5 mm)

		composition during t_1.	
	III	Channels in the inside of the sample, physically separated from the bath	18 hour sample (> 1.5 mm)
	IV	Part of the brick between first and last blockage	18 hour sample (0.5-1.5 mm)

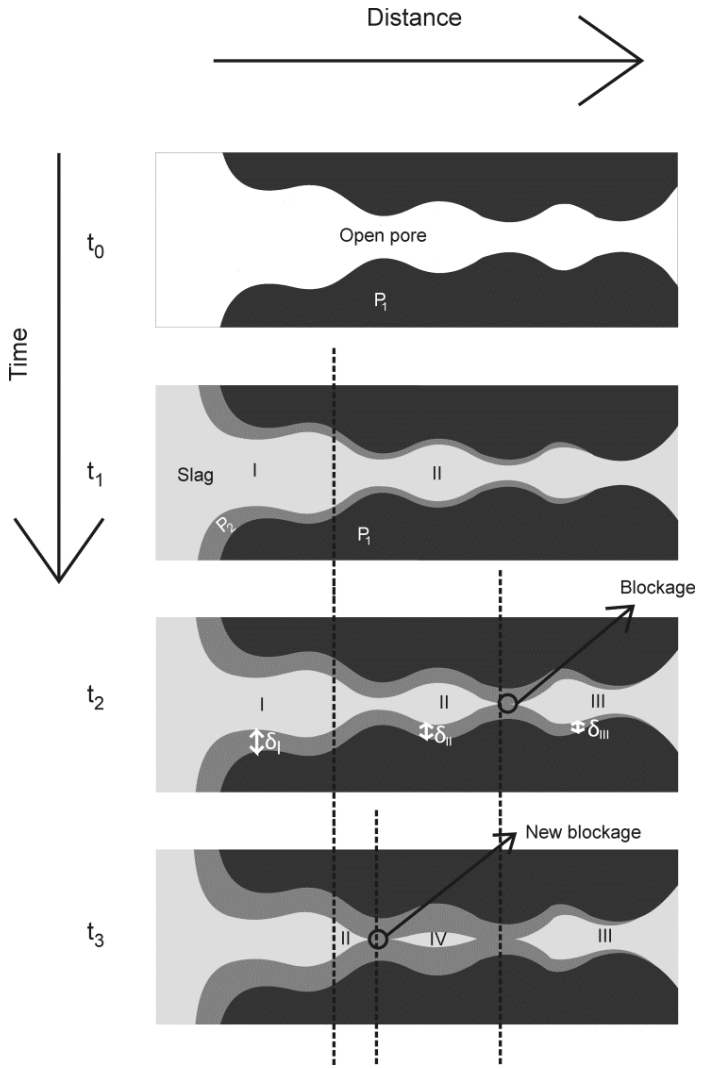

Figure 6.6: Schematic representation of the reaction between liquid slag and a refractory brick for different reaction times.

The initial stage t_0 (Figure 6.6) describes the state before any contact with the slag and subsequent reaction occurred. The refractory consists solely of original refractory phases and pores, filled with gas. Once the sample is brought into contact with the slag (t_1), capillary forces cause infiltration of the liquid into the open pores. At the same time, the C_2 components start reacting with refractory components to form new P_2 phases according to the following overall reaction:

$$C_2+C_4 => P_2 \qquad (6\text{-}1)$$

thereby removing C_2 components from the infiltrating liquid. Fresh C_2 components are constantly supplied from the bath into the liquid channel by diffusion, allowing the P_2 phases to grow with time until they start blocking the pores (stage t_2). In zone I and II the P_2 phase growth continues leading to the formation of new blockages during t_3 creating a new part of the brick between several blockages (zone IV).

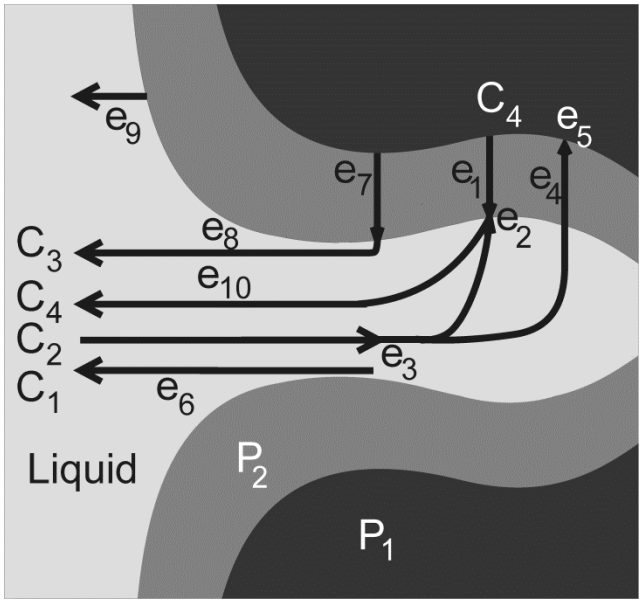

Figure 6.7: Schematic representation of the elemental steps taking place during reaction (6.1).

Elemental steps

The overall reaction to form new P_2 phases, described by formula 6-1, may involve several elemental steps (e_1-e_{10}) shown in Table 6.3 and Figure 6.7. The formation of these P_2 phases removes C_2 components from the infiltrated liquid and, thus, leads to a concentration gradient from the bath to the interior of the brick, causing C_2 components to diffuse from the liquid slag bath into the channels (e_3). At the same time there is an opposite gradient in C_1 components, causing counter diffusion along the liquid channels from the refractory towards the bath (e_6).

When the P_2 phases separate the C_2 and C_4 components from one another, they prevent further growth of the phase unless new C_2 and C_4 components are supplied to the P_2 interface. Whether e_2 or e_5 is the dominant reaction depends on the ratio between the supply rate of the C_2 and C_4 components. If $R_{C2} < R_{C4}$ (with R_x: supply rate of component x), then the P_2 phase grows preferentially at the interface between P_2 and the liquid (e_2). If $R_{C2} > R_{C4}$ the P_2 phase layer grows preferentially at the interface between P_1 and P_2 (e_5). R_{C4} depends solely on the diffusion of C_4 components through the P_2 phase (e_1), while the C_2 components have to diffuse from the bath through both the liquid channel (e_3) and the P_2 phases (e_4).

If the bath is unsaturated in refractory components, both the C_3 and C_4 components can dissolve into the liquid. This mostly requires solid state diffusion of these components through the newly formed P_2 layer (e_1, e_7). Once they are dissolved in the liquid they are removed to the unsaturated bath by liquid diffusion through the liquid channels (e_8, e_{10}). At the interface between the lining and the bath, a steady state thickness of the P_2 phases is reached when the dissolution of the P_2 phases into the unsaturated bath is equally fast as the growth of the P_2 phases, the latter being controlled by the diffusion of C_4 through these phases. The net result is a gradual dissolution of the brick in the liquid bath. This will continue over time until the bath is saturated in refractory components or until the entire lining is dissolved.

These elemental steps occur in zones I and II all the time. Zone III and IV on the other hand are physically separated from the liquid bath, thereby suppressing steps e_3, e_6, e_8, e_9 and e_{10} resulting in a local equilibrium state.

Time and position variation of the slag composition and amount

The formation of P_2 phases requires C_2 components, thereby removing them from the liquid until the liquid reaches its minimal C_2 concentration, controlled by the equilibrium between liquid, P_1 and P_2 phases (C_{2equil} in Figure 6.8a). This minimal level is reached deep inside zone II and eventually for all the liquid in the sealed off parts of the brick (zones III and IV). In zone I and II C_2 components are supplied by diffusion from the liquid slag bath through the liquid channels and convection in zone I. If this mass transfer is significantly faster than the removal of C_2 due to the formation of P_2 phases, then the concentration slopes in Figure 6.8a may level off with time, as seen in t_2-t_3. If the reverse is true the composition of the liquid will lie between bath composition and the equilibrium composition (as seen in Figure 6.8a for t_1).

The same trend is shown in the ternary diagram (Figure 6.8b). Inside the refractory sample, the composition of the liquid initially takes different compositions between $C_{Slag,intf}$ and C_{equil}. C_{equil} corresponds to the composition of the liquid containing the lowest concentration of C_2, determined by the equilibrium between liquid, P_1 and P_2 phases. At this composition no further reactions occur. The phase diagram shows that the liquid with a composition in between C_{equil} and the bath composition cannot be in equilibrium with the original P_1 phases. A new P_2 phase is formed to overcome this, thereby removing C_2 components from the liquid, moving away from the top corner in the ternary diagram. The liquid at each point is in equilibrium with the P_2 phases and its composition will thus follow the liquidus line. With time the liquid composition moves towards two distinct positions: one equal to C_{equil} for zone III and IV due to additional P_2 formation in the sealed off zones of the brick. The other equal to $C_{Slag,intf}$ for zone I and II due to new C_2 supply if the supply of new C_2 components by mass transfer is significantly faster than the removal due to the formation of P_2 phases. If this is not true the liquid will take different position on the liquidus line similar to t_2.

If the slag bath is unsaturated in refractory components the C_3 and C_4 components will first dissolve into the slag at the interface with the lining, until the 2 phase region ($L+P_2$) is reached. The liquid composition at the interface thus lies on the liquidus line ($C_{Slag,intf}$) as seen in Figure 6.8b. This differs from the bulk bath composition and a composition gradient will develop over time between the interface ($C_{Slag,intf}$) and the bulk bath

($C_{Bulk,bath}$) resulting in the continuous dissolution of the lining into the bulk bath (as can be seen in Figure 6.8a and b).

Table 6.3: Description of the different elementary steps occurring during the reaction between the infiltrated liquid and the refractory phases.

Step	Description
e_1	Diffusion of C_4 through newly formed P_2 solid layer
e_2	Reaction between C_4 and C_2 ($C_2+C_4=>P_2$) at the P_2 – Liquid interface
e_3	Diffusion of C_2 components from the slag bath into the liquid channel
e_4	Diffusion of C_2 through newly formed P_2 solid layer
e_5	Reaction between C_4 and C_2 ($C_2+C_4=>P_2$) at the P_1 – P_2 interface
e_6	C_1 counter diffusion from the liquid channel into the slag bath
e_7	Diffusion of C_3 through newly formed P_2 solid layer
e_8	Diffusion of C_3 components from the liquid channel into the slag bath
e_9	Dissolution of the solid phase P_2 into the liquid bath
e_{10}	Diffusion of C_4 components from the liquid channel into the slag bath

The phase formation is closely related to the composition of the liquid and is therefore also position and time dependent as can be seen in Figure 6.8c. If no new phases are formed, the liquid fraction will be constant and equal to the initial porosity (assuming all pores are filled and the local variation in porosity is not taken into account) while the formation of new solid phases causes the liquid fraction to drop. Once the C_2 components drop to their minimum value the P_2 phases stop growing and the liquid fraction will no longer change over time. This is the case for zones III and IV as well as the deeper parts of zone II. Because of the longer reaction time the phase growth is more pronounced in zone IV than in zone III. Due to the constant supply of new components in zone I and II the phases continue to grow with time, leading to the highest P_2 fraction (and lowest liquid fraction) in this part of the brick (see Figure 6.8c: $S_3< S_2< S_1<S_0$).

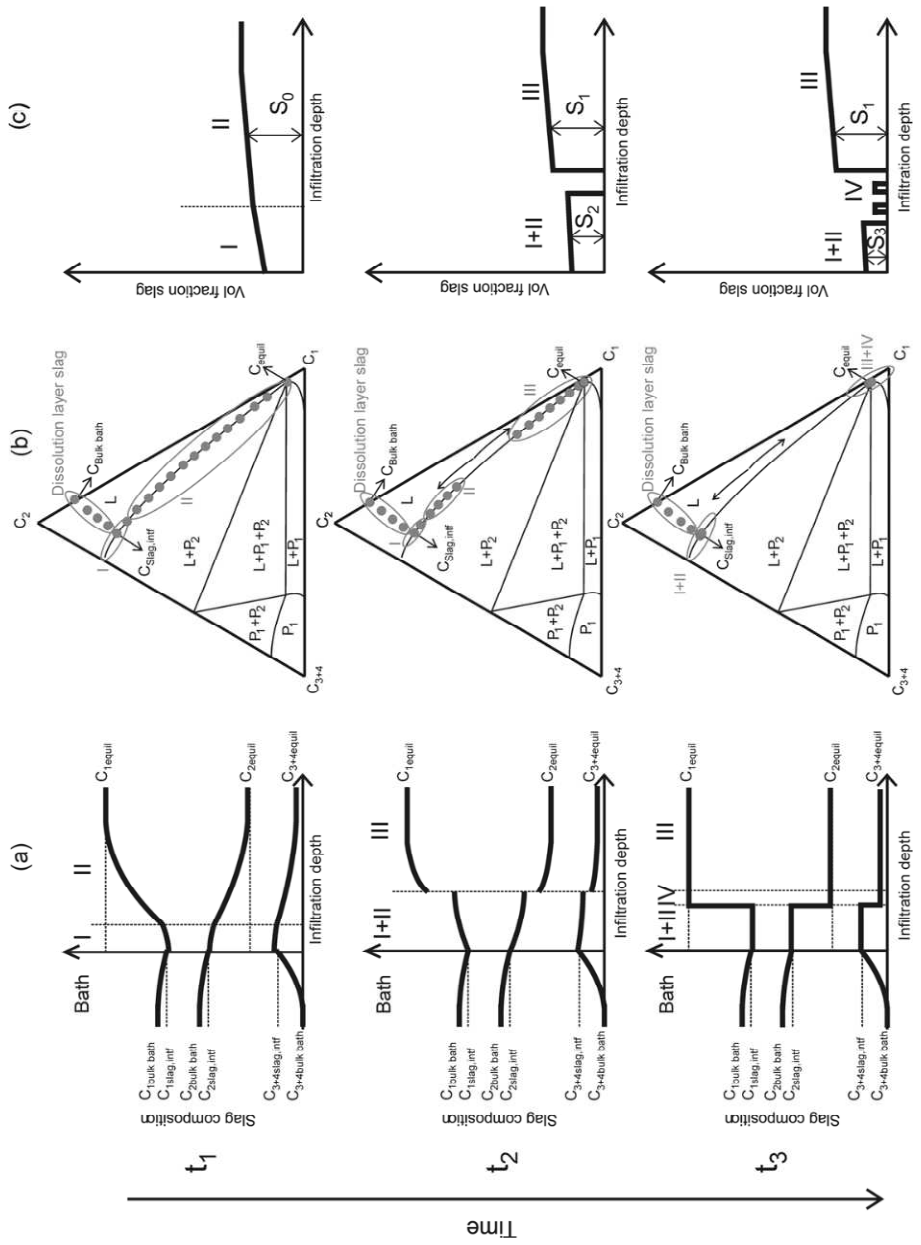

Figure 6.8: Effect of the reaction between refractory phases and infiltrating liquid on some of the liquid composition and amount for the different stages. The composition of the liquid phase is given a) as a function of depth and b) projected on a ternary phase diagram. c) volume fraction of the liquid phase.

Application to the studied system

The previous general discussion is applied to the studied PbO-SiO_2-MgO slag system, where the only new phase forsterite is formed by the following reaction:

$$SiO_{2slag}(C_2) + 2MgO_{ref}(C_4) \rightarrow Mg_2SiO_{4ref}(P_2) \quad (6\text{-}2)$$

Unlike the spinel phase in Chapter 5 the forsterite phase does not form as a continuous layer but instead as separate grains. The elemental steps during this reaction can be identified using the results of Gardés et al. [23]. They studied the diffusion of MgO and SiO_2 in forsterite (Mg_2SiO_4) and enstatite ($MgSiO_3$) layers growing between pure periclase (MgO) and quartz (SiO_2) and determined that the interlayer growth rate is controlled by MgO, the fastest diffusing component. The elemental steps during reaction 6.2 are therefore (e_1-e_3), making the forsterite grow at the forsterite-liquid interface.

The different stages, zones, components and phases are identified (see Table 6.2). The experiments are chosen to be in two different time stages (15 min = t_1 and 18 hours = t_3). After 15 min (t_1) no blockages are formed yet and as no convection is applied, the liquid phase composition differs noticeably from the bath slag composition (see Figure 6.4) and only zone II is present in the sample (no zone I with the liquid composition close to the bath composition can be identified). This leads to the slow and continuous decline in silica seen in Figure 6.4. After 18 hour (t_3) the liquid composition (Figure 6.5) in zone I and zone II becomes equal to the bath composition (for the experiment C_{Bulk} bath is equal to $C_{slag,intf}$ in Figure 6.8b as the slag already contains MgO) indicating that the supply of SiO_2 is significantly faster than the forsterite formation in this part of the sample, while in the sealed off interior of the brick (zone III and IV), the liquid composition is constant and equal to the composition deep inside the 15 min sample (C_{equil} in Figure 6.8b). The liquid fraction (Figure 6.3) after 18 hour (t_3) has a minimum value between 1-2 mm (zone IV), this is at the same position that liquid composition also changes drastically. In zone III the liquid fraction increases again until it reaches the same value as during t_1 (15 min).

Position of blockage

The physical and chemical properties controlling the blockage formation are identified and linked to the furnace parameters, namely the furnace temperature and the slag composition, making it possible to control the position where the blockages form. Practically, the blockages close to the slag-refractory interface are beneficial as they seal off the largest part of the brick from the aggressive bath. However, in some cases growing phases in a larger part of the brick may be more desirable. For example: when two different slag systems are used, one during the first run of a new lining specifically to protect the lining. During the rest of the lining lifetime the normal slag system can then be used. By forming blockages in a larger part of the brick, the refractory lining stays protected for a longer time when a part dissolves into the slag bath. During the selection of the first "protecting" slag system it is important that the P_2 phases being formed do not dissolve into the second slag system.

The position of the blockages is primarily controlled by the ratio between the phase growth rate and the supply rate of new components. If the phase formation is faster than the supply of the chemical components, the phases grow near the bath-lining interface and the liquid composition is constant in the rest of the infiltrated brick. If the reverse is true, the C_2 components infiltrate deeply inside the sample allowing phase growth throughout the infiltrated part of the brick. The supply of new components is controlled by liquid diffusion while the removal of these components (by phase formation and growth) is mostly controlled by solid state diffusion through the new solid layer. Liquid state diffusion is usually orders of magnitude faster than solid state diffusion, but the distance that has to be bridged is also orders of magnitude different: a few microns for the solid state diffusion while the liquid state diffusion through the infiltrated part of the sample can go from a few millimeters up to several centimeters.

Moving the position of the blockages towards the interface with the bath requires a decrease in the ratio of the liquid diffusion over the solid state diffusion rate in the P_2 phases. This can be achieved by increasing the temperature. Even though higher temperatures may help to move the position of the blockages in the case of diffusion controlled growth of the blocking phase, at the same time they can limit (or even prevent) the precipitation of solid phases, thereby preventing the sealing of the pores altogether. It also increases the solubility of the refractory components into

the slag bath, thereby increasing the chemical degradation at the slag-refractory interface when the liquid is unsaturated in refractory components. Furthermore, it will increase the mechanical loading of the brick and therefore induce crack formation and propagation that might result in spalling of the brick or formation of new channels through which slag can infiltrate in the brick. An alternative approach in controlling the position of the phases is not merely raising the temperature but applying a thermal gradient over the lining, increasing the ratio of the diffusion coefficients D_{liq}/D_{P2} with distance from the bath. The new solid phases grow faster closer to the bath-lining interface, where the temperature is highest (and equal to the bath temperature). Besides the temperature, the composition of the slag bath is a second process parameter which can influence the position of the blockages. By changing the liquid composition, the viscosity can be increased (for example by increasing the silica content) thereby decreasing the liquid diffusion and thus hindering the supply of new C_2 components. A low viscosity is, however, often a requirement for an efficient process operation. By modifying the slag composition it is also possible to change the P_2 phases being formed, thereby changing the diffusion coefficient for the C_2 and C_4 components and thus the growth rate of the new phase. By careful selection of the phase being formed it is possible to move the position of the blockages.

6.4 Conclusion

In this paper a conceptual description of the interaction between refractory bricks and infiltrating slag is developed, based on results obtained from constant temperature finger experiments at 1200°C using a synthetic PbO-SiO_2-MgO slag in contact with magnesia-chromite refractory samples for 2 different interaction times. The main conclusions are:

- The reaction between the refractory sample and the infiltrating liquid leads to the formation of new phases. For the studied system the MgO of the brick reacts with the infiltrating silica from the slag to form forsterite (Mg_2SiO_4).
- The new forsterite phase is able to seal off the pores inside the refractory. This happens after infiltration of the sample as the infiltration rate is higher than the phase growth rate. The sample is thus completely infiltrated.
- The interaction is time dependent due to the supply of fresh silica from the bath through the liquid channels, thereby allowing the forsterite to continue to grow with time, creating blockages.

- The composition of the infiltrated liquid is position dependent. By the formation of forsterite, silica is constantly removed from the liquid until the liquid reaches its minimal concentration. This is the case for all the liquid blocked off from the slag bath. Due to the supply of fresh silica, the liquid composition near the slag bath approaches that of the bath composition.
- The composition of the liquid phase is controlled by local equilibrium between the infiltrating liquid and the newly formed and original refractory phases, as first described by Zhang and Lee [24]. Phase diagrams can thus be used to predict the compositional changes of the liquid.

Based on the experiments a generic description of the interaction between the infiltrating slag and the refractory sample is given, focusing on the formation of new solid phases and its effect on both the liquid composition and fraction as a function of time and position in the sample. From this analysis the ratio between the liquid state and solid state diffusion is identified as the dominant factor controlling the position of the blockages. This ratio in turn depends on the furnace temperature and the slag composition. Using these insights, industrial slag systems can be modified to create sealing layers inside the refractory lining, thereby increasing the lifetime of the furnace. This finding is particularly relevant for industrial furnaces or reactors which operate at a more or less constant temperature. In this case the degradation of the lining is dominated by chemical corrosion and not by thermally-induced wear. The use of phase formation during use is thus a promising, yet not universally applicable technique, to increase the lifetime of refractory lining in pyrometallurgical processes.

6.5 Acknowledgement

This research was supported by the Agency for Innovation by Science and Technology in Flanders (IWT Baekeland mandate 100700) and by Umicore R&D.

References

1. Köffel, M. and Taschler, T., *Refractories for the copper and lead industry.* World of Metallurgy, 2006. **59**(3): p. 133-142.
2. Petkov, V., Jones, P.T., Boydens, E., Blanpain, B., and Wollants, P., *Chemical corrosion mechanisms of magnesia-chromite and chrome-free refractory bricks by copper metal and anode slag.* Journal of the European Ceramic Society, 2007. **27**(6): p. 2433-2444.
3. Lee, W.E. and Zhang, S., *Melt corrosion of oxide and oxide-carbon refractories.* International Materials Reviews, 1999. **44**(3): p. 77-104.
4. Zhang, S., Sarpoolaky, H., Marriott, N.J., and Lee, W.E., *Penetration and corrosion of magnesia grain by silicate slags.* British Ceramic Transactions, 2000. **99**(6): p. 248-255.
5. Kaur, R.R., Swinbourne, D.R., Wadsley, M.W., and Nexhip, C., *Comparison of ferrous calcium silicate slag and calcium ferrite slag interactions with magnesia-chrome refractories.* Metallurgical and Materials Transactions B-Process Metallurgy and Materials Processing Science, 2011. **42**(3): p. 451-459.
6. Poirier, J., Qafssaoui, F., Ildefonse, J.P., and Bouchetou, M.L., *Analysis and interpretation of refractory micro structures in studies of corrosion mechanisms by liquid oxides.* Journal of the European Ceramic Society, 2008. **28**(8): p. 1557-1568.
7. Liu, J., Guo, M., Jones, P.T., Verhaeghe, F., Blanpain, B., and Wollants, P., *In situ observation of the direct and indirect dissolution of MgO particles in CaO-Al_2O_3-SiO_2-based slags.* Journal of the European Ceramic Society, 2007. **27**(4): p. 1961-1972.
8. Gregurek, D., Majcenovic, C., Spanring, A., and Kirschen, M., *Forsterite bursting in magnesia chromite bricks - two case studies from lead and copper smelting furnaces.* RHI Bulletin, 2011(2): p. 49-53.
9. Yan, S., Sun, S., and Jahanshahi, S., *Reactions of dense MgO with calcium ferrite-based slags at 1573 K.* Metallurgical and Materials Transactions B-Process Metallurgy and Materials Processing Science, 2005. **36**(5): p. 651-656.
10. Mukai, K., Tao, Z., Goto, K., Li, Z., and Takashima, T., *In-situ observation of slag penetration into MgO refractory.* Scandinavian Journal of Metallurgy, 2002. **31**(1): p. 68-78.

11. Matsui, T., Hiragushi, K., Ikemoto, T., and Sawano, K., *Penetration behavior of silicate slag into magnesia refractory bricks.* Journal of the Technical Association of Refractories, 2002. **22**(4): p. 302-309.
12. Diaz, L.A., Torrecillas, R., de Aza, A.H., and Pena, P., *Effect of spinel content on slag attack resistance of high alumina refractory castables.* Journal of the European Ceramic Society, 2007. **27**(16): p. 4623-4631.
13. Sako, E.Y., Braulio, M.A.L., and Pandolfelli, V.C., *The corrosion and microstructure relationship for cement-bonded spinel refractory castables.* Ceramics International, 2012. **38**(3): p. 2177-2185.
14. Cherif, K., Pandolfelli, V., and Rigaud, M., *Factors affecting the corrosion by fayalite slags and the thermal shock performance of magnesia-chrome bricks.* Canadian Ceramics Quarterly, 1997. **66**(3): p. 210-216.
15. Bradley, L., Li, L., and Stott, F., *Flame-assisted laser surface treatment of refractory materials for crack-free densification.* Materials Science and Engineering: A, 2000. **278**(1): p. 204-212.
16. Bradley, L., Li, L., and Stott, F.H., *Surface modification of alumina-based refractories using a xenon arc lamp.* Applied Surface Science, 2000. **154–155**: p. 675-681.
17. Deng, Y.Y., Wang, H.Z., and Zhao, H.Z., *Influence of chrome-bearing sols vacuum impregnation on the properties of magnesia-chrome refractory.* Ceramics International, 2008. **34**(3): p. 573-580.
18. Kaneko, T.K., Bennett, J.P., and Sridhar, S., *Effect of temperature gradient on industrial gasifier coal slag infiltration into alumina refractory.* Journal of the American Ceramic Society, 2011. **94**(12): p. 4507-4515.
19. Kaneko, T.K., Zhu, J., Thomas, H., Bennett, J.P., and Sridhar, S., *Influence of oxygen partial pressure on synthetic coal slag infiltration into porous Al_2O_3 refractory.* Journal of the American Ceramic Society, 2012. **95**(5): p. 1764-1773.
20. Kim, H.B. and Oh, M.S., *Changes in microstructure of a high chromia refractory due to interaction with infiltrating coal slag in a slagging gasifier environment.* Ceramics International, 2008. **34**(8): p. 2107-2116.
21. Puente-Ornelas, R., Lizcano-Zulaica, C.J., Guzman, A.M., Zambrano, P.C., and Das-Roy, T.K., *Dissolution of refractories for gasification process of petroleum coke for the steel industry.* Fuel, 2012. **93**(1): p. 581-588.
22. Chen, S., Zhao, B., Jak, E., and Hayes, P.C., *Experimental study of phase equilibria in the PbO-MgO-SiO_2 system.* Metallurgical and

Materials Transactions B-Process Metallurgy and Materials Processing Science, 2001. **32**(1): p. 11-16.

23. Gardes, E., Wunder, B., Wirth, R., and Heinrich, W., *Growth of multilayered polycrystalline reaction rims in the MgO-SiO_2 system, part I: experiments.* Contributions to Mineralogy and Petrology, 2011. **161**(1): p. 1-12.
24. Zhang, S. and Lee, W.E., *Use of phase diagrams in studies of refractories corrosion.* International Materials Reviews, 2000. **45**(2): p. 41-58.

Chapter 7 The effect of a temperature gradient on the phase formation inside a magnesia-chromite refractory brick in contact with a non-ferrous PbO-SiO_2-MgO slag

L. Scheunis[1], A. Fallah-Mehrjardi[2], M. Campforts[3], P.T. Jones[1], B. Blanpain[1], A. Malfliet[1] and E. Jak[2]

Submitted to the Journal of the European Ceramic Society

[1] Department of Materials Engineering, KU Leuven, Kasteelpark Arenberg 44, Box 2450, 3001 Heverlee, Belgium

[2] Pyrometallurgy Research Centre, School of Engineering, The University of Queensland, Brisbane, Queensland, Australia

[3] Research & Development, Umicore, Kasteelstraat 7, 2250 Olen, Belgium

Contribution Lennart Scheunis: Lennart Scheunis performed the experiments, analyzed the samples, interpreted the results and wrote the paper. The contribution of the co-authors consisted in discussion of the experimental setup design and of the results and reviewing of the paper before final publication.

Abstract

Furnace relinings represent a major operating cost in pyrometallurgy. External cooling is, therefore, often used to reduce the chemical wear by limiting the slag infiltration depth, reducing the reaction kinetics and lowering the solubility of refractory components into the liquid slag. In this chapter a new experimental setup is used to study the reaction between a synthetic PbO-SiO_2-MgO based slag and a magnesia-chromite refractory under a temperature gradient. Forsterite (Mg_2SiO_4) is formed throughout the sample, removing SiO_2 from the infiltrated liquid slag. The resulting change in slag composition causes the liquidus temperature and the viscosity of the liquid to decrease, partially countering the effect of the applied temperature gradient and resulting in the complete infiltration of the sample. The extent to which external cooling prolongs the lifetime of an industrial furnace thus depends on the slag properties and how they are modified after reaction with the refractory.

7.1 Introduction

Ceramic magnesia-chromite refractory bricks are commonly used in non-ferrous smelting furnace linings because of their high melting point, good mechanical properties at elevated temperatures and their ability to withstand aggressive conditions [1]. Despite these properties, wear still occurs, eventually requiring a costly replacement of the lining. Reducing the wear increases the time between replacements, leading to a more efficient operation. To minimize the refractory degradation it is important to both identify the main degradation mechanisms as well as understand how these mechanisms depend on the process conditions (slag composition, temperature, pO_2, …). Based on these insights, modifications to the process conditions and/or the used brick type can be made in order to reduce the wear rate in the slag zone of the reactor. By reducing the wear either the lining's lifetime can be prolonged or, for the same lifetime, a thinner lining can be used, increasing the usable volume and thus the capacity of the reactor. A better understanding of the degradation mechanisms can also be used to increase the predictability of lining's lifetime, allowing a better planning of the downtime. When metal is produced in several stages, each in a different reactor, the unexpected downtime of one reactor can cause a production stop for the entire plant.

Refractory wear is caused by a combination of chemical, thermal and mechanical stresses, with the chemical attack by liquid slag often being the

most critical. The identification of the main degradation mechanisms in industrial environments is typically done using post mortem analyses [2, 3]. In post mortem analyses samples are taken from the lining after the final cooling of the reactor and the microstructure of these samples is analyzed and compared with the microstructure of the original bricks, thereby identifying the degradation. Post mortem analyses, thus, provide the best possible insight into the degradation mechanisms present inside the lining towards the end of its use. Unfortunately some disadvantages are associated to this method: it is impossible to quench samples from the reactor lining. The investigated samples are therefore allowed to slowly cool, leading to changes in the microstructure and the composition of the phases, hindering a correct identification of the degradation. Samples can only be taken at the end of the lining's lifetime so that the effect of changes in operating conditions can only be obtained during the next relining of the furnace, implying a slow learning curve. It also means that when the chemical stresses vary during the lining's lifetime, for example when different slag compositions are used or when the pO_2 varies with time, linking the final microstructure of the lining to one specific parameter is difficult, hindering a clear identification of the main causes of the degradation. For some phenomena it is even impossible to observe them as the reaction products are removed from the lining before the samples are taken.

To overcome these disadvantages, the effect of chemical degradation is studied using experiments under controlled conditions [4, 5], making it possible to better link the effect of a single parameter to the occurring wear mechanism. To perform these experiments several simplifications are made with respect to the industrial process: a single (often simplified) slag composition is used; the turbulence of the bath is in most cases not taken into account; the pO_2 is assumed to remain constant and, finally, most experiments are performed at constant temperature, typically the working temperature of the furnace. In reality, however, all industrial refractory linings have a temperature gradient between the hot face (i.e. the side in contact with the liquid bath) and the cold face (i.e. the side in contact with the shell of the steel vessel). Some furnaces even apply additional cooling of the lining by using water cooled copper plates at the cold face side in order to solidify the infiltrating slag and limit the reaction surface between slag and the porous refractory lining. The assumption of an isothermal system is, therefore, only valid when the slag does not deeply infiltrate the lining and

the temperature in the infiltrated part of the refractory is thus close to the operating temperature of the furnace. For slag systems that deeply infiltrate the lining, the local conditions in the lining can vary significantly with position, affecting the degradation as the solubility, phase stability and reaction rates all change with temperature. It is thus essential to directly measure the effect of a temperature gradient on the degradation for this type of slags.

To investigate the effect of a temperature gradient on an infiltrated refractory sample a new setup is developed, based on an experimental setup typically used for freeze lining experiments [6-15] consisting of a water or air cooled probe, where the flow rate can be used to control the temperature at the probe side. In this paper a refractory sample is placed between the cooling probe and the liquid slag bath, thereby creating a temperature gradient over the refractory sample. This approach differs from the experimental setup currently used by Kaneko et al. [16-18] where a refractory sample is partially put in the hot zone of a furnace while the bottom of the refractory is kept in a colder part of the furnace resulting in a temperature gradient over the sample. A hole is drilled in the part of the sample in the hot zone and filled with slag. The main differences between this setup and the one used in this work are the ability of the latter to quench the samples after the experiment, the large slag volume in contact with the refractory sample and the ability to control the cold face temperature by the gas flow (and thus also the gradient).

This new setup is used to investigate the effect of a temperature gradient on the infiltration behavior and the phase formation inside a porous magnesia-chromite refractory sample in contact with a synthetic PbO-SiO_2-MgO slag. PbO systems are known to deeply infiltrate the sample and previous research [19] studied the behavior of such a PbO-SiO_2-MgO slag in contact with the same refractory brick under isothermal conditions. The goal of this work is to determine the effect of the temperature gradient on the infiltration behavior of the slag, the formation of reaction phases and the modification in slag composition.

7.2 Experimental procedure

The refractory samples were tested under a temperature gradient using a newly designed experimental setup, shown in Figure 7.1. It consists of a refractory sample, a cooling probe and a crucible containing liquid slag. The cylindrical refractory samples, having a diameter of 30 mm and a height of

70 mm, were machined out of commercially available fused grain rebonded magnesia-chromite bricks. The global composition, detailed description of the microstructure and the composition of all the present phases have been previously described by the present authors [19]. In the center of the samples a cylindrical hole was drilled with a diameter of 10 mm and a depth of 60 mm. In this hole a cold finger probe was inserted and fixed to the refractory using castable alumina, thereby also ensuring no air is left between the refractory sample and the cooling probe, as this would drastically decrease the heat removal to the probe. The cooling probe consists of two concentric stainless steel tubes; the external tube has a diameter of 9.5 mm (3/8 inch) and is closed at the bottom while the interior tube has a diameter of 6.35 mm (1/4 inch). Air was blown at a flow rate of 100l/h through the interior tube and released through the gap between both tubes, thereby removing heat from the probe surface and cooling the refractory sample. The obtained temperature gradient was measured at 3 different positions: (1) in a groove in the surface of the cooling probe, (2) midway inside the refractory sample (5 mm from the cooling probe surface) and, finally, (3) in a groove in the surface of the refractory sample in contact with the liquid slag. All the thermocouples were placed at a depth of 4 cm (taken from the top of the sample). 5 mm from the hot face, this required the creation of a hole to place the thermocouple in. Because of the depth it was impossible to have the same thickness as the thermocouple. The diameter of the created hole was approximately 2 mm. The thermocouples were positioned non-collinear to ensure that the measurements did not influence each other. The local replacement of refractory phases by a hole and thermocouple with a different conductivity and heat capacity could otherwise influence the other temperature measurements. For the same reason the sample taken for investigation of the microstructure was taken at the opposite side of the sample to the thermocouples.

The PbO-SiO_2-MgO slag was produced by mixing pure oxides (Alfa Aesar, purity level of 99.9 wt%) powders in the desired ratio (54 mole% PbO, 41 mole% SiO_2 and 5 mole% MgO) to a total weight of 3 kg. It was heated in open air at a rate of 40 °C/hour in an MgO crucible using a resistance furnace until a temperature of 1100 °C was reached. After 1100 °C was obtained, the refractory sample, attached to the cold finger probe, was slowly lowered into the furnace. It was kept above the liquid bath for at least 30 min while air was blown through the probe, creating a temperature gradient over the sample before the sample was partially submerged into

the liquid slag bath. After the required reaction time the sample was taken out of the bath and quenched in water to preserve the high temperature microstructure and composition. The time between removal of the sample from the liquid bath and quenching was approximately 2-3 s. Three different reaction times were tested: 15 min, 1 h and 2.5 h.

After the experiment a sample was taken from the refractory finger for microstructural investigation. The location of sampling is shown in Figure 7.1. Before this sample was analyzed it was embedded in an epoxy resin and polished. After coating the sample with a conducting carbon layer, both its microstructure and the composition of the different phases were analyzed using a fully quantitative EPMA-WDS (JEOL JXA-8530F) system. It was operated using an acceleration voltage of 15 kV and a probe current of 15 nA. The oxygen content was not measured directly; instead the oxidation state of the element was selected a priori. Although both Fe^{2+} and Fe^{3+} can be present in the sample under consideration here, only "Fe_2O_3" was selected for presentation purposes because the experiments were performed in open air making Fe^{3+} the most likely form of iron in the slag. Inside the chromite spinel phases some Fe^{2+} may still be present.

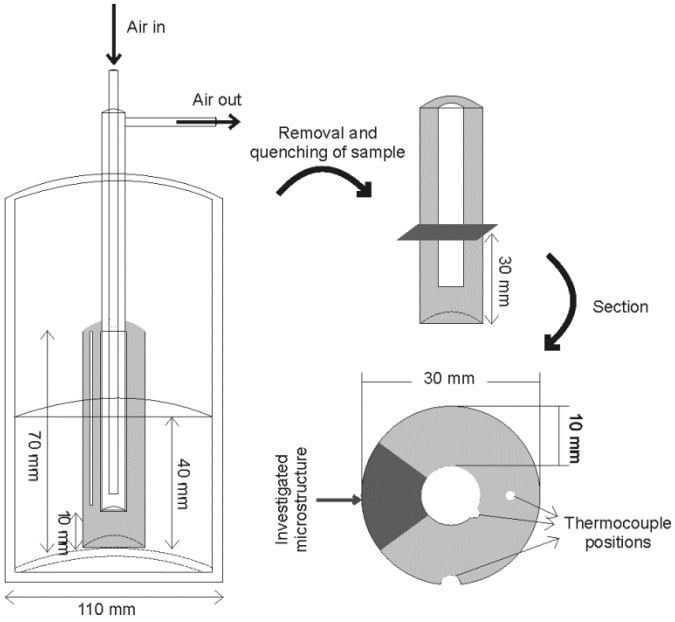

Figure 7.1: Schematic representation of the experimental setup and a top view of the sample showing the position of the thermocouples.

7.3 Results

7.3.1 Temperature measurements

Figure 7.2 shows the variation of the temperature at 3 different positions in the refractory sample as a function of the submersion time. After contact with the slag, the temperature at the slag-sample interface (called the hot face) and 5 mm from the hot face decrease with time, while the temperature at the cooling probe surface increases. All three temperatures level off with time. The average temperatures (taken from 5000 s onwards) during the steady state are: 740 °C for the cold face, 982 °C 5 mm from the hot face and 1078 °C at the hot face.

Using these measured values the temperature throughout the entire sample can be estimated using the heat transport equation, which in cylindrical coordinates (r, φ, z) is given below:

$$\frac{1}{r}\frac{\partial}{\partial r}\left(rk\frac{\partial T}{\partial r}\right)+\frac{1}{r^2}\frac{\partial}{\partial \varphi}\left(k\frac{\partial T}{\partial \varphi}\right)+\frac{\partial}{\partial z}\left(k\frac{\partial T}{\partial z}\right)+\ q_{gen}=\rho c_p\frac{\partial T}{\partial t} \quad (7\text{-}1)$$

Where q_{gen} is the heat generation, k is the heat conductivity, ρ is the density, c_p is the heat capacity, T is the temperature and t is the time. Equation 7-1 can be simplified by only considering the steady state (∂T/∂t=0) and by making the following assumptions: (1) the heat generated (or used) by reactions between the infiltrated slag and the refractory brick is negligible compared to the heat removed by the cooling probe (q_{gen}=0) and (2) the heat conductivity (k) of the sample is independent of temperature. The geometry of the sample can also be used by assuming (3) the sample is homogeneous and the effect of the different phases in the microstructure is thus not taken into account, which for a cylindrical sample means ∂T/∂φ=0. Finally, (4) the sample is considered to be sufficiently long that the temperature in the investigated part of the sample can be considered to be independent of the height (∂T/∂z=0). Equation 7-1 then becomes:

$$\frac{1}{r}\frac{\partial}{\partial r}\left(r\frac{\partial T}{\partial r}\right)=0 \quad (7\text{-}2)$$

Solving of this equation gives the temperature as a function of position:

$$T(r)=C_1\,ln(r)+C_2 \quad (7\text{-}3)$$

Equation 7-3 requires 2 boundary conditions to determine C_1 and C_2. Using the measured steady state temperatures at the hot (T_{HF}) and cold face (T_{CF}) this gives:

$$T(r) = T_{CF} + \frac{T_{HF} - T_{CF}}{ln\left(\frac{r_{HF}}{r_{CF}}\right)} \, ln\left(\frac{r}{r_{CF}}\right) \qquad (7\text{- }4)$$

The measured sample thickness from Figure 7.3 is used as the difference between the cold face radius (r_{CF}=5 mm) and the hot face radius (r_{HF}). The obtained temperature profile is plotted in Figure 7.5 together with the slag measurements at each position.

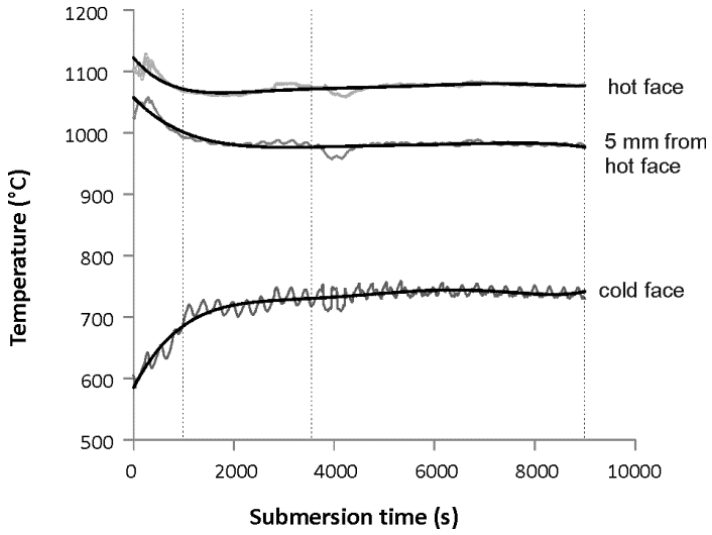

Figure 7.2: Temperature data at different positions in the sample. The bath temperature was kept at 1100 °C. The curves in black are fitted polynomials (order 5) for the experimentally obtained data (shown in gray). The dotted vertical lines indicate the times when samples were taken.

7.3.2 Microstructure

Figure 7.3 shows a cross section of the microstructure from the liquid bath (hot face) to the cooling probe (cold face) as well as detailed images at different positions inside each sample. The liquid slag, seen as the white phase in Figure 7.3, forms a thin layer at the hot face but also infiltrates the refractory samples; only the first 1.5 mm for the 15 min sample, while the samples after 1 h and 2.5 h are both completely infiltrated. The cold face of the 15 min sample is identical to the microstructure of an unreacted fused grain rebonded magnesia-chromite brick, consisting of primary chromite spinel (PC, $[Mg,Fe^{2+}][Cr,Al,Fe^{3+}]_2O_4$) and fused grains (FG), which consist of chromite spinel particles in a periclase (MgO) matrix [1, 20-22]. These phases remain clearly visible inside the infiltrated parts of all samples. The slag infiltrates the pores, which are still clearly visible in the unreacted part of the 15 min sample. Some pores and cracks (C) are also present in the infiltrated part of the brick and are formed either by (1) thermal shock during quenching, (2) mechanical load during sample preparation or (3) were closed off from the slag during infiltration.

Detailed images of the hot face (a-c) show that for all samples forsterite grains are present inside the liquid bath near the refractory sample. Inside the samples this phase also forms grains between the periclase of the fused grains and the liquid slag, but it is not detected in contact with primary or secondary chromite spinel grains. Finally, for the 1 h and 2.5 h samples, melilite (M, $[Ca,Pb]_2[Fe,Mg,Al][Si,Al,Fe]_2O_7$) is detected near the cold phase (between 7-10 mm from the bath). At the same position some forsterite particles are also present, although they are much smaller than the melilite grains.

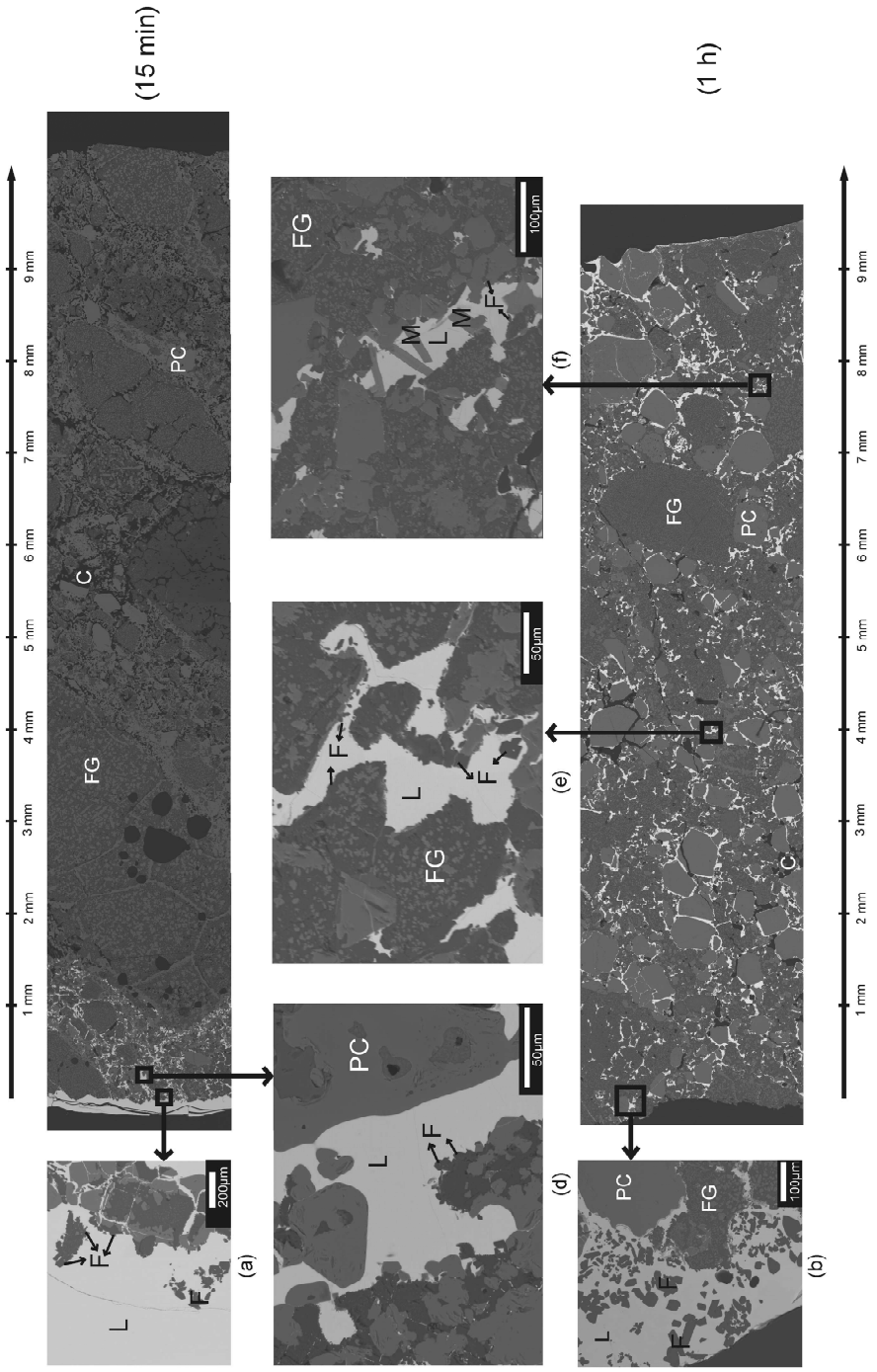
(15 min)
(1 h)
1 mm
2 mm
3 mm
4 mm
5 mm
6 mm
7 mm
8 mm
9 mm
PC
C
FG
L
F
M
200µm
100µm
50µm
(a)
(b)
(d)
(e)
(f)

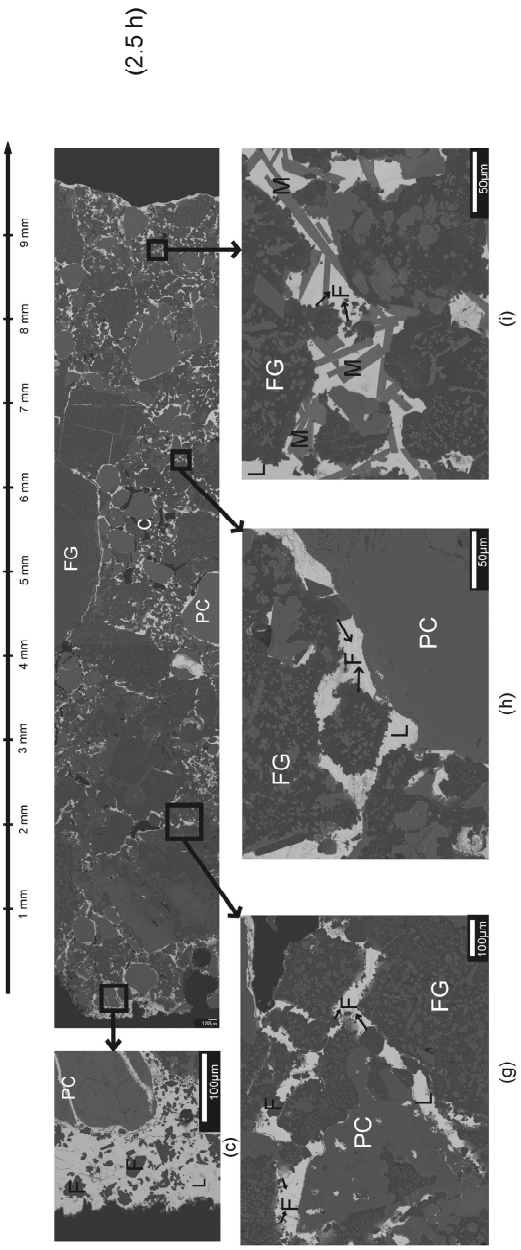

Figure 7.3: BSE images of the microstructure showing a cross section after 15 min, 1 h and 2.5h as well as detailed images at the hot face (a-c) and deeper inside the samples (d-i). With FG: fused grain, PC: primary chromite, L: liquid slag during experiment, C: cracks and pores, F: forsterite and M: melilite.

The forsterite grains at the hot face (Figure 7.3 a-c) appear to be larger than inside the sample and, furthermore, their size appears to increase with time, although quantification of these grains inside the sample is difficult based on the images, because forsterite has the same BSE brightness as periclase. The forsterite amount is therefore determined by WDS mapping of several rectangular areas of 400 µm by 1300 µm, taken between the hot and the cold face of the sample. The first analysis is taken with the center of the measured area at the contact interface between slag and sample with the shortest side of the rectangle in the direction towards the cold face. For the subsequent analyses, the measurement area is always moved an additional 1 mm towards the cold face. For each area a WDS analysis is performed every micron for 10 ms. By analyzing the results at each point it is possible to determine which phase is present: forsterite (when both MgO and SiO_2 are detected), slag (based on the presence of PbO), chromite (when Cr_2O_3 is detected) or periclase (only MgO). Based on this result, the forsterite area fraction is calculated for each measured area.

Most of the detected forsterite formed after reaction between the slag and the refractory sample. The presence of larger grains in the measured area will lead to a lower forsterite area fraction as there is less slag and therefore less reaction leading to new forsterite. As seen in Figure 7.3, the forsterite only formed when the slag is in contact with periclase and not in contact with chromite spinel phases. When a lot of these chromite grains are present in the analyzed area, the detected forsterite amount is also lower. To identify the effect of the temperature gradient and the reaction time on the forsterite formation, the effect of the local microstructure is countered by scaling the forsterite amount to the reaction surface. Only the periclase-slag and forsterite-slag interfaces are taken into account for the reaction surface. The result is given in Figure 7.4, showing that the detected amount of forsterite increases with time and that this increase is larger closer to the hot face of the sample.

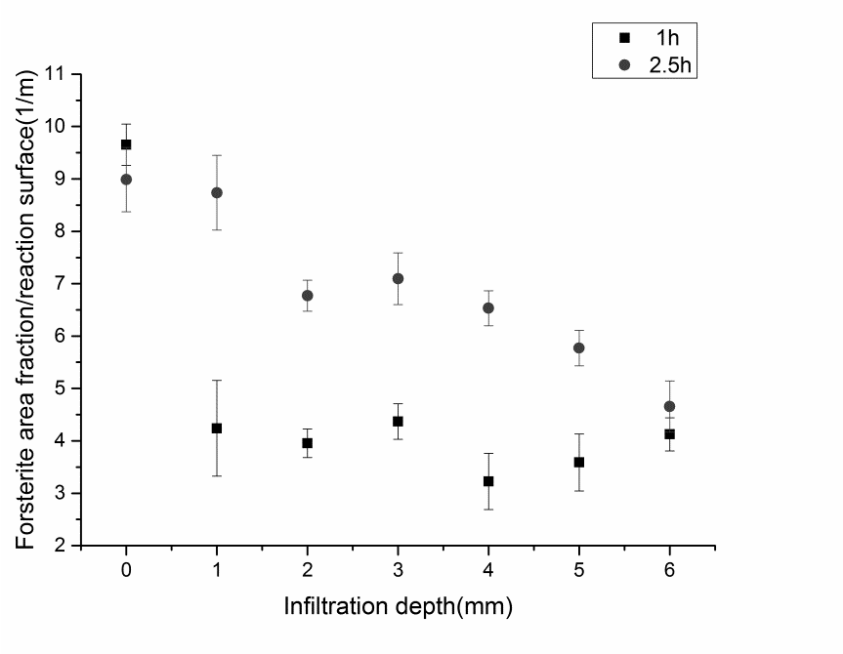

Figure 7.4: The measured amount of forsterite per reaction surface (slag-MgO interface and slag-forsterite interface) for two different reaction times.

7.3.3 Slag composition as a function of position

The composition of the infiltrated slag is measured with EPMA-WDS at different positions inside each sample. Figure 7.5 shows the content of the main slag components (PbO, SiO_2 and MgO) with position inside the sample. The PbO content of the slag varies in the opposite direction with respect to the SiO_2 and MgO content of the slag. The PbO content increases towards the cold face and this increase is most pronounced in the first 1-2 mm of the sample. The PbO content levels off deeper inside the sample, reaching a constant value 3 mm from the hot face. With increasing reaction time this constant value increases. In the final millimeter of the 2.5 h sample, the PbO content decreases again.

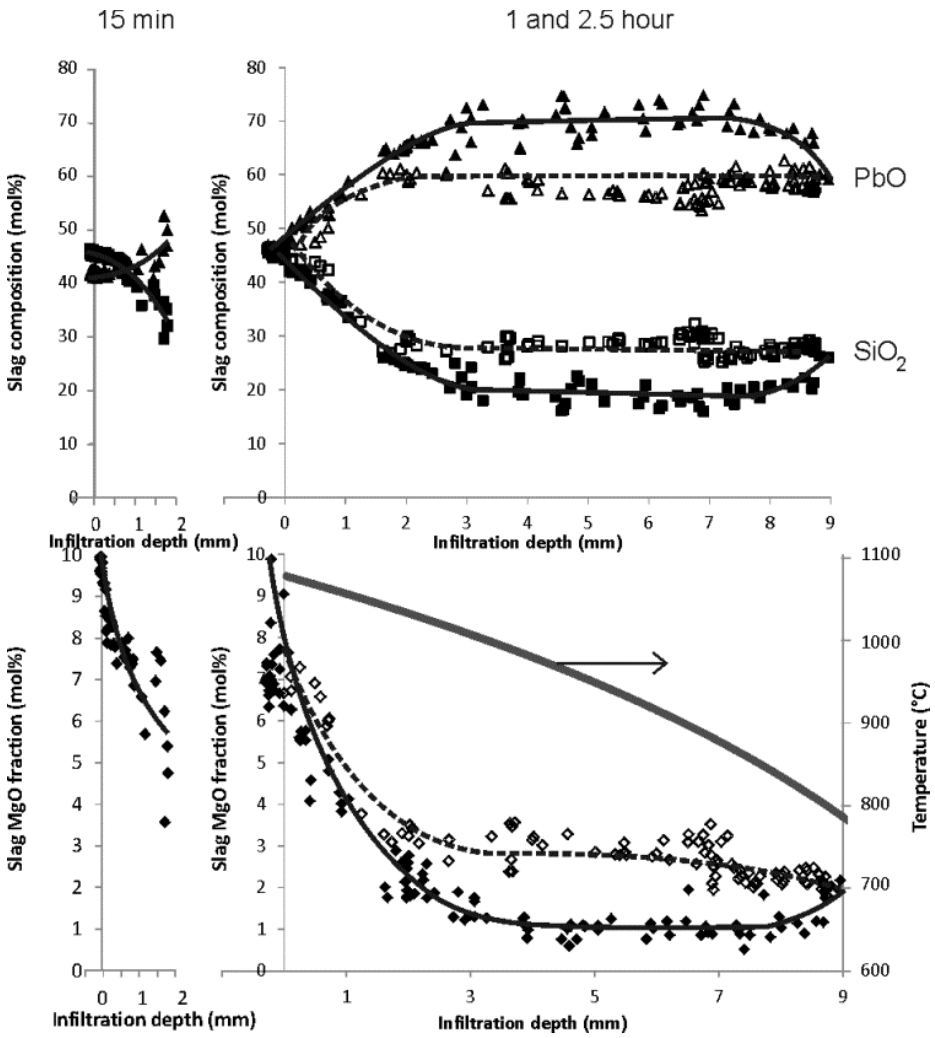

Figure 7.5: Concentration of the major slag components (PbO, SiO_2, MgO) as a function of position and reaction time. (1h open markers and dotted lines and 2.5h filled markers and full lines) obtained using EPMA-WDS.

Figure 7.5 only showed the variation of the main slag components. However, some other components are also detected, which dissolved from the refractory phases into the liquid slag. Due to the large dataset, an average composition is given in Table 7.1. This average has been taken for 1 mm sections, except for the first 3 mm where the average of a 0.5 mm section is taken due to the large change in composition with position. For each section at least 6 points were used to calculate the average. Table 7.1 shows that the concentration of the spinel components (Cr_2O_3, Fe_2O_3 and Al_2O_3) in the liquid slag all increase towards the cold face of the sample.

Table 7.1: Composition of the slag measured using EPMA-WDS and calculated temperature at different positions for the tested reaction times.

			15 min						
Section			MgO	SiO_2	Cr_2O_3	"Fe_2O_3"	PbO	Al_2O_3	CaO
A	bath		9.8	45.7	0.0	0.1	42.0	1.2	1.2
B	0-0.5		8.4	45.4	0.3	0.2	42.0	1.6	2.1
C	0.5-1		7.6	43.2	0.6	0.4	42.5	1.4	4.3
D	1-1.5		6.7	38.2	1.2	1.0	43.3	1.6	8.0
E	1.5-2		5.5	33.9	2.1	1.2	48.0	1.7	7.5
			1 h						
Section		Calculated temperature	MgO	SiO_2	Cr_2O_3	"Fe_2O_3"	PbO	Al_2O_3	CaO
A	bath	1078	6.7	44.3	0.0	0.1	47.6	0.9	0.4
B	0-0.5	1072	7.0	44.2	0.0	0.2	47.3	0.9	0.4
C	0.5-1	1061	6.3	40.8	0.2	0.7	50.3	1.1	0.6
D	1-1.5	1049	3.8	32.7	0.4	2.2	56.3	3.1	1.5
E	1.5-2	1037	3.2	27.2	0.2	2.9	60.6	3.2	2.7
F	2-2.5	1024	3.3	29.2	0.3	2.8	59.6	2.7	2.2
G	2,5-3	1011	2.9	27.2	0.4	3.4	60.2	2.9	3.0
H	3-4	990	3.0	28.1	0.2	3.5	58.0	3.3	3.9
I	4-5	960	2.5	28.4	0.2	3.5	58.2	3.1	4.1
J	5-6	927	2.8	28.8	0.4	3.6	56.4	3.3	4.6
K	6-7	889	2.5	28.9	0.6	3.7	56.5	3.1	4.7
L	7-8	847	2.4	26.9	0.9	4.1	58.7	3.1	4.0
M	8-9	798	1.7	27.7	1.0	4.3	58.6	2.5	4.1
N	9-9.5	755							

Section		Calculated temperature	2.5 h						
			MgO	SiO_2	Cr_2O_3	"Fe_2O_3"	PbO	Al_2O_3	CaO
A	bath	1078	7.2	45.8	0.1	0.1	46.3	0.3	0.2
B	0-0.5	1072	5.7	41.5	0.2	0.7	50.7	0.8	0.3
C	0.5-1	1061	4.4	36.8	0.6	1.1	55.3	1.3	0.5
D	1-1.5	1049	4.1	33.5	0.1	1.3	58.8	1.3	0.8
E	1.5-2	1037	2.2	25.2	0.3	2.8	64.7	2.2	2.5
F	2-2.5	1024	2.2	24.1	0.3	2.8	66.0	2.1	2.5
G	2,5-3	1011	1.4	21.6	0.7	3.8	68.8	1.6	1.9
H	3-4	990	1.3	20.5	0.8	4.9	68.8	1.7	2.0
I	4-5	960	0.9	18.8	1.0	5.0	70.9	1.6	1.8
J	5-6	927	1.0	19.3	1.1	4.9	69.9	1.7	2.0
K	6-7	889	1.1	17.6	1.1	4.6	71.9	1.6	2.1
L	7-8	847	1.1	19.2	1.2	4.7	70.0	1.6	2.2
M	8-9	798	1.5	22.7	1.5	4.5	64.8	1.9	3.0
N	9-9.5	755	2.3	29.8	1.3	4.3	55.4	2.3	4.5

To achieve a better insight into the mechanisms responsible for the changing slag composition the results from Table 7.1 are projected onto a PbO-SiO_2-MgO phase diagram in Figure 7.6, by rescaling the slag composition in Table 7.1 to only MgO, SiO_2 and PbO. This phase diagram is created using the phase equilibria results for the liquidus lines of the forsterite primary phase field of the PbO-MgO-SiO_2 system obtained from Chen et al. [23] for 3 different temperatures (1100, 1000 and 900 °C). Interpolation of these values gives the liquidus lines for each temperature in Figure 7.6 (full lines). The liquidus lines are further extrapolated using the data from Scheunis et al. [19] (dotted lines). The local temperature in the center of each section is calculated using equation 7-4 and is provided in Table 7.1 making it possible to check how the slag composition varies with position in the sample with respect to the liquidus lines. The slag composition inside the refractory moves towards the PbO corner of the phase diagram with time and infiltration depth, while all points stay on the liquidus lines.

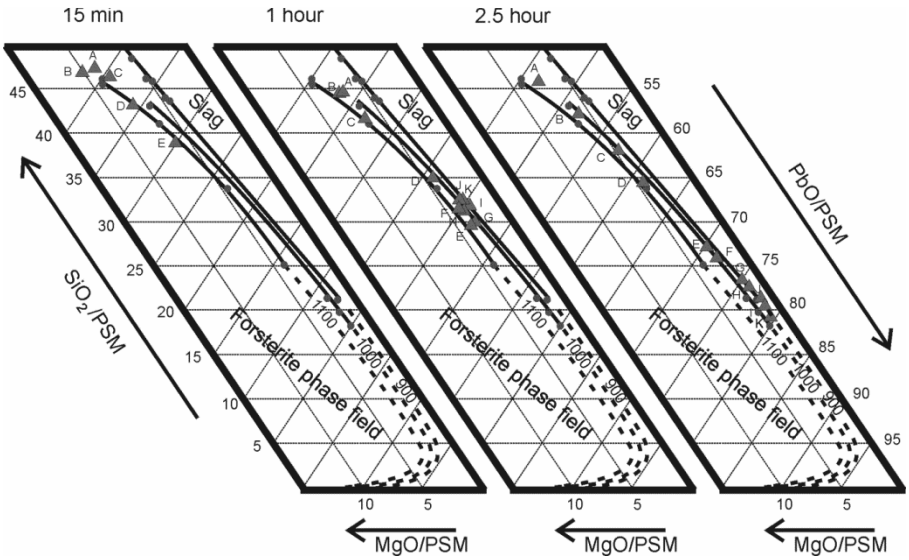

Figure 7.6: Projection of the slag composition in mole % on the PbO-MgO-SiO_2 ternary phase diagram for the different section of the samples given in Table 7.1 at 3 different reaction times (15 min, 1 h and 2.5 h). The liquidus lines at 1100 °C, 1000 °C and 900 °C are interpolated (full lines) and extrapolated (dotted lines) based on the phase equilibria results (●) obtained from Chen et al [23].

7.4 Discussion

To minimize the refractory wear it is vital to understand how the degradation mechanism changes inside the lining. The degradation in the interior of the lining is controlled by local equilibrium [24], which is the equilibrium between the refractory phases and the local slag composition at the local temperature. It is thus essential to know how the slag composition and temperature vary with position. For a sample under a temperature gradient not only the slag composition and temperature, but also the infiltration behavior varies with position and time. The study of these effects is further complicated as they influence each other. Therefore, the local temperature, infiltration behavior and slag composition are discussed separately, starting with the variation in local temperature.

7.4.1 Local temperature

As seen in the microstructural images (Figure 7.3), the slag infiltrates the refractory during the first hour of reaction, while the measured temperature inside the sample varies continuously (Figure 7.2). The temperature variation is, therefore, probably due to a difference in thermal conductivity between the infiltrated and original refractory part of the sample due to the replacement of entrapped air in the pores by more conductive slag. After full infiltration of the sample (1 h reaction time in Figure 7.3) the measured temperatures reach a steady state condition with a smaller temperature difference between the hot and cold face, further supporting the hypothesis that the infiltration of slag causes the thermal conductivity to increase. The local temperature throughout the sample is calculated during this steady state. The simplifications made to do this can be evaluated by comparing the measured (982 °C) and calculated (944 °C) temperature values 5 mm from the hot face. The difference is probably due to two main errors: (1) the assumption of a temperature independent thermal conductivity of the infiltrated refractory is not valid for the large temperature range between the hot and cold face of the sample and, probably the most important effect is (2) the size of the hole for the thermocouple at 5 mm from the hot face which as a diameter of approximately 2 mm. A variation of 1.5 mm already causes the calculated temperature to increase to 990 °C the 944 °C calculated at 5 mm from the hot face.

7.4.2 Slag composition

The slag composition is a function of the infiltration behavior and the local temperature. A slow infiltration rate leads to a longer reaction time between slag and refractory before the slag infiltrates deeper into the lining, while the temperature controls the thermodynamics and kinetics of all reactions. The local slag composition (Figure 7.5) and the detected forsterite content (Figure 7.4) are therefore closely related. For the studied system, the slag composition changes due to removal of SiO_2 by the formation of forsterite:

$$2MgO_{ref} + SiO_{2slag} \rightarrow Mg_2SiO_{4ref} \quad (7\text{-}5)$$

This reaction continues until equilibrium is reached between the slag, forsterite and periclase phases. Based on Figure 7.6, the slag equilibrium composition is not reached for any of the measurements. From a thermodynamic point of view, reaction 7.5 will therefore continue. This

explains why the detected forsterite amount increases with time, while the SiO_2 decreases. This change is most pronounced near the hot face where the local temperature and thus the reaction rate is higher.

Based on the PbO-SiO_2-MgO phase diagram (Figure 7.6), the MgO content in the liquid slag follows the liquidus lines, indicating that the liquid is in equilibrium with the newly formed forsterite. Deviations from the liquidus lines can be caused by (1) imperfect quenching of the sample, due to its large size, (2) the effect of the minor components (see Table 7.1), which up till now has been neglected or (3) the limited size of the measurement areas in the sample (1–5 µm), leading to some overlap of the X-ray excitation volume during the EPMA measurements with the surrounding (MgO rich) phases.

7.4.3 Infiltration behavior

The infiltration behavior is controlled by both the slag composition and the local temperature. For an isothermal non-reactive liquid the infiltration depth increases with √t, according to the following equation [25]:

$$l = \sqrt{\frac{r\sigma \cos\theta t}{2\eta}} \tag{7-6}$$

Where l is the infiltration depth, r is the pore radius, σ is the surface tension of the liquid slag, θ is the contact angle between the liquid slag and the refractory, t is the reaction time and η is the viscosity of the liquid slag.

Without reaction, the presence of a temperature gradient will increase the viscosity of the liquid deeper inside the sample, thereby slowing down the infiltration rate compared to the isothermal case. Most slag systems, however, react with the refractory, changing the liquid composition. Two cases can be identified based on the slag components being removed: (A) the reaction between the liquid and the refractory phases hinders further infiltration [25] or (B) the change in liquid composition accelerates the infiltration [19].

Figure 7.7 shows the time dependency of the infiltration depth as well as the variation of the viscosity with position, with and without the presence of external cooling. For an isothermal, non-reactive slag the viscosity remains constant over the entire sample. According to equation 7-6 the infiltration depth thus increases with √t. The slag's viscosity increases exponentially with the inverse temperature. The infiltration of the slag will

therefore go much slower in a gradient and will also stop before full infiltration of the sample when the slag solidifies inside the sample.

When the slag reacts with the refractory phases, components are selectively removed from the infiltrating liquid, rendering the slag composition a function of the infiltration depth. When this reaction leads to an increase of the slag's viscosity (case A) with depth, the infiltration rate will be slower than for a non-reactive slag system. The additional application of a temperature gradient will increase the viscosity even further resulting in an even slower infiltration behavior.

Finally, the reaction can lower the slag viscosity (case B), leading to a faster slag infiltration compared to a non-reactive system. A temperature gradient will increase the viscosity and decrease the infiltration rate, although the rate may still be higher than the isothermal non-reactive case, if the effect of reaction has a bigger influence on the viscosity than the temperature. Towards the cold face the changes in the slag composition will be limited, due to the slower kinetics, and the change in viscosity is dominated by the temperature. It is therefore still possible to stop the infiltration of the slag if the temperature gradient is sufficiently large.

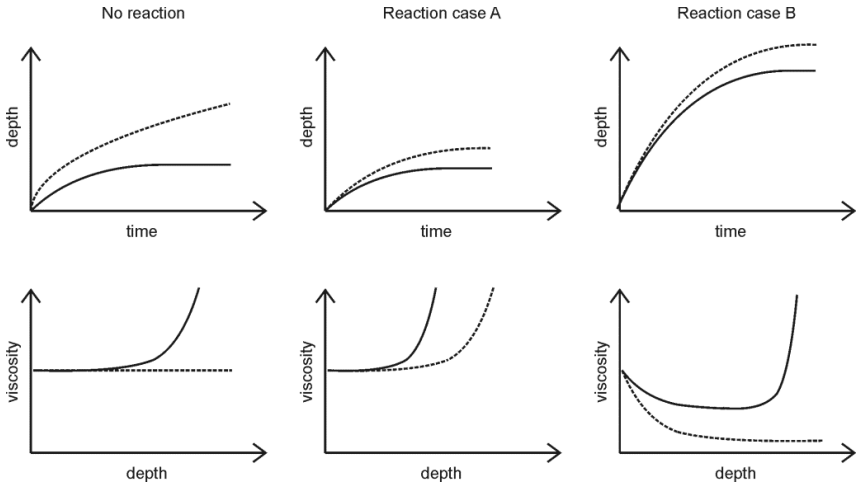

Figure 7.7: Conceptual description of the effect of a temperature gradient on the infiltration depth with time for three different slag systems: (1) without reaction with the refractory phases, (2) reaction with the refractory phases hindering further infiltration and (3) reaction accelerating infiltration of the liquid. For all three cases the isothermal situation (dotted lines) is compared to the situation when a temperature gradient is applied (full lines).

The viscosity of the liquid slag as a function of depth for all samples is calculated based on data used by [26] and given in Figure 7.8. Despite the decreasing temperature, the viscosity significantly drops in the first 2 mm of the sample due to the changing liquid composition. At the cold face the viscosity increases again due to the limited change in slag composition and is thus controlled by the decrease in temperature. This matches reaction case B discussed in Figure 7.7. With time the reaction between the refractory phases and the liquid continues, causing the slag composition to change, in turn leading to a drop in viscosity from 1 h to 2.5 h reaction time.

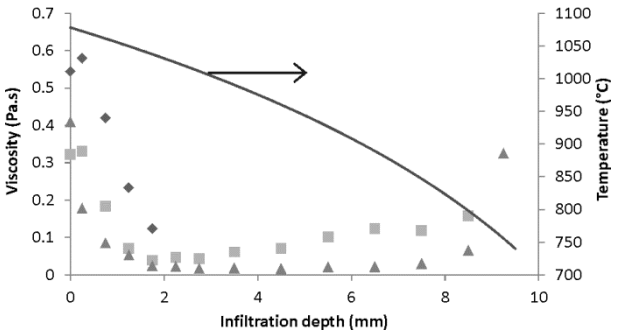

Figure 7.8: The temperature and viscosity for 3 reaction times (♦: 15 min, ■:1 h and ▲: 2.5 h) as a function of the distance from the slag-refractory interface. The calculations are done using the FactSage viscosity module [27, 28] based on the average composition and temperature given in Table 7.1.

Equation 7-6 shows that the infiltration behavior depends on several slag properties (viscosity, surface tension and contact angle with the refractory phases), all changing with slag composition. For the studied PbO-SiO_2-MgO slag, the infiltration depth is calculated for the minimum and the maximum values for each slag property, while all other parameters in equation 7-6 are kept constant. In this way the relative significance of the slag properties on the infiltration behavior can be determined. The viscosity varies between 0.579 Pa.s (0.25 mm from the hot face after 15 min) and 0.039 Pa.s (2 mm from the hot face after 1 h), resulting in a ratio of 3.9 for both infiltration rates. To estimate the effect of the surface tension of the slag, the available data for the PbO-SiO_2 system at 850 °C is used [29]. The PbO content of the slag varies between 50 mole% (218.6 10^{-3} N/m) up to 70 mole% (175.2 10^{-3} N/m), resulting in a ratio of 1.1 for the infiltration rate. For the contact angle (θ) no data are available. Because the slag completely wets the pores

for all compositions (as seen in Figure 7.3), cos θ can be considered close to 1, which is a common assumption in refractory research [4]. No large influence on the infiltration behavior is therefore expected. The slag viscosity significantly influences the infiltration behavior. To a first approximation the infiltration behavior can be studied by only considering the effect of the viscosity. The studied PbO-SiO_2 slag system is clearly an example of a case B reaction discussed in Figure 7.7.

Equation 7-6 is only valid if all parameters remain constant during the reaction. A more accurate description of the infiltration behavior of the liquid slag requires the solution of the following equation:

$$\frac{dl}{dt} = \frac{r\sigma \cos\theta}{4\eta l} \tag{7-7}$$

Using equation 7-7, the increase in infiltration depth (Δl) is determined after each time step (Δt) using the local values for the viscosity (η), contact angle (θ) and surface tension (σ). All these parameters, however, depend on both the liquid composition and the local temperature. To determine the temperature distribution for a partially infiltrated sample, the heat equation (equation 7-1) has to be solved which requires the thermal conductivity of an infiltrated brick, which, to the best of the authors' knowledge, is not available. Predicting the local slag composition is also impossible as both the reaction kinetics of the phase formation, causing the compositional change, and the local temperature are unknown. Due to these practical difficulties, a full description of the infiltration as a function of time has not been performed.

7.4.4 Effect of external cooling on chemical degradation

External cooling is applied in industrial furnaces to limit refractory wear by (1) reducing the dissolution of the refractory components in the slag, (2) freezing the slag in the lining and thus reducing the exposed part of the lining and (3) by lowering the reaction kinetics, reducing the densification by new phases being formed. Each of these three effects is discussed below for the studied PbO-SiO_2-MgO system.

The MgO content of the liquid slag decreases towards the cold face of the sample (Figure 7.5). According to the PbO-SiO_2-MgO phase diagram (Figure 7.6) the decrease in MgO solubility of the liquid can be due to both a lower temperature and/or a lower SiO_2 content in the liquid. By comparing the results in Figure 7.5 with those from an isothermal study on the interaction between a PbO-SiO_2 slag and a refractory sample [19], it is seen that the

MgO content of the liquid decreases faster and closer to the hot face for the isothermal case. The faster SiO_2 removal (by faster forsterite formation) thus appears to have a larger effect on the MgO solubility than the decreasing temperature.

The infiltration rate decreases due to the applied temperature gradient, but this effect is (partially) countered by the change in liquid composition over time. Eventually the decreasing temperature will freeze the slag inside the refractory lining. The isothermal study showed that the slag reaches a composition of almost pure PbO in the interior of the sample after 15 min reaction time. Based on the result for this isothermal case, one would expect the slag in a temperature gradient to freeze below the melting point of PbO (880 °C). This is, however, not the case in the performed experiment. Due to the lower temperatures (and slower kinetics) towards the cold face, the liquid does not remove all the SiO_2 before the infiltration is arrested and the slag will only freeze at its lowest eutectic temperature (717 °C for a 25 mole% SiO_2-75 mole% PbO slag [30]). The temperature when the liquid freezes, thus, depends on the liquid composition, which in turn, depends on the slag composition and, hence, on the SiO_2 removal. The SiO_2 in turn depends on the forsterite growth (which depends on the temperature) and the specific reaction surface (which depends on the pore size distribution).

The application of external cooling clearly lowers the kinetics (Figure 7.5) and thus the forsterite formation (Figure 7.4) and the densification this may cause. The presence of large amounts of forsterite can lead to failure of the lining, a mechanism referred to as forsterite bursting [31]. The risk for forsterite bursting therefore decreases when external cooling is applied.

The interaction between a synthetic PbO-SiO_2-MgO slag and a magnesia-chromite refractory sample has previously been studied under isothermal conditions [19], showing the same forsterite formation as in this paper. For both the isothermal and temperature gradient experiments the SiO_2 content decreased towards the center of the sample due to this forsterite formation. For the isothermal case, the SiO_2 content of the slag reaches a value of 5 mole% in the center of the sample, considered to be the equilibrium concentration of the slag in contact with periclase and forsterite. At lower temperatures, the SiO_2 equilibrium concentration in the slag will be even lower. Figure 7.6 clearly shows that this low SiO_2 content has

not been reached yet and the formation of forsterite is expected to continue.

7.5 Conclusion

A newly developed experimental setup has been used to examine the effect of a temperature gradient on the reaction between a synthetic PbO-SiO_2 slag and a porous magnesia-chromite brick. Based on the results the following conclusions can be drawn:

- The temperature inside the sample changes with infiltration depth of the liquid. The replacement of air in the pores by more conductive slag increases the thermal conductivity of the infiltrated part of the sample. As the infiltration progresses the difference in thermal conductivity between the infiltrated and original part of the lining leads to a continuous temperature variation in the sample. After full infiltration, the temperature gradient remains constant, but is less steep compared to the original sample.
- The reaction between the slag and the refractory changes with temperature. Higher temperatures lead to faster kinetics of forsterite formation, and thus faster SiO_2 removal from the liquid slag, while in the cooler part of the sample both the phase formation and change in slag composition occur more slowly.
- The infiltration rate changes with slag composition and temperature. At the hot face the effect of the slag compositional change is most dramatic, decreasing the SiO_2 content in the liquid slag and leading to a drop in the liquid's viscosity. Near the cold face the removal of SiO_2 is limited and the change in viscosity is determined by the decreasing temperature.

Whether the applied gradient has a beneficial effect on the refractory lifetime depends on the studied slag system and on the dominant refractory degradation mechanisms causing the wear. For the studied PbO-SiO_2 slag, applying a temperature gradient limits densification in the lining but also leads to a relatively high MgO solubility of the liquid slag near the hot face, as the removal of SiO_2 is hindered by slower kinetics inside the sample.

References

1. Malfliet, A., Lotfian, S., Scheunis, L., Petkov, V., Pandelaers, L., Jones, P.T., and Blanpain, B., *Degradation mechanisms and use of refractory linings in copper production processes: A critical review.* Journal of the European Ceramic Society, 2014. **34**(3): p. 849-876.
2. Gregurek, D., Majcenovic, C., Spanring, A., and Kirschen, M., *Wear phenomena of basic brick linings in the copper industry*, in *Copper*2013: Santiago de Chile. p. 473-484.
3. Braulio, M.A.L., Zinngrebe, E.W., van der Laan, S.R., and Pandolfelli, V.C., *Steel ladle well block post mortem analysis.* Ceramics International, 2012. **38**(2): p. 1447-1462.
4. Lee, W. and Zhang, S., *Melt corrosion of oxide and oxide–carbon refractories.* International Materials Reviews, 1999. **44**(3): p. 77-104.
5. Gregurek, D., Ressler, A., Reiter, V., Franzkowiak, A., Spanring, A., and Prietl, T., *Refractory wear mechanisms in the nonferrous metal industry: testing and modeling results.* JOM: The Journal of The Minerals, Metals & Materials Society (TMS), 2013. **65**(11): p. 1622-1630.
6. Campforts, M., Blanpain, B., and Wollants, P., *The importance of slag engineering in freeze-lining applications.* Metallurgical and Materials Transactions B-Process Metallurgy and Materials Processing Science, 2009. **40**(5): p. 643-655.
7. Campforts, M., Jak, E., Blanpain, B., and Wollants, P., *Freeze-lining formation of a synthetic lead slag: Part I. Microstructure formation.* Metallurgical and Materials Transactions B-Process Metallurgy and Materials Processing Science, 2009. **40**(5): p. 619-631.
8. Campforts, M., Jak, E., Blanpain, B., and Wollants, P., *Freeze-lining formation of a synthetic lead slag: Part II. Thermal history.* Metallurgical and Materials Transactions B-Process Metallurgy and Materials Processing Science, 2009. **40**(5): p. 632-642.
9. Campforts, M., Verscheure, K., Boydens, E., Van Rompaey, T., Blanpain, B., and Wollants, P., *On the mass transport and the crystal growth in a freeze lining of an industrial nonferrous slag.* Metallurgical and Materials Transactions B-Process Metallurgy and Materials Processing Science, 2008. **39**(3): p. 408-417.

10. Campforts, M., Verscheure, K., Boydens, E., Van Rompaey, T., Blanpain, B., and Wollants, P., *On the microstructure of a freeze lining of an industrial nonferrous slag.* Metallurgical and Materials Transactions B-Process Metallurgy and Materials Processing Science, 2007. **38**(6): p. 841-851.
11. Verscheure, K., Campforts, M., Verhaeghe, F., Boydens, E., van Camp, M., Blanpain, B., and Wollants, P., *Water-cooled probe technique for the study of freeze lining formation.* Metallurgical and Materials Transactions B-Process Metallurgy and Materials Processing Science, 2006. **37**(6): p. 929-940.
12. Fallah-Mehrjardi, A., Hayes, P.C., and Jak, E., *Investigation of freeze lining in copper-containing slag systems: Part III. High-temperature experimental investigation of the effect of bath agitation.* Metallurgical and Materials Transactions B-Process Metallurgy and Materials Processing Science, 2013. **44**(6): p. 1337-1351.
13. Fallah-Mehrjardi, A., Hayes, P.C., and Jak, E., *Investigation of freeze-linings in copper-containing slag systems: Part I. Preliminary experiments.* Metallurgical and Materials Transactions B-Process Metallurgy and Materials Processing Science, 2013. **44**(3): p. 534-548.
14. Fallah-Mehrjardi, A., Hayes, P.C., and Jak, E., *Investigation of freeze linings in copper-containing slag systems: Part II. Mechanism of the deposit stabilization.* Metallurgical and Materials Transactions B-Process Metallurgy and Materials Processing Science, 2013. **44**(3): p. 549-560.
15. Jansson, J., Taskinen, P., and Kaskiala, M., *Freeze-lining formation in continuous converting calcium ferrite slags. I.* Canadian Metallurgical Quarterly, 2013. **53**(1): p. 1-10.
16. Kaneko, T.K., Bennett, J.P., and Sridhar, S., *Effect of temperature gradient on industrial gasifier coal slag infiltration into alumina refractory.* Journal of the American Ceramic Society, 2011. **94**(12): p. 4507-4515.
17. Kaneko, T.K., Zhu, J., Howell, N., Rozelle, P., and Sridhar, S., *The effects of gasification feedstock chemistries on the infiltration of slag into the porous high chromia refractory and their reaction products.* Fuel, 2014. **115**: p. 248-263.
18. Kaneko, T.K., Zhu, J., Thomas, H., Bennett, J.P., and Sridhar, S., *Influence of oxygen partial pressure on synthetic coal slag infiltration into porous Al_2O_3 refractory.* Journal of the American Ceramic Society, 2012. **95**(5): p. 1764-1773.
19. Scheunis, L., Fallah Mehrjardi, A., Campforts, M., Jones, P.T., Blanpain, B., and Jak, E., *The effect of phase formation during use*

on the chemical corrosion of magnesia–chromite refractories in contact with a non-ferrous PbO–SiO_2 based slag. Journal of the European Ceramic Society, 2014. **34**(6): p. 1599-1610.

20. Jones, P.T., Vleugels, J., Volders, I., Blanpain, B., Van der Biest, O., and Wollants, P., *A study of slag-infiltrated magnesia-chromite refractories using hybrid microwave heating.* Journal of the European Ceramic Society, 2002. **22**(6): p. 903-916.
21. Jones, P.T., Desmet, D., Guo, M., Durinck, D., Verhaeghe, F., Van Dyck, J., Liu, J., Blanpain, B., and Wollants, P., *Using confocal scanning laser microscopy for the in situ study of high-temperature behaviour of complex ceramic materials.* Journal of the European Ceramic Society, 2007. **27**(12): p. 3497-3507.
22. Jones, P.T., Blanpain, B., Wollants, P., Ding, R., and Hallemans, B., *Degradation mechanisms of magnesia-chromite refractories in vacuum-oxygen decarburisation ladles during production of stainless steel.* Ironmaking & Steelmaking, 2000. **27**(3): p. 228-237.
23. Chen, S., Zhao, B., Jak, E., and Hayes, P.C., *Experimental study of phase equilibria in the PbO-MgO-SiO_2 system.* Metallurgical and Materials Transactions B-Process Metallurgy and Materials Processing Science, 2001. **32**(1): p. 11-16.
24. Lee, W.E., Argent, B.B., and Zhang, S.W., *Complex phase equilibria in refractories design and use.* Journal of the American Ceramic Society, 2002. **85**(12): p. 2911-2918.
25. Mukai, K., Tao, Z., Goto, K., Li, Z., and Takashima, T., *In-situ observation of slag penetration into MgO refractory.* Scandinavian Journal of Metallurgy, 2002. **31**(1): p. 68-78.
26. Kim, W.-Y., Pelton, A., and Decterov, S., *Modeling the viscosity of silicate melts containing lead oxide.* Metallurgical and Materials Transactions B, 2012. **43**(2): p. 325-336.
27. Bale, C.W., Chartrand, P., Degterov, S.A., Eriksson, G., Hack, K., Ben Mahfoud, R., Melancon, J., Pelton, A.D., and Petersen, S., *FactSage thermochemical software and databases.* Calphad-Computer Coupling of Phase Diagrams and Thermochemistry, 2002. **26**(2): p. 189-228.
28. Bale, C.W., Belisle, E., Chartrand, P., Decterov, S.A., Eriksson, G., Hack, K., Jung, I.H., Kang, Y.B., Melancon, J., Pelton, A.D., Robelin, C., and Petersen, S., *FactSage thermochemical software and databases - recent developments.* Calphad-Computer Coupling of Phase Diagrams and Thermochemistry, 2009. **33**(2): p. 295-311.

29. Kuromitsu, Y., Yoshida, H., Takebe, H., and Morinaga, K., *Interaction between alumina and binary glasses.* Journal of the American Ceramic Society, 1997. **80**(6): p. 1583-1587.
30. Jak, E., Hayes, P.C., Degterov, S., Pelton, A.D., and Wu, P., *Thermodynamic optimization of the systems PbO-SiO_2, PbO-ZnO, ZnO-SiO_2 and PbO-ZnO-SiO_2.* Metallurgical and Materials Transactions B, 1997. **28**(6): p. 1011-1018.
31. Gregurek, D., Majcenovic, C., Spanring, A., and Kirschen, M., *Forsterite bursting in magnesia chromite bricks - two case studies from lead and copper smelting furnaces.* RHI Bulletin, 2011(2): p. 49-53.

Chapter 8 Conclusions and future work

8.1 Conclusions

This work investigated the chemical degradation of magnesia-chromite bricks in contact with PbO-containing slags to identify methods to mitigate the refractory wear rate caused by slag attack. This chemical degradation can be controlled by changing the properties of either the slag or the brick. The literature review showed that the fused grain rebonded magnesia-chromite bricks, used in this work, are the most resistant to chemical degradation. Hence improvements to limit the refractory wear require modification of the slag composition.

Labscale experiments and synthetic slag systems are used determine how the modifications in slag composition influence specific degradation mechanisms.

Experimental data indicate that the chemical wear caused by PbO-SiO_2 containing slags is due to two main degradation mechanisms: (1) the much deeper infiltration of the liquid slag compared to other slag systems and (2) the dissolution of MgO from the refractory sample into the liquid slag. In this work different slag compositions were studied to minimize each of these mechanisms separately.

By using a slag that is saturated in spinel components, a protective spinel layer is formed on the entire hot face of the sample leading to a significant reduction of the dissolution rate of MgO from the refractory sample into the liquid slag. Dissolution of the refractory brick into the bath is only possible when MgO can diffuse through the newly-formed spinel phase. This mechanism is significantly slower than the diffusion through the liquid slag phase, when the refractory phases are in direct contact with the liquid bath.

Unfortunately, this protective layer does not form throughout the entire sample. Because of previous reactions between the infiltrating slag and the refractory phases, the spinel forming components are selectively removed from the liquid during its infiltration into the porous sample. When insufficient spinel forming components remain in the liquid the spinel phase

no longer forms, leading to direct contact between the liquid slag and the refractory phases. This, in turn, results in an increase in the MgO dissolution in the interior of the brick compared to the hot face.

The second main cause for chemical degradation is the deep infiltration associated with PbO slags. The strategy used in this work to stop this deep infiltration is to seal off the open pores of the refractory brick before the slag can infiltrate the brick completely. This is done by forming new phases in the pores by reaction between the infiltrating liquid and the refractory phases. A PbO-SiO_2 slag has been selected in order to form forsterite (Mg_2SiO_4) as the phase sealing off the open pores. Unfortunately, the infiltration rate of the liquid is higher than the forsterite phase formation rate, leading to complete infiltration of the sample before the open pores are sealed off by the newly formed forsterite. Once the forsterite seals the pores, the interior of the brick is physically separated from the bath. Over time an equilibrium situation occurs in the interior of the brick, ceasing any further chemical reaction in this part of the brick. This finding is particularly relevant for industrial furnaces or reactors which operate at a more or less constant temperature. In this case the degradation of the lining is dominated by chemical corrosion and not by thermally-induced wear and the formation of forsterite can be used to limit the chemical degradation in the interior of the lining, with a limited risk of forsterite bursting due to temperature variations.

The last method used to slow down the chemical degradation consists of applying a temperature gradient over the refractory sample to slow down the infiltration rate and allow more time to form sealing phases at the hot face. To study this, a new experimental setup was developed capable of applying the desired temperature gradient. The gradient did slow down the infiltration rate, which is primarily controlled by the viscosity of the liquid. The forsterite formation is also slowed down due to the lower temperatures. The decrease in SiO_2, due to the formation of forsterite, however, leads to a lower viscosity. This effect is more important than the temperature difference leading to a faster infiltration once the sealing phases are formed. This means that the sample is completely infiltrated before the open pores are closed by the formation of forsterite.

8.2 Future work

The following suggestions for future work are made:

- Investigation of the possibility a two slag approach, where the first slag is used solely during the first run after each relining. The first contact between the new bricks and this slag can thus be used to seal off the pores. After this initial run a second slag system can be used, modified to form a protective layer, leading to indirect dissolution. By the combination of both slags, it is possible to limit both the chemical degradation in the interior of the brick (by sealing off the pores) and at the hot face (by forming the protective layer) of the sample. However, this approach still requires additional research, specifically to determine the effect of the interaction between both slags. When the second slag comes into contact with the slag still present in the pores, this can change the liquid composition at the hot face, in turn affecting the formation of the protective layer. Over time the slag composition in the pores will change to the composition of the second slag, possibly leading to the dissolution of the blocking phases. To use this two slag approach it is therefore vital that the interaction between both slags is understood and that this is taken into account when selecting the compositions of both slags.

- Investigate the influence of pO_2 variation on the refractory wear. In bath processes the pO_2 can vary during the campaign, affecting the chemical wear of the lining. The stability of the protective spinel layer, for example, depends on the oxidation state of the iron in the slag, which in turn depends on the applied pO_2. Reducing the pO_2 during the use of the reactor can thus result in the disappearance of the protective spinel layer, significantly affecting the chemical wear of the lining.

- Investigate the effect of temperature variation on the refractory wear. The temperature in a reactor can vary. An increase in temperature has a direct influence on the stability of the protective layer but also on the solubility of the refractory components in the liquid bath.

- Linking the interior of degradation of the brick to the thermo-mechanical behavior of the lining. It is known that the chemical attack results in a modification of the microstructure and thus in a deterioration of the properties of the brick, increasing the spalling risk. However, up till now a quantification of the change in brick properties has not been performed yet. Determine the effect of the chemical reaction on the thermal expansion, thermal conductivity, stiffness and strength of the brick will make it possible to model the influence of chemical interaction on thermo-mechanical failure, leading to a better understanding of the synergetic effect between the different degradation mechanisms.

List of publications

International academic journal papers

Published

Scheunis L., Campforts M., Jones P.T., Blanpain B., Malfliet A. (2015). The influence of slag compositional changes on the chemical degradation of magnesia-chromite refractories exposed to PbO-based non-ferrous slag saturated in spinel. Journal of the European Ceramic Society, 35(1),347-355.

Scheunis L., Fallah-Mehrjardi A., Campforts M., Jones P.T., Blanpain B., Jak E. (2014). The effect of phase formation during use on the chemical corrosion of magnesia–chromite refractories in contact with a non-ferrous PbO–SiO_2 based slag. Journal of the European Ceramic Society, 34 (6), 1599-1610.

Malfliet A., Lotfian S., Scheunis L., Petkov V., Pandelaers L., Jones P.T., Blanpain B. (2014). Degradation mechanisms and use of refractory linings in copper production processes: A critical review. Journal of the European Ceramic Society, 34 (3), 849-876

Submitted

Scheunis L., Fallah Mehrjardi A., Campforts M., Jones P.T., Blanpain B., Malfliet A., Jak E., The effect of a thermal gradient on the phase formation inside a magnesia-chromite refractory in contact with a non-ferrous PbO-SiO_2 slag, submitted to the Journal of the European Ceramic Society.

In preparation

Scheunis L., Campforts M., Jones P.T., Blanpain B., Malfliet A. Spinel saturation of a PbO based slag as a method to limit the chemical degradation of magnesia-chromite bricks.

Book chapter

Malfliet A., Scheunis L., Jones P.T., Blanpain B., Refractories in copper production (2013) in Seetharaman S.(Ed.) Treatise on Process Metallurgy, Volume 3: Industrial Processes, Elsevier, 600-620

Conference proceedings

Scheunis L., Jones P.T., Blanpain B., Malfliet A., Campforts M. (2013). The effect of in-situ phase formation on the infiltration and chemical degradation of magnesia-chromite bricks in contact with a synthetic non-ferrous slag. In Bassa, R. (Ed.), Parra, R. (Ed.), Luraschi, A. (Ed.), Demetrio, S. (Ed.), Proceedings of Copper 2013: Vol. 3. Copper 2013. Santiago de Chile, Chile, 1-4 December, 2013, 485-496

Scheunis L., Campforts M., Jones P.T., Blanpain B. (2011). Influence of simultaneous infiltration and reaction on the chemical degradation of magnesia-chrome bricks in contact with a synthetic lead slag, Proceedings of Fray International symposium, Vol. 1, Cancun, Mexico, November 27 – December 1, 2011, 371-387

Curriculum Vitae

Personal data

Full name: Lennart Scheunis

Current address: Hooistraat 33, 3582 Beringen, Belgium

Place of birth: Hasselt

Date of birth: 05/05/1986

Education

2010 – 2014: PhD, faculty of Engineering, KU Leuven

Umicore IWT-Baekeland (mandate 100700).

2008 – 2010: Master in Materials Engineering, KU Leuven

2004 – 2008: Bachelor in Engineering, KU Leuven